AEDC-TR-90-7

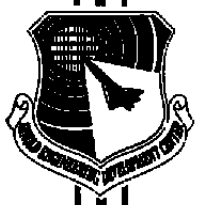

Calibration of the PARC Program for Propulsion-Type Flows

G. D. Garrard and W. J. Phares
Sverdrup Technology, Inc., AEDC Group

July 1990

Final Report for Period October 1, 1988 — June 1, 1990

ARNOLD ENGINEERING DEVELOPMENT CENTER
ARNOLD AIR FORCE BASE, TENNESSEE
AIR FORCE SYSTEMS COMMAND
UNITED STATES AIR FORCE

NOTICES

When U. S. Government drawings, specifications, or other data are used for any purpose other than a definitely related Government procurement operation, the Government thereby incurs no responsibility nor any obligation whatsoever, and the fact that the Government may have formulated, furnished, or in any way supplied the said drawings, specifications, or other data, is not to be regarded by implication or otherwise, or in any manner licensing the holder or any other person or corporation, or conveying any rights or permission to manufacture, use, or sell any patented invention that may in any way be related thereto.

Qualified users may obtain copies of this report from the Defense Technical Information Center.

References to named commercial products in this report are not to be considered in any sense as an endorsement of the product by the United States Air Force or the Government.

This report has been reviewed by the Office of Public Affairs (PA) and is releasable to the National Technical Information Service (NTIS). At NTIS, it will be available to the general public, including foreign nations.

APPROVAL STATEMENT

This report has been reviewed and approved

Mark S. Briski

MARK S. BRISKI, Capt, USAF
Facility Technology Division
Directorate of Technology
Deputy for Operations

Approved for publication:

FOR THE COMMANDER

Keith L. Kushman

KEITH L. KUSHMAN
Technical Director
Directorate of Technology
Deputy for Operations

REPORT DOCUMENTATION PAGE

Form Approved
OMB No. 0704-0188

1. AGENCY USE ONLY (Leave blank)	2. REPORT DATE	3. REPORT TYPE AND DATES COVERED
	July 1990	Final, October 1, 1988 -- June 1, 1990

4. TITLE AND SUBTITLE
Calibration of the PARC Program for Propulsion-Type Flows

5. FUNDING NUMBERS
65807F

6. AUTHOR(S)
Garrard, G. D. and Phares, Sverdrup Technology, Inc., AEDC Group

7. PERFORMING ORGANIZATION NAME(S) AND ADDRESS(ES)
Arnold Engineering Development Center/DOT
Air Force Systems Command
Arnold AFB, TN 37389-5000

8. PERFORMING ORGANIZATION REPORT NUMBER
AEDC-TR-90-7

9. SPONSORING/MONITORING AGENCY NAMES(S) AND ADDRESS(ES)
Arnold Engineering Development Center/DO
Air Force Systems Command
Arnold AFB, TN 37389-5000

10. SPONSORING/MONITORING AGENCY REPORT NUMBER

11. SUPPLEMENTARY NOTES
Available in Defense Technical Information Center (DTIC).

12a. DISTRIBUTION/AVAILABILITY STATEMENT
Approved for public release; distribution is unlimited.

12b. DISTRIBUTION CODE

13. ABSTRACT (Maximum 200 words)

The purpose of this Technical Report is to provide documentation of recent efforts towards the calibration of the PARC program for various types of flows experienced in the testing of turbine engines and rocket motors. This report provides a systematic and comprehensive assessment of the PARC program's capabilities and provides a baseline capability against which future modifications to the PARC program can be assessed. The work documented herein is based on a building block calibration approach and is a continuation of efforts started in FY 87. The present work revisits some of the earlier cases and expands into other, more complex flow problems with features similar to those found in the ETF test environments. The discussion of each calibration case is broken down into three parts. The motivation for selecting a particular flow problem for the PARC calibration is dicussed first. That section will identify how each calibration case is related to typical testing problems within ETF and why it is important that it be included in this report. The actual test cases used for each calibration case are discussed. Particular emphasis is placed on where the data were obtained. The CFD results obtained in the study are documented and discussed in the third section, along with a description of grids, boundary conditions, and initial conditions used in the study.

14. SUBJECT TERMS		15. NUMBER OF PAGES
Navier-Stokes code	**diffuser performance**	**108**
program calibration	**2-D/C-D nozzle**	**16. PRICE CODE**
free jet	**backstep**	

17. SECURITY CLASSIFICATION OF REPORT	18. SECURITY CLASSIFICATION OF THIS PAGE	19. SECURITY CLASSIFICATION OF ABSTRACT	20. LIMITATION OF ABSTRACT
UNCLASSIFIED	**UNCLASSIFIED**	**UNCLASSIFIED**	**SAME AS REPORT**

PREFACE

The work reported herein was conducted by the Arnold Engineering DevelopmentCenter (AEDC), Air Force Systems Command (AFSC). The results of the research were obtained by Sverdrup Technology, Inc., AEDC Group, operating contractor for the engine test facilities at the AEDC, AFSC, Arnold Air Force Base,Tennessee, under Project DB84EW. The Air Force Project Manager was Capt. Mark Briski/DOT. The data analysis was completed on October 1, 1989, and the manuscript was submitted for publication on June 21, 1990.

CONTENTS

ILLUSTRATIONS

Figure Page

Figure Page

TABLES

Table Page

APPENDIXES

1.0 INTRODUCTION

The use of computational fluid dynamics (CFD) in ground level propulsion system testing has been steadily increasing in recent years. This increase has been driven by the need to reduce the high costs and technical risks associated with propulsion system testing. In the Engine Test Facility (ETF) at the Arnold Engineering Development Center (AEDC), CFD has been successfully applied to help reduce the costs and risks related to turbine engine and rocket motor testing. The PARC program (a general purpose CFD tool that provides aerodynamic flow-field simulation using the Reynolds-averaged Navier-Stokes equations) has recently been used to support complex propulsion system tests. These CFD applications have included the design of an exhaust gas management system for thrust reversing turbojet engines, numerous free-jet engine/inlet compatibility studies, and diffuser sizing studies for rocket motor testing. Two versions of the PARC program are available. Two-dimensional (2-D) and axisymmetrical flow problems have been simulated by the PARC2D program, and three-dimensional (3-D) flow simulations have been provided by the PARC3D program.

A problem that has been present during the application of CFD within the ETF is the lack of program calibration. The use of the PARC program without an understanding and appreciation of the program's strengths and weaknesses as applied to specific test problems could result in inappropriate use and lead to erroneous conclusions. Exact solutions from the PARC program for most problems should not be expected because the driving force behind the PARC program development has been free-shear-layer-type flows. Emphasis has not been placed on wall-bounded-type flows. By necessity, PARC program calibration efforts have been performed concurrently with the application, yielding potential compromises in schedule and cost. Of equal importance is the availability of validation standards against which code modifications can be evaluated.

The purpose of this Technical Report is to provide documentation of recent efforts towards the calibration of the PARC program for various types of flows experienced in the testing of turbine engines and rocket motors. This will facilitate the resolution of the two major difficulties discussed in the previous text by (1) providing a systematic and comprehensive assessment of the PARC program's capabilities, and (2) providing a baseline capability against which future modifications to the PARC program can be assessed.

The work documented herein is based on a building block calibration approach and is a continuation of efforts started in FY 87 (Ref. 1). The Ref. 1 document recorded the comparison of PARC program results to test data for three types of fundamental flow fields occurring in test environments. They were (1) flow over a flat plate with no pressure gradient, (2) a matched expansion axisymmetric supersonic free-jet wake, and (3) very low subsonic flow over a rearward-facing step (backstep). Past validation and calibration of the PARC

program is summarized in Section 2. The present work revisits some of these earlier cases and expands into other, more complex flow problems with features similar to those found in the ETF test environments. The subject of free-jet flows is revisited in Section 3, with particular emphasis placed on an improvement to the PARC program that corrects a problem encountered in Ref. 1 for far-field flows. The calibration of the PARC program for determining steady-state diffuser performance is discussed in Section 4. The capability to accurately compute wall viscous flows in strong pressure gradients is evaluated in Section 5 through analysis of 2-D converging/diverging nozzle flows. The reaward-facing step analysis is extended to included comparisons of PARC program results to data for supersonic flow in Section 6.

The discussion of each calibration case will be broken down into three parts. The motivation for selecting a particular flow problem for the PARC calibration will be discussed first. This section will identify how each calibration case is related to typical testing problems within ETF and why it was important that it be included in this report. The actual test cases used for each calibration will then be discussed. Particular emphasis will be placed on where the data were obtained. The CFD results obtained in the study will be documented and discussed in the third section, along with a description of grids, boundary conditions, and initial conditions used in the study.

2.0 LITERATURE SURVEY

The calibration and validation of CFD programs have been very active research topics in the recent past. As more and more dependence is placed on CFD simulations, the sources of error in the computational algorithms must be fully understood. It is important that CFD programs be tested by comparing them to appropriate experiments, both to ensure their validity and to define their applicable range. Several examples of the calibration of the PARC program exist in recent literature, and are summarized in Table 1. The calibration cases include such flow calculations as supersonic inlets, axisymmetric and 2-D nozzles, diffusers, and exhaust-gas management systems. The following literature survey summarizing Refs. 1 through 6 is intended to acknowledge earlier calibration efforts on the PARC program. It also provides a means to capture the status of PARC program calibration activities prior to this effort. It is not intended to completely cover all of the available literature relating to CFD program calibration.

The terminology used in the present discussion will be based on the definitions for calibration and validation as given in Ref. 7. This work has received considerable attention in the literature (Refs. 8 and 9, for example), and was based on the work of a National Aeronautics and Space Administration (NASA) ad hoc committee on validation. The pertinent definitions are

CFD Program Validation — Validation provides detailed surface and flow-field comparisons with experimental data. The purpose of the comparison is to verify the program's ability to correctly model the critical physics of the flow. It is required that the accuracy and limitations of both the experimental data and the program be thoroughly known and understood over a range of specified parameters.

CFD Program Calibration — Calibration provides a comparison of a program's ability to accurately predict certain aspects of the flow field by comparing the program output to experimental data obtained from geometries that are similar to the one under consideration. It is only important to ensure that the parameters of interest are reliably predicted and not that all aspects of the flow are correctly modeled.

As a general observation, the concept of a validated PARC program is presently an unachievable goal. The current state-of-the-art in many aspects of CFD dictates that proper modeling of the critical flow physics can not occur (Ref. 10). The most obvious example of this is in the modeling of turbulence. Turbulence modeling as it currently stands, with empirically based models, has a long way to go before an accurate reproduction of the flow physics is obtained (Ref. 11).

The first recorded example of the calibration of the PARC program was provided by Huddleston, Cooper, and Phares (Ref. 2). This effort used the PARC2D program to study the effects of test cell exhaust-gas recirculation on the surface pressure distributions occurring on a high-bypass turbofan engine. Two geometries were considered, the first being a subscale test configuration and the second being an actual turbine engine installation in an ETF test cell. The subscale test case geometry is shown in Fig. 1. The PARC2D calculations matched the test data to within approximately ± 5 percent for both the center pipe surface pressures and the cell wall pressures. The comparison plots are shown in Figs. 2 and 3. The subscale case provided a calibration of the PARC2D program and indicated that further effort was warranted. The actual turbine engine test case had a geometry similar to that shown in Fig. 4. Measured and computed fan cowl surface pressures are compared in Fig. 5. Likewise, core plug surface pressures are compared in Fig. 6. Although the computed values were within ± 25 percent (with a few exceptions), the exact location of the predicted peak locations were somewhat shifted from those recorded. The discrepancy was considered to be the result of both the axial and normal spacing of the gridding, and further investigation was recommended.

Another example of using the PARC2D program in a turbine engine testing environment was provided by Phares et al. (Ref. 3). This example discusses several applications of the PARC2D program to problems occurring in propulsion testing. Pertinent applications included a study of test cell heating caused by diffuser and engine interaction, the prediction of diffuser wall pressures in a variable area ejector, and the prediction of base pressures for a centered

propulsive jet. The study of test cell heating caused by diffuser and engine interaction was a qualitative comparison of PARC2D calculations to experimentally obtained Thermovision® camera pictures. The geometry of the hardware is shown in Fig. 7. For a given test cell pressure, the PARC2D program was able to qualitatively predict the presence of exhaust gas recirculation from the diffuser. The geometry of the variable area ejector case is shown in Fig. 8. The results, which compared PARC2D calculations to both test data and an integral analysis method (Ref. 4), are plotted in Fig. 9. The PARC2D program calculations matched diffuser wall static pressure to within ±5 percent if the diffuser wall boundary condition was defined as a constant, specified temperature. If the wall was treated as adiabatic, errors as large as 25 percent were generated. In addition, the centered propulsive-jet case was used to determine the capability of the PARC2D program to determine base pressures. The geometry of the case is shown in Fig. 10. Comparison of the PARC2D results to test data is shown in Fig. 11. The solution compares reasonably well with the test data, with an error of approximately ±10 percent.

Hunter and Kent (Ref. 5) document the use of the PARC2D program to analyze two hypersonic inlets at Mach 7.4. The geometry for the two inlets, which were designated in Ref. 5 as P-2 and P-12 inlets, is presented in Fig. 12. Calibration of the PARC2D program was obtained by comparing program output to centerbody static pressures and cowl static pressures. Comparisons for the P-2 and P-12 inlets are shown in Fig. 13. The PARC2D program predicted centerbody and cowl static pressure distributions for the P-2 inlet to within approximately 15 percent. Centerbody static pressure distributions for the P-12 inlet indicated a discrepancy between the program results and the data of as much as 30 percent. No discussion was included as to why the differences might have occurred. The cowl static pressure predictions were within 10 percent of the data.

The work performed by Semmes, Arbiter, and Dyer (Ref. 6) is an excellent example of a calibration effort applied to the PARC2D program. Three different configurations were considered for the calibration effort, including a 2-D hypersonic inlet (same data set generated by the P-2 inlet in Ref. 5), an axisymmetric convergent/divergent nozzle, and an axisymmetric subsonic diffuser. For the 2-D hypersonic inlet, a considerably broader amount of data were considered in Ref. 6 than were considered in Ref. 5. For example, the boundary-layer growth along the centerbody and cowl predictions compared to test data are shown in Fig. 14. The PARC2D boundary-layer thickness predictions were as much as 50 percent larger than the test data. The differences were attributed to both the uncertainty in determining the experimental boundary-layer edge and the fact that the PARC2D calculation was switched from laminar to turbulent at the location where the onset of transition was observed in the actual flow field.

The geometry for the axisymmetric convergent/divergent nozzle is given in Fig. 15. Surface static pressure along the top wall is shown in Fig. 16. The PARC2D program predicted the wall static pressures to within 10 percent both upstream and downstream of the nozzle throat. In the throat region, the pressure predictions were off by as much as 50 percent, mainly because of a slight shift in the pressure profile relative to the data. The surface static pressure distribution for the subsonic diffuser is plotted in Fig. 17. The errors in the PARC2D predictions were near 0 percent at the inlet of the nozzle and increased to approximately 5 percent at the exit of the diffuser. The error was attributed to the type of boundary condition used to specify outflow at the nozzle exit.

The final selection that was reviewed was the work reported by Cooper, Garrard, and Phares (Ref. 1). This work was performed to validate the PARC2D program for three fundamental flows typical of turbine engine and rocket motor testing at the AEDC. Laminar and turbulent flow over a flat plate was investigated, as was a supersonic, axisymmetrical jet issuing from a Mach 2.22 nozzle into quiescent air and subsonic flow over a rearward-facing step. The geometry applied in the flat plate analysis is shown in Fig. 18. Numerous comparisons to data were made for both laminar and turbulent flow. Several different inflow and outflow Reynolds numbers were studied as were adiabatic and fixed temperature plates, different inflow Mach numbers, and different grids. The discrepancies between the PARC2D calculations and the calibration data were limited from 5 to 10 percent, even for such parameters as skin friction and Stanton number.

The supersonic nozzle geometry is presented in Fig. 19. The test case was a Mach 2.22 flow exhausting into quiescent air with no thermal gradient. The near-field results (Fig. 20) indicate that the PARC2D program matched the spread rate of the turbulent jet. Far-field results (Fig. 21) showed that the PARC2D program underpredicted the spread rate by approximately 40 percent at X/Rne = 140. The divergence was believed to be the result of underpredicting the turbulence level of the flow in the far-field region.

The geometry of the rearward-facing step is presented in Fig. 22. The PARC2D program results are compared to data in Fig. 23. The PARC2D program predictions matched velocity profiles to within ± 10 percent everywhere except in the separated region just downstream of the step. In the separated region, the difference between the predictions and data were as high as 30 percent. This relatively large error was attributed to the use of an algebraic turbulence model. Other efforts reported herein have also shown equally large errors for separated flows because of the use of an algebraic turbulence model.

The examples of PARC program calibration presented above are summarized in Table 1 and demonstrate the versatility and strength of the PARC program. Many different fundamental types of flow were considered and the results were generally excellent. Most

cases where the errors were large were attributable to slight shifts in the results in regions of high gradients. Even where the maximum error was large, most cases predicted the correct trends in the data.

3.0 FREE-JET FLOWS

3.1 MOTIVATION

Free-jet flows are included in this report because most of the tests performed in the ETF involve some form of free-jet flow. Particular examples of free-jet flows in the ETF include exhaust flows from turbine engines and rocket motors and free-jet flow provided by a subsonic or supersonic nozzle during engine/inlet compatibility testing. These test installations are generically sketched in Fig. 24. The exhaust flows for turbine engines and rocket motors are expelled into the test cell environment and then collected by the exhaust diffuser. The test article and diffuser can not be directly connected because of thrust measurement requirements, requiring the exhaust to travel as a free-jet for some distance. Engine/inlet compatibility testing requires a free-jet environment to correctly simulate free-flight conditions to the test article.

3.2 TEST CASES

The test cases considered in this section are a continuation of the work performed during FY 88 and reported in Ref. 1. The work is broken into three parts. The first part discusses the axisymmetric Mach 2.22 nozzle flow documented by Eggers (Ref. 12). The Ref. 1 effort had considerable problems with the far-field spread rate. The current effort consisted of various modifications to the algebraic turbulence model in the PARC program and resulted in an improved capability to predict far-field flow conditions. The second part of the study expanded the range of free-jet flows by considering a subsonic free jet (Mach 0.2). The results for the subsonic case were compared to theory as defined by Schlichting (Ref. 13). The third and final part of the study considered the spread rate of a supersonic free jet at various Mach numbers (1.0, 1.6, 3.0, and 4.0). The supersonic cases were compared to data presented by Rudy and Bushnell (Ref. 14). Both the subsonic and supersonic free-jet cases were analyzed using the modified turbulence model developed in the first part of the study. All cases were analyzed with PARC2D, the 2-D, axisymmetric version of the PARC program.

The uncertainty of the velocity data presented in Ref. 12 is reported to be ± 0.75 percent on the centerline. The uncertainty increases to ± 1.0 percent where $U/U_{max} = 0.3$ and ± 15 percent for $U/U_{max} = 0.1$. There is no discussion of the uncertainty of the theory presented in Ref. 13. The velocity profile theory does, however, fall within the spread of the compiled data, which have a mean deviation of less than 5 percent for U/U_{max} greater than 25 percent.

The supersonic data presented in Ref. 14 are based on a compilation of data obtained from a multitude of sources. The uncertainty of the entire database is not presented. The uncertainty of the Mach 5.0 data is presented as ±2.5 percent. It is expected that the remaining data will fall within this band.

3.3 RESULTS

The three test cases considered in this section all consisted of similar geometry. The gridding, boundary conditions, and initial conditions used in the study were nearly identical and are discussed in the following.

The grid used to generate the results for the supersonic free-jet cases was constructed using the techniques developed in Ref. 15. The grid started upstream of the nozzle throat and extended 159 X/R_{ne} downstream of the nozzle exit. The grid was constructed of 18,900 grid points made up of the intersections of 189 vertical lines (referred to as the I indices) and 100 horizontal lines (referred to as the J indices). The nozzle exit was modeled with 60 grid points along the first I index. The grid spacing off the nozzle wall was exponentially packed with an initial spacing of 0.0005 in. At the nozzle exit, the J indices above the nozzle lip were packed exponentially towards the nozzle with the same initial spacing as inside the nozzle.

The grid for the subsonic test case, likewise generated using the techniques developed in Ref. 15, started just upstream of the nozzle exit and extended 50 X/R_{ne} downstream of the nozzle exit. The grid was constructed of 12,231 grid points made up of the intersections of 151 vertical lines (referred to as the I indices) and 81 horizontal lines (referred to as the J indices). The nozzle exit was modeled with 30 grid points along the first I index. The J indices were packed exponentially towards the nozzle lip on either side with an initial spacing of 0.0001 in.

Boundary conditions for the grids were identical. The vertical wall extending from the nozzle lip to the top of the grid was treated as a slip wall. The boundaries defined by the uppermost J index and the last I index were treated as free boundaries. The pressure and temperature of the ambient surroundings were specified along these two boundaries. The centerline of the flow (J index 1) was specified as the axis of symmetry. It was about this index that the problem was considered to be axisymmetric.

The flow was introduced to the grid along the boundary defined by I index 1. As stated earlier, 60 points were used to define the supersonic nozzle exit and 30 grid points defined the subsonic nozzle exit. Flow conditions were specified along the boundary so that the correct pressure ratio was obtained with the ambient conditions. This ensured that the correct nozzle

exit Mach number was obtained. For Eggers' Mach 2.22 nozzle case, the flow conditions at the nozzle exit were obtained from a solution of the flow in the nozzle and then transferred to this grid. The remaining cases based the flow profile exiting the nozzle on one-dimensional (1-D) isentropic flow conditions. The boundary layer at the nozzle exit was specified using the $1/7^{th}$ power law (Ref. 16). The flow properties at the nozzle exit for all three cases were not permitted to vary during the solution.

The initial flow properties specified downstream of the nozzle exit depended upon the location in the grid. If the point under consideration was located on or below the J index that defined the nozzle lip, the flow was considered to have the same properties as given at the nozzle exit. Above the J index that specified the nozzle lip, the flow was assumed to have a very low velocity (Mach number of 0.001) and was at the pressure and temperature used along the free boundaries.

EGGERS' MACH 2.22 NOZZLE — The data presented by Eggers in the Ref. 12 report provides a broad collection of data describing the flow field downstream of an axisymmetric Mach 2.22 nozzle exhausting into quiescent air. Previous work indicated that the PARC program could successfully handle the near-field flow, matching the centerline Mach number, jet spread rate, and velocity profiles at various stations downstream of the nozzle exit to within ± 20 percent. Once the core region of the flow collapsed, the PARC program was unable to change the rate of mixing layer growth to match that indicated by the data. A schematic of the nozzle and flow field is shown in Fig. 19.

In order to facilitate a better match to the data, a modification to the algebraic turbulence model used by the PARC program was made. The original turbulence model generated a value for the turbulent viscosity based on the formulation by Thomas (Ref. 17) of the Baldwin and Lomax model (Ref. 18). The final value of the turbulent viscosity was obtained by multiplying the model output by a constant turbulence mixing coefficient (defined as the variable COFMIX in the PARC program), nominally equal to 0.1. This coefficient was required since the level of turbulent viscosity calculated by the model was higher than indicated by data. The modification based the value of the mixing coefficient at any particular point in the flow on the local Mach number. The modification is described in detail in Appendix A.

The calculated radial location of the point where the velocity equaled one-half the centerline velocity along a given I index is compared to data in Fig. 25. The modification to the algebraic turbulence model provides excellent results, with the PARC program predictions remaining within ± 10 percent of the data.

The X-velocity profiles of the solution are compared to data at various locations downstream of the nozzle exit in Fig. 26. Compared to the Ref. 1 results, the PARC program calculations yielded centerline velocity within ± 10 percent of the data.

SUBSONIC FREE JET — Based on the results that were obtained with the Mach 2.22 nozzle case, the second part of the free-jet study was conducted using the modified version of the algebraic turbulence model. This part of the study considered an axisymmetric subsonic free jet (Mach 0.2) issuing from a wall.

The calculations for this case were compared to the theory presented by Schlichting in Ref. 13 for turbulent subsonic circular jets. Based on empirical data, the boundary of the free jet relative to the nozzle exit radius where the velocity is equal to one-half the centerline velocity is given by $b_{1/2} = 0.0848x$. A comparison of the PARC program calculations to this equation is shown in Fig. 27. The program, with the modified turbulence model, provided an excellent match, deviating from the empirical theory by less than 10 percent.

The velocity profiles at various locations downstream of the nozzle exit plane were also compared to theory as developed in Ref. 13. Schlichting compares the theory to data in Fig. 24.8 in Ref. 13, nondimensionalizing the results by U_{max} and $Y_{(½U_{max})}$. Except at the jet edge where U/U_{max} falls below 0.25, the theory falls within the scatter of test data. The PARC program results are compared to the theory in Fig. 28 for two locations downstream of the nozzle exit. Again, the results were good, with deviations from the theory being less than 10 percent.

SUPERSONIC FREE JET — The third and final section of this study considered a supersonic free jet operating at four different exit Mach numbers, 1.0, 1.6, 3.0, and 4.0.

The calculations for this study were compared to data compiled by Rudy and Bushnell in Ref. 14. The Reference presents a broad collection of data that have been correlated with the spreading parameter, which is described by the following relationship:

$$\sigma = \frac{1.855\ (X_B - X_A)}{Y_B - Y_A}$$

where Y_A and Y_B are the lateral distances between the points at which u/u_1 is 0.1 and 0.9 at longitudinal stations X_A and X_B, respectively. The spreading parameter σ can also be viewed as the reciprocal of the spreading rate of the shear layer. The comparison of the PARC program calculations to the Ref. 14 data is shown in Fig. 29. The PARC calculations matched the data closely, with maximum deviations on the order of 5 percent.

4.0 DIFFUSER FLOWS

4.1 MOTIVATION

Diffusers are commonly used in the ETF for the ground testing of turbine engines and rocket motors. The ETF routinely tests a wide variety of propulsion systems at simulated altitude conditions. A sketch of a typical turbine engine test installation is shown in Fig. 24a. A typical rocket motor installation is sketched in Fig. 24b. By capturing the exhaust products from a propulsion system, the diffuser either directly produces the simulated altitude pressure in the test cell or enhances the performance capabilities of an exhaust plant. The pressure rise provided by the diffuser is a direct function of the kinetic energy of the driving fluid stream and the amount of secondary flow captured from the test cell (Ref. 19).

Testing of propulsion systems in ground test facilities is becoming more stringent, both in terms of test simulation requirements and in controlling cost. Proper sizing of the diffuser system to match the operating characteristics of the test article is vitally important. In many cases, testing requirements dictate that a diffuser system be used that can both increase the maximum altitude pressure simulation capabilities of the facility and that can reduce the exhauster pressure ratio requirements in order to decrease power usage. The nonrepeatable nature of many tests places a high level of importance on the proper sizing of the diffuser system. For example, a solid-propellant rocket motor test can not be repeated since the motor can be fired only once.

The physical nature of the flow in a diffuser can be extremely complex and a purely theoretical description of the flow is generally not feasible. Several 1-D, semiempirical methods have been developed for designing diffusers for various applications (Refs. 20 and 21). Because of the simplifying assumptions needed to keep the analysis 1-D, the designer does not know quantitatively important aspects of the flow in the diffuser (such as heat-transfer rates and wall pressure loadings) that will permit the proper design of all components of the diffuser system. CFD is showing promise as an analysis tool to provide detailed knowledge of diffuser operation. This will improve the design process by ensuring the diffuser is properly sized to match the test requirements. As with any analysis tool, the constraints and limitations of the tool must be known before it can be intelligently applied.

4.2 TEST CASES

To address the previously discussed issues, a calibration of the axisymmetric version of the PARC program, PARC2D, for diffuser systems found in turbine engine and rocket motor testing has been accomplished. The study is broken into two parts. The first part of the study compares the analysis results to a simple ejector system using a single-specie, single-stream,

nonreacting flow. The simplicity of the test configuration removed as many unknown variables as possible. The data for the study were taken from the available literature. The second part of the study considers three rocket test installations. These three cases provide a database against which to compare the PARC program performance for "real world" type flows.

The data used for the first part of the calibration of the CFD program were presented by Fortini in Ref. 21. That report discusses the effects of various dimensions on the performance of a small axisymmetrical diffuser system using high-pressure nitrogen as the primary fluid. The test apparatus is sketched in Fig. 30. The diffuser system consisted of a primary chamber, a primary nozzle, a cylindrical test cell, and a diffuser tube.

Four diffusers were provided for the study. The inside tube diameters were 1.00, 1.25, 1.50, and 1.75 in. The tube lengths were initially 12 in., with the tubes being shortened to study the effects of the length-to-diameter ratio (L/D). Each tube had 30 static pressure taps located symmetrically along the length of the diffuser.

The data used in the second part of the diffuser study were obtained from test data taken in the ETF during actual rocket motor firings. Three rocket motor configurations were selected. The configurations of the three motor/diffuser combinations are sketched in Fig. 31. In this figure, the length measurements were nondimensionalized by the total diffuser length. The total pressure of the primary flow and the resulting cell pressure as determined from test data are presented in Table 2.

The uncertainty of the data presented in Ref. 21 is not discussed; however, mercury manometers were used to obtain the pressure measurements. The pressure recordings were photographed and then determined from the photographic negative. Although it is impossible to definitively deduce the uncertainty of the data from this information, it is expected that the uncertainty should be approximately the same as other reported pressure measurements obtained by the mercury manometer method during this time period. A review of several references published in the middle to late 1950's (Refs. 22 through 25) indicates that the uncertainty of mercury manometer readings can vary from as low as ± 0.01 in. of mercury to as high as ± 0.1 in. of mercury. At the high level this equates to an uncertainty of only ± 0.05 psia.

The uncertainty of the data used in the second part of the analysis was found to be ± 10.4 percent on cell pressure for Motors 1 and 2, and ± 1.1 percent for Motor 3. Chamber pressure for Motors 1 and 2 had an uncertainty of ± 1.9 percent, whereas the chamber pressure for Motor 3 had an uncertainty of ± 0.4 percent.

4.3 RESULTS

FORTINI DIFFUSER SYSTEM — Several aspects of the calibration study have been consistently applied throughout. Rather than duplicate the presentation of these aspects for each case, they will be discussed in the following text. The parameters of interest include gridding, boundary conditions, initial conditions, and convergence criteria.

Since the calibration effort was limited to only two nozzle/diffuser configurations, it was necessary to provide only two different grids. The grids were created using the techniques developed in Ref. 15. Each grid was constructed of 18,000 points along 180 vertical lines (referred to as the I indices) and 100 horizontal lines (referred to as the J indices). The first grid provided the computational domain for the 1.5-in.-diam, 6-in.-long diffuser (L/D = 4), and the second grid modeled the 1.0-in.-diam, 12-in.-long diffuser (L/D = 12). Exponential grid packing with spacings of 0.0001 in. was used in the nozzle wall viscous layer and at the nozzle exit lip where the shear layer would form.

The boundary conditions were specified so that all walls were treated as no-slip and adiabatic with the exception of the bottom and front wall of the cell volume, which were considered as slip surfaces. Because of the low flow velocity expected in these regions, it was judged that resolving a boundary layer along the wall would not contribute to the solution and would in fact degrade the solution by requiring significant computer processing time. The exit of the diffuser provided the outflow boundary. This boundary condition was provided by using the diffuser exit pressure from Ref. 21, which varied from 14.3 to 14.4 psia. For this study, the exit pressure was held a constant 14.3 psia. Flow into the system was controlled on I index 1, J indices 1 to 40. The total pressure of the nitrogen flow was applied there, the value of which depended on the condition being studied.

The initial conditions applied over the computational domain were varied, depending on the expected performance from the diffuser. For a started diffuser, the flow properties inside the nozzle were based on the total pressure required for the data point of interest and the nozzle flow area at the I index under consideration. One-dimensional, isentropic flow was assumed, with subsonic flow defined upstream of the nozzle throat and supersonic flow defined downstream of the nozzle throat. Downstream of the nozzle exit, the flow continued down the diffuser with the nozzle wall boundary (J = 40) extended to the diffuser exit to provide an artificial boundary for the flow. The cell volume and the remaining grid points in the diffuser were given properties corresponding to very low velocity flow at a pressure near the desired answer.

For an unstarted diffuser, the flow in the nozzle was exactly identical to the started case. Outside of the nozzle, however, the entire grid was set to the pressure and flow velocity as

in the cell region of the preceding case. The initial conditions were set this way because of difficulties that were present when the initial conditions for the started cases were used on some of the unstarted cases. With the diffuser filled with supersonic flow, the solution resulted in the diffuser starting. Before the unstarted pressure could be obtained in the cell volume, a shock would have to travel up the diffuser. Waiting for the shock to reach the entrance to the diffuser was time-consuming and required a large number of iterations on the computer (greater than 20,000 iterations). By starting the supersonic flow from the nozzle exit, the convergence problem was accelerated without impacting the final results.

Four cases were considered in the study. The first three cases considered the diffuser having an L/D of 4. The first case simulated the diffuser system operating in the started mode, whereas the second and third cases used data from unstarted conditions. The second configuration used the diffuser having an L/D of 12. A started case was considered in the study. The study was conducted using the version of the PARC2D program that did not include the modifications to the algebraic turbulence model described in Appendix A. This was dictated by the fact that both work efforts were conducted concurrently. Three of the cases were rerun using the modified PARC program. The PARC2D program was calibrated when operating in the started mode using the turbulent mixing coefficient (COFMIX) to obtain the correct cell pressure. Then, once the required value of COFMIX was determined, the program was exercised with the remaining flow cases.

Case 1 — This case was based on the maximum pressure case for the L/D = 4 diffuser. The total pressure for the primary nitrogen flow was 629 psia. In order to obtain the correct cell pressure of 0.5 psia, values of 0.11, 0.115, and 0.12 were tried for COFMIX. The value of 0.115 provided a cell pressure very nearly equal to the data and was used in the remainder of the study. The resulting flow field, shown by Mach number contours and velocity vectors, is given in Fig. 32.

A comparison between the calculated and measured wall static pressures down the diffuser length is presented in Fig. 33. The calculations matched the data until just downstream of where the nozzle exit flow reached the diffuser wall. At that point, the PARC2D program overpredicted the rate of pressure increase along the wall, resulting in the sudden pressure recovery seen in the figure. These results indicate that the PARC2D program did not correctly model the flow in the diffuser. Based on the discussion of normal shocks in ducts in Ref. 26 and the test data from Ref. 21, it was expected that the pressure recovery in the diffuser would result from a series of normal shocks. The computational results shown in Figs. 32 and 33, however, indicated that the PARC2D program set up a single strong normal shock in order to effect the needed pressure rise.

Case 2 — This case was a condition operating with the diffuser unstarted. The total pressure of the nitrogen primary fluid was 208 psia. At this operating pressure, the diffuser was not flowing full, and the flow was separated inside the nozzle (Ref. 21). The turbulence mixing coefficient was set to 0.115 as defined previously.

A converged solution was obtained after 100,000 iterations. The cell pressure was calculated to be 12.7 psia. This was 30 percent higher than the test data value of 9.5 psia. The plots of Mach number contours and velocity vectors are shown in Fig. 34. Figure 35 reveals that the flow did not separate from the nozzle wall until just before the nozzle exit. Since the data in Ref. 21 do not include the location of the flow separation point in the nozzle, it was not known if the computed flow field separated at the correct location. Based on past experience (Ref. 1), it was suspected that the algebraic turbulence model was a major factor in the poor performance. Wall static pressures, both calculated and measured, are plotted in Fig. 36. There was not much to be concluded from this plot since the cell pressure was considerably higher than the test data. There was an indication of a region of accelerating flow, however, which was not expected given the adverse pressure gradient in the diffuser.

Other values of COFMIX were investigated to see if perhaps one value would be required for started cases and another value for unstarted cases. A higher mixing coefficient of 0.13 did effect a lowering of the cell pressure by approximately 0.8 psia within 6,000 iterations. It should be mentioned, however, that the time-step size had to be reduced in order to keep the flow solution stable. Given these results, the mixing coefficient was raised to 0.15. At that level, the flow solution became unstable and could not be converged. It was therefore concluded that the PARC2D program could not adequately handle this regime of the diffuser performance map.

Case 3 — This case was to be used to investigate the operation of the diffuser system when the nozzle flows full but the diffuser does not. For this particular case, the total pressure of the nitrogen primary fluid was 360 psia. As with Case 2, the turbulence mixing coefficient was set to 0.115. Given the results from Case 2, which indicated that the diffuser started during the first part of the solution, the initial conditions assumed no flow values in the diffuser.

The results obtained for this case showed that, although the PARC2D program was converging to the correct cell pressure, the solution was highly transient and cyclical in nature. A total of 100,000 iterations were required to develop the cyclical nature of the solution, and it was not determined if additional iterations would have resulted in the solution converging to a constant pressure. The PARC2D solutions were obtained using a local time-stepping approach, and therefore, were not time-accurate. Thus, no time-dependent conclusions could be drawn from the results. It is interesting to note, however, that Ref. 21 describes the diffuser

operation in this regime as being unstable, and in fact identifies several points (including this one) as having a "buzzing" nature.

The flow solution obtained for this case is presented in Fig. 37. The velocity vector plot indicates a region along the diffuser wall where the flow has reversed direction. This qualitatively agrees with AEDC testing experience where water from exhaust gas coolers downstream of the diffuser has been observed to travel up into the test cell when the diffuser is operating in the unstarted mode. It should also be noted that this phenomena was also present in Case 2, as shown in Fig. 35.

The wall static pressure down the diffuser, both calculated and data, is shown in Fig. 38. The PARC2D values were obtained at 100,000 iterations. Again, as in Case 2, it appears that although the test cell pressure is over 10 percent too low, the pressure recovery in the diffuser occurs as it should with the pressure rise spread over the entire length of the diffuser.

Case 4 — This case was a simulation of the diffuser system operating in the started mode with the diffuser having an L/D of 12. The total pressure of the nitrogen primary fluid was 460 psia. The turbulence mixing coefficient was set to the nominal 0.115. Since the diffuser was operating in the started mode, full flow initial conditions were used.The cell pressure quickly converged to the test data value of 1.55 psia. The overall flow field calculated by the PARC2D program is shown in Fig. 39.

The wall static pressure along the diffuser is plotted in Fig. 40 for both the calculated values and the data. For this particular case, the PARC2D program does an excellent job of predicting the wall static pressure. Unlike the Case 1 results, the program did not overpredict the shock strength in the diffuser. The wall static pressures remained within 10 percent of the data until nearly half way down the diffuser. Beyond this point, the pressures appear to be shifted slightly with nominally correct peak-to-peak pressure levels compared to the experimental data.

ROCKET DIFFUSER SYSTEMS — Three rocket motor/diffuser systems were considered in the calibration effort. These rocket motors were selected from the large ETF database because of the availability of data and their similarity to the bulk of rocket motors tested in the ETF. Particular geometrical data is given in Table 2 for each of the three motors. As with the Fortini diffuser study, there were several aspects of the work that were consistent for all three cases. These will be discussed now, rather than during the discussion of each rocket motor.

The grids used in the study were all similar, with the differences in the diffuser geometry being the only variable. Each grid was constructed of 25,351 points. There were 251 I indices

and 101 J indices. The grid extended from just upstream of the nozzle exit plane to the diffuser exit. The grid started upstream of the nozzle exit to keep the vertical wall (I index = 1) from interfering with the recirculating flow coming off the exhaust gas plume. There was no attempt to grid the full test cell volume as was done in the Fortini effort. The nozzle exit plane was located at I index 20 with the J indices varying from 1 to 50. The grid was packed exponentially towards the nozzle wall with the spacing of the first grid point being 0.01 in. away from the wall.

The boundary conditions applied on the computational domain are shown in Fig. 41. The boundary conditions specified in the diffuser were similar to those used in the Fortini study. However, there were two basic changes from the previous cases. Secondary inflow was provided by defining the front wall of the cell volume as being an inflow boundary. The amount of secondary flow was determined as a percentage of the nozzle exit flow rate. The nozzle exit flow properties were determined using the Solid-Propellant Rocket Motor Performance Prediction Computer Program (SPP) described in Ref. 27. Given the rocket motor solid-propellant composition and the nozzle geometry, SPP provided the intrinsic properties of the inviscid flow field with a correction applied for the nozzle boundary layer. The gaseous ratio of specific heats provided by SPP was used as an input to the PARC program. By fixing the flow properties at the nozzle exit, the need to solve the flow field in the nozzle with the inherent complex chemical reactions (such as hydrogen burning) was avoided. The reactions in the flow downstream of the nozzle were not considered, since the PARC program is limited to single-specie flow. It should be noted that this limitation requires that the secondary flow properties be equal to the primary flow properties. In actual practice, this would not be the case as most of the secondary flow is nitrogen rather than rocket exhaust gas. The diffuser exit pressure was set to an arbitrary value that insured diffuser operation in the started mode.

The initial conditions used in the analysis were similar to the started diffuser initial conditions described in the Fortini results. Following the J index that defined the nozzle wall surface (J = 50), isentropic flow conditions were specified for the grid points lying on or below the J = 50 index. Points lying above the J = 50 index were given a low flow velocity so that static properties were equal to total properties.

The flow-field solution that was obtained for the Motor 1 configuration is shown in Fig. 42. The results are presented as Mach number contours and velocity vectors. The Motor 2 results, likewise shown as Mach number contours and velocity vectors, are shown in Fig. 43. Finally, the Motor 3 results are presented in Fig. 44. All three solutions shown were obtained with nominal levels of secondary flow entering the system.

The PARC2D program was used with the turbulence mixing modification described in Appendix A to quantify test cell pressure as a function of secondary flow. The results of the study are shown in Fig. 45. The calculated cell pressure predictions for all three motors at various levels of secondary flow are plotted. The secondary flow is expressed in terms of percent of the primary flow (which includes all of the rocket exhaust constituents). The differences between the data and the PARC2D predictions for both Motors 1 and 3 were less than 5 percent. Motor 2, however, missed the actual test data cell pressure by 50 percent. As stated earlier, the cell pressure value had an uncertainty of ± 10.4 percent, which could account for some of the error. Additional error sources, which were present during the test but could not be quantified (and were present for all three motors), included the uncertainty of the secondary flow rate and the effect of taking transient data and treating it as steady-state data. There was also some uncertainty concerning the nozzle geometry for Motor 2. For the secondary flow-rate uncertainty, the total amount of air leaking into the test cell is not well-defined, and was often based on values obtained from leakage checks that included large volumes of ducting in addition to the test cell. The concern about the transient data was that the transducers used in the measurement of cell pressure were not optimized for quick response. It is not known what lag was present in the system that would have resulted in a cell pressure measurement different from reality.

The trend in cell pressure, as predicted by the PARC2D program as secondary flow was varied, is presented in a qualitative fashion in Fig. 45. With no secondary flow, the cell volume is pumped to some minimum pressure by the mass entrainment of the rocket exhaust plume. The addition of a small amount of secondary flow, however, causes the cell pressure to rise considerably. The Motor 1 cell pressure jumped over 150 percent with less than 1 percent secondary flow. The same trend appeared to occur for Motor 3, where the addition of 5-percent secondary flow raised the calculated cell pressure approximately 600 percent. Based on the data, it was expected that Motor 2 would have a cell pressure increase of approximately 200 percent for the 3.5-percent secondary flow rate. The PARC2D program predicted only a 100-percent rise at the low secondary flow rate.

5.0 TWO-DIMENSIONAL CONVERGING/DIVERGING NOZZLE

5.1 MOTIVATION

The calibration of the PARC program for two-dimensional converging/diverging (2-D/C-D) nozzle flows is driven by both test articles and facility concerns. The use of 2-D/C-D nozzles on test articles has increased significantly in recent years. This increase has been caused by the advantages that 2-D/C-D nozzles provide over axisymmetrical nozzles, such as high nozzle performance without excessive aft-end drag and easier integration of the nozzle geometry into the airframe design. The capability of thrust vectoring has also been a big factor in the

use of 2-D/C-D nozzles. Within the ETF, 2-D/C-D nozzles are regularly used to provide free-jet flows for inlet/engine compatibility testing. Variable Mach number capability is considerably easier to design into a 2-D/C-D nozzle than in an axisymmetric nozzle.

5.2 TEST CASES

Two test cases are included to calibrate the PARC program performance for a test-article-type configuration and a facility free-jet-type nozzle. The first case used the data presented by Mason et al., in Ref. 28. The test case considered a Mach 1.35 2-D/C-D nozzle operating with a nozzle pressure ratio (nozzle flow total pressure divided by the ambient total pressure) of approximately 6. The calibration parameter was the wall static pressure along the nozzle length. Variations in the computational gridding and the importance of the viscous terms were investigated. Six cases were analyzed during the calibration effort using the 2-D version of the PARC program. The second calibration case compared PARC3D program calculations to test data obtained from Ref. 29 for a small supersonic free-jet nozzle. A test case with the nozzle operating at a nozzle exit velocity of Mach 2.59 was selected. The calculations were compared to test data for nozzle exit plane Mach number profiles, nozzle exit plane flow pitch angularity profiles, and boundary-layer displacement thickness at various locations around the nozzle exit plane.

The data uncertainty for the two test cases were not given in either reference. The method of acquiring the data was discussed, however, and indicated that the data sets were of good quality. The Ref. 28 report identified the data acquisition system as a magnetic tape system that recorded a series of data frames for each data point. The average of the frames was presented as the steady-state data. The Ref. 29 pressure data were acquired through a system similar to the setup used in Ref. 21 in that manometer boards were photographed for later analysis. A maximum uncertainty of approximately ± 0.05 psia was deduced for this type of setup in Section 3.2. Temperature measurements in the form of millivolts were recorded on a strip chart recorder, which also provided the ability for posttest analysis of the results.

5.3 RESULTS

2-D/C-D EXHAUST NOZZLE — The test configuration described in Ref. 28 is shown in Fig. 46. The configuration was identified as A1 in the reference. Multiple static pressure measurements were made at three vertical plane stations on both the top and bottom surfaces during the test. Because the PARC2D solution was 2-D, only the centerline data on the top plate was used for the calibration effort.

Two grids were used in the study. The first grid consisted of 10,431 grid points with 171 I indices and 61 J indices. Packing of the grid points off the nozzle wall was exponential

with the first grid point 0.001 in. away from the wall. Spacing in the I indices was exponentially centered around the nozzle throat, with a minimum spacing of 0.01 in. This grid was considered to be of high resolution. The second grid decreased the number of grid points to 10,126, with 166 I indices and 61 J indices. The spacing of the grid points off the nozzle wall was increased so that the first grid point from the wall was 0.005 in. away. There were also five fewer I indices in the diverging section of the nozzle.

Along the top wall, the boundary condition was specified as a no-slip, adiabatic surface. The flow into the nozzle was specified along the I = 1 index by specifying the flow total pressure and temperature. Outflow for subsonic points was controlled at the nozzle exit (the I index varied depending on the grid) by specifying the ambient static pressure and temperature. The bottom surface defined by the J = 1 index was treated as a slip surface. This provided the plane of symmetry about the nozzle vertical plane centerline.

The initial conditions specified on the computational domain, which were used to start the convergence process, were similar to those used previously. Isentropic flow conditions were assumed, with subsonic flow specified upstream of the nozzle throat and supersonic flow specified downstream. The boundary layer along the nozzle wall was defined by the $1/7^{th}$ power law as discussed in Ref. 16.

The calculated static-pressure-to-total-pressure ratio (P/P_t) along the nozzle wall using the 177-by-61 grid is compared to test data in Fig. 47. Upstream of the nozzle throat (at X/L = 0), the comparison between the PARC calculations and the test data was excellent. At the nozzle throat, however, the calculated level of P/P_t was approximately 8 percent lower than the test data. Downstream of the nozzle throat the calculations match the test data to within 3 percent.

The P/P_t comparisons were also performed for the 166-by-61 grid. This case was used to study the effects of reducing the axial grid resolution in the diverging section of the nozzle and the influence of the grid packing in the viscous boundary-layer region. As with Case 1, the values of P/P_t calculated by the PARC program upstream of the nozzle throat agreed with the test data. The reduction in the grid resolution downstream of the nozzle throat caused some change in the flow solution, with the maximum error increasing to approximately 8 percent.

The results of these two cases indicated that the PARC2D program can provide excellent results for 2-D/C-D nozzles. Care must be exercised, however, to ensure that an adequate number of grid points are provided. These results also demonstrate that 2-D flow calculations can be successfully used as long as the point of reference in the 3-D nozzle is close to the nozzle centerline. It should also be noted that the viscous effects in 2-D/C-D nozzles are

important. Solutions obtained for inviscid flows were not as accurate. Wall static pressure errors as large as 30 percent were obtained because of improper pressure peak locations.

SUPERSONIC FREE-JET NOZZLE — The data presented in Ref. 29 were obtained using a subscale free-jet nozzle with a nozzle exit area of 36 in.^{2} (6 in. on each side). The coordinates are for a nozzle exit Mach number of 2.59. The basic free-jet installation is shown in Fig. 48. The flexible nozzle wall coordinates, obtained from unpublished sources, are given in Table 3. The 3-D version of the PARC program was used. As previously stated, the basic flow structure in the nozzle is 2-D. This particular effort, however, was initiated to study certain 3-D flow characteristics such as the boundary-layer displacement thickness around the nozzle exit plane. Only a quarter section of the nozzle was modeled. The grid was constructed of 836,500 points divided between 239 I indices, 70 J indices, and 50 K indices. The grid spacing off both the nozzle flex and flat walls was 0.0005 in. in the nozzle throat region. At the nozzle exit, the packing was increased to 0.001 in. to account for the thicker boundary layer.

The nozzle wall surfaces were treated as no-slip and adiabatic. The centerline surfaces were treated as slip walls since it was assumed that the nozzle flow had two planes of symmetry. The inflow boundary condition was formulated by specifying the proper total pressure and temperature on the I = 1 surface. The entering mass was assumed to flow normal to the I = 1 surface. The outflow boundary condition was defined on the I = 239 surface by specifying the proper static pressure and temperature for subsonic points so that the nozzle was operating at the design pressure ratio for a nozzle exit Mach number of 2.59.

The initial conditions applied to the computational domain were defined assuming 1-D, isentropic flow. The boundary-layer profile was defined using the $1/7^{th}$ power law as described in Ref. 16.

Calculated flow-field Mach number contours are shown in Fig. 49. Both the axial centerline plane and the nozzle exit plane are presented. In the axial centerline plot, the vertical axis has been scaled by a factor of two for clarity. The nozzle exit plane plot shows several 3-D flow effects such as the constant boundary-layer thickness on the flexible wall and the variable boundary-layer thickness on the flat wall. The corner region also shows 3-D flow effects.

The results of the PARC3D calculations are compared to test data in Fig. 50. The flow field at the nozzle exit plane is presented in terms of Mach number contours. The experimental data are shown over the entire nozzle exit plane, and the PARC3D data are limited to a one-quarter section. The Mach number level is off slightly between the two plots (2.58 for the test data, 2.52 for the PARC3D solution). No attempt was made to correct the PARC3D solution to the test data. Since the calibration data were Mach number uniformity, absolute

Mach number level was not of primary interest. The inviscid core flow Mach number uniformity across the exit plane was equal to 0.01 for both the experimental data and the PARC3D calculations.

The calculated nozzle exit plane flow angularity is compared to test data in Fig. 51. The flow angularity is defined in the vertical plane only (alpha). As with the Mach number uniformity comparison, the test data were presented across the entire nozzle exit plane, whereas the PARC3D calculations were limited to one-quarter section of the exit plane. The flow angularity of the test data varied from -1.0 to 0.4 deg. The PARC3D results, however, varied from 0. to 0.8 deg. Although the magnitude was unknown, it was felt that numerical truncation errors played a significant part in the differences.

The calculated nozzle exit plane boundary-layer displacement thickness (δ^*) is compared to test data in Fig. 52. The test data δ^* is given at Mach numbers of 2.0 and 2.95. There were no data presented for the Mach 2.59 case. The calculated δ^* is shown on the plot as squares for selected locations around the nozzle perimeter. In all cases the PARC3D predictions were within 10 percent of the test data based on an interpolation of the two Mach number cases. The largest deviation occurred in the nozzle corner region where the Mach number contour plots (shown in Figs. 49 and 50) indicated a localized, complex, high-gradient corner flow region.

The final comparison of the PARC3D calculations to test data for the 2-D/C-D nozzle is shown in Fig. 53. Boundary-layer profiles at the nozzle exit centerline of the flexible wall are plotted. The comparisons between test data and the calculated profile showed that the PARC3D profile was considerably more linear than the test profiles. The PARC3D prediction of the boundary-layer thickness was approximately 30 percent lower than the test data. The poor performance of the PARC3D program in predicting boundary-layer profiles was attributed to the algebraic turbulence model that has been optimized for wake-type flows such as discussed in Section 3.

6.0 REARWARD-FACING STEP

6.1 MOTIVATION

The selection of a rearward-facing step (or backstep) as a calibration test case was based on its flow analogy to nozzle exhaust/diffuser configurations. The rearward-facing step provided a fundamental test case to evaluate PARC program predictions of regions of separating and reattaching flow. Common occurrences of rearward-facing steps in the ETF include regions downstream of the diffuser where the facility ducting increases diameter in a step fashion. Typical nozzle/diffuser geometries also can be represented as a rearward-facing step.

6.2 TEST CASES

The test cases considered in this study were selected to expand the work reported in Ref. 1 for subsonic flow over a rearward-facing step to include supersonic flow as presented in Ref. 30. Three test cases were selected with inlet flow Mach numbers of 2.5, 3.5, and 5.0. The calibration parameters selected for the study were the wall static pressures downstream of the step and the locations of the reattachment compression shock.

The measurement uncertainties reported in Ref. 30 were given as ± 1.0 percent for the pitot pressure transducers. The location of the reattachment shock was determined from shadowgraphs reproduced in Ref. 30. The measurement uncertainty of the shock location obtained from the shadowgraphs was not reported.

6.3 RESULTS

The geometry of the test hardware along with a generic description of the flow field that would be present is shown in Fig. 54. The rearward-facing step height was 0.443 in. for all three cases. It was assumed in the calibration effort that the rearward-facing step hardware was sufficiently wide to neglect end effects. Given this assumption, the 2-D version of the PARC program was used in the study.

The grid used in the study consisted of 24,321 points divided between 201 I indices and 121 J indices. The packing of the grid points off the wall surface upstream of the rearward-facing step (defined by the J = 60 index) was exponential with the initial grid point being 0.001 in. off the wall. The spacing off the wall downstream of the rearward-facing step was identical. The I indices were packed into the rearward-facing step (defined by the I = 60 index) so that distance from the first I index in either direction to the rearward-facing step index was 0.001 in.

The boundary conditions applied on the computational domain are shown in Fig. 55. The surface downstream of the rearward-facing step was treated as no-slip and adiabatic. The top surface of the grid (the J = 121 index) was defined as a slip surface. The vertical surface of the rearward-facing step was treated as a slip surface since the flow across the surface was low-speed and the resolution of the boundary layer was not critical to the calibration effort. The surface upstream of the rearward-facing step was also defined as a slip surface. The inflow boundary was specified by fixing the proper flow conditions for the given Mach number case and holding them constant during the iteration process. The outflow boundary was generated by specifying the proper static pressure and temperature in the subsonic region for the particular case. The initial conditions used in the analysis specified the free-stream conditions over the entire computational domain.

Case 1 — The flow field that was developed for the Mach 2.5 case is shown as Mach number contours in Fig. 56. The computed wall static pressures on the surface downstream of the rearward-facing step are compared to test data in Fig. 57. The values of pressure and distance were nondimensionalized by the flow total pressure and total plate length, respectively. The PARC program overpredicted the pressure in the region of separation by approximately 30 percent. The reattachment point was too close to the rearward-facing step based on the data. The pressure downstream of the reattachment point effectively matched the test data with minimal error. These results were consistent with the results obtained in Ref. 1 and with other separated flow studies, and were attributed to the use of the zeroth-order turbulence model.

Case 2 — The flow field that was developed for the Mach 3.5 case is shown as Mach number contours in Fig. 58. The computed wall static pressures on the surface downstream of the rearward-facing step are compared to test data in Fig. 59. The PARC program calculations underestimated the separated flow region just downstream of the rearward-facing step by approximately 5 percent. In the region of flow reattachment, the PARC calculations reattached to the wall prematurely causing the pressure data to include errors as large as 100 percent. Once the flow reattached to the wall, however, the PARC calculations and the test data agree to within less than 1 percent, which is within the uncertainty of the measurements.

Case 3 — The flow field that was developed for the Mach 5.0 case is shown as Mach number contours in Fig. 60. The computed wall static pressures on the surface downstream of the rearward-facing step are compared to test data in Fig. 61. The value of the static-to-total-pressure ratio in the separated flow region was underpredicted by the PARC program by nearly 50 percent. The PARC program also missed the location of flow reattachment by initiating the pressure rise to near the rearward-facing step. The pressure comparison downstream of the reattachment point compares favorably, with a maximum error between the PARC program calculations and the test data of 5 percent.

The comparison of the location of the reattachment compression shock downstream of the rearward-facing step is shown in Fig. 62. The test data were obtained by measuring the shock location off the shadowgraphs presented in Ref. 30. The PARC program predictions were obtained from the Mach number contour plots as shown in Figs. 56, 58, and 60. The PARC program was able to predict the shock location to within 20 percent for all cases. Case 1, operating at Mach 2.5, provided the least maximum error of only 10 percent.

7.0 SUMMARY AND CONCLUSIONS

The primary objective of this research effort was the calibration of the PARC program for various fundamental flow problems commonly found in the testing of turbine engines

and rocket motors in the ETF. The results of the present calibration efforts are summarized in Table 4. Four types of flow problems have been addressed. The first calibration effort addressed free-jet-type flow fields. A modification to the algebraic turbulence model was demonstrated to provide significantly better results than the previous version for predicting the far-field flow characteristics of a Mach 2.22 jet exhausting into quiescent air. Both the location of where the flow velocity was equal to one-half the centerline velocity and the velocity profiles were predicted to within 10 percent of the test data. A subsonic free jet (Mach 0.2) was also modeled. Results were compared to empirical theory. As with the Mach 2.22 free jet, the results for both the location where the local velocity was equal to one-half the centerline velocity and the velocity profiles were within 10 percent of the data. The final free-jet comparison calibrated the PARC program for predicting the spread rate of supersonic free jets. Cases operating with nozzle exit Mach numbers of 1.0, 1.6, 3.0, and 4.0 were modeled, and the results were shown to be within 5 percent of the test data.

The second type of flow problem addressed in the calibration effort was diffuser flow. The study addressed a small-scale air ejector/diffuser system and three different rocket motor/diffuser configurations. The air ejector/diffuser study considered the system operating in three modes: (1) the diffuser unstarted and the flow separated in the nozzle, (2) the diffuser unstarted and the nozzle flowing full, and (3) the diffuser started and the nozzle flowing full. Two diffuser sizes were considered with diffuser-to-nozzle-throat-area ratios of 36 and 16 with the diffuser length-to-diameter ratio of 4 and 12, respectively. The results from the case operating with the diffuser unstarted and the flow in the nozzle separated were poor, with the test cell pressure predicted to be 30 percent higher than that of the test data. The differences were attributed to the zeroth-order turbulence model used by the PARC2D program. The results from the case operating with the nozzle flowing full and with the diffuser unstarted were inconclusive. The test cell pressure calculation was unsteady and cyclic in nature. The calculation did appear to be varying about the test data value. The diffuser pressure rise ratio was successfully predicted for cases operating with the nozzle flowing full and the diffuser started. The wall static pressure predictions with the diffuser operating started were qualitatively correct, with the exact location of pressure peaks and valleys being slightly incorrect. The rocket motor/diffuser configurations considered installations having diffuser to nozzle throat area ratios varying from 500 to 600. Two cases used a second throat diffuser, and the other used a cylindrical diffuser. The results were inconclusive. Two of the cases matched the cell pressure data to within 5 percent, whereas one case underpredicted the test data by approximately 50 percent. The reason for the differences was not known but could be the result of improper nozzle geometry.

The third calibration study addressed 2-D/C-D nozzles. Two cases were considered. The first case modeled a 2-D/C-D nozzle typical of the type used on turbine engines. The PARC program was able to match the wall static pressure data along the nozzle top wall centerline

to within 8 percent for a high-resolution grid. The second case considered a 2-D/C-D nozzle similar to the nozzles used for free-jet testing. The solution used the 3-D version of the PARC program. Mach number deviations and flow angularity were compared at the nozzle exit. The PARC program matched the test data for Mach number deviation, and predicted a flow angularity approximately 0.5 deg higher than the test data. The boundary-layer displacement thickness around the nozzle exit was also assessed, with the PARC program matching the test data to within 10 percent. The shape of the boundary-layer profile predicted by the PARC3D program at the nozzle exit, however, did not agree with the test data. The predicted boundary-layer edge was approximately 30 percent lower than indicated by the test data. The profile was also considerably more linear than the measured profile.

The fourth and final calibration study addressed supersonic flow over a rearward-facing step. Wall static pressures and reattachment compression shock locations were compared for three Mach numbers, 2.5, 3.5, and 5.0. The PARC program provided excellent results downstream of the flow reattachment point, with the PARC calculations missing the test data by a maximum of 5 percent. The PARC program consistently underpredicted the length of the separated zone. These separation length trends are consistent with results from other calibration efforts where an algebraic turbulence model was used. For the Mach 2.5 case, the wall static pressures in the separated region were overpredicted by 30 percent. The pressures for the Mach 3.5 case were underpredicted by 5 percent, and the pressures for the Mach 5.0 case were underpredicted by 50 percent. The location of the reattachment compression shock was predicted to within 20 percent for all three cases.

The calibration results summarized above have demonstrated that the PARC program is a highly versatile tool and can provide calculated results with acceptable levels of error for many different types of flow problems. In many instances where the calculated parameter level may be incorrect, the PARC program can provide important trend information that can not be obtained from any other source. As with any numerical tool, however, there are certain areas where additional improvements are needed. The most obvious improvement would be in the area of turbulence modeling. As stated earlier, the PARC program was developed and optimized for free-shear-layer-type flows. It has been shown that the algebraic turbulence model can handle this type of flow field, but problems involving wall-bounded flows were not acceptably handled. A development effort is currently underway to include a $k - \epsilon$ turbulence model in the PARC program, which should provided better results for wall-bounded flow problems. The $k - \epsilon$ turbulence model will be included in the next release of the PARC program.

REFERENCES

1. Cooper, G. K., Garrard, G. D., and Phares, W. J. "PARC Code Validation for Propulsion Flows." AEDC-TR-88-32 (AD-A204293), January 1989.

2. Huddleston, D. H., Cooper, G. K., and Phares, W. J. "A Computational Fluid Dynamics Evaluation of Test Cell Recirculation Effects on High-Bypass Turbofan Engine Surface Pressure Distributions." AIAA-86-1384,AIAA/ASME/SAE/ASEE 22nd Propulsion Conference, Huntsville, Alabama, June 16-18, 1986.

3 Phares, W. J., Cooper, G. K., Swafford, T. W., and Jones, R. R. "Application of Computational Fluid Dynamics to Test Facility and Experiment Design." AIAA-86-1733, June 1986.

4. Peters, C. E. and Phares, W. J. "Integral Analysis of Ducted Two-Stream Mixing with Recirculation." AEDC-TR-77-115 (AD-A053053), March 1978.

5. Hunter, L. G. and Kent, T. J. "Inlet Analysis Using Computational Fluid Dynamics." AIAA-86-2611, AIAA/AHS/ASEE Aircraft Systems, Design and Technology Meeting, Dayton, Ohio, October 20-22, 1986.

6. Semmes, R. G., Arbiter, D. G., and Dyer, R. D. "Efforts Toward the Validation of a Computational Fluid Dynamics Code for Analysis of Internal Aerodynamics." AGARD N89-18643, December 1988.

7. Bradley, R. G. "CFD Validation Philosophy." Paper No. 1., AGARD Symposium on Validation of Computational Fluid Dynamics, May 1988, Lisbon, Portugal.

8. Marvin, J. G. "Accuracy Requirements and Benchmark Experiments for CFD Validation." NASA TM 100087, May, 1988.

9. Povinelli, L. A. "CFD Validation Experiments for Internal Flows." NASA TM 100797, May 1988.

10. Bobbitt, P. J. "The Pros and Cons of Code Validation." NASA TM 100657, July 1988.

11. Kutler, P. "A Perspective of Computational Fluid Dynamics." NASA TM 88246, May, 1986.

12. Eggers, James M. "Velocity Profiles and Eddy Viscosity Distributions Downstream of a Mach 2.22 Nozzle Exhausting to Quiescent Air." NASA TND-3601, September 1966.

13. Schlichting, Herman. *Boundary-Layer Theory*. McGraw-Hill Book Company, New York, NY, 1968, pp. 699-702.

14. Rudy, D. H. and Bushnell, D. M. "A Rational Approach to the Use of Prantdtl's Mixing Length Model in Free Turbulent Shear Flow Calculations." NASA SP-321, Free Turbulent Shear Flows, Volume 1—Conference Proceedings, Langley Research Center, July 20-21, 1972.

15. Soni, B. K. "Two- and Three-Dimensional Grid Generation for Internal Flow Applications of Computational Fluid Dynamics." AIAA Paper 85-1526, AIAA 7th Computational Fluid Dynamics Conference, Cincinnati, Ohio, 1985.

16. Schlichting, Herman *Boundary-Layer Theory.* McGraw-Hill Book Company, New York, NY, 1968, pp. 565.

17. Thomas, P. D. "Numerical Method for Predicting Flow Characteristics and Performance on Nonaxisymmetric Nozzles—Theory." Langley Research Center, NASA CR 3147, September 1979.

18. Baldwin, B. S. and Lomax, H. "Thin Layer Approximation and Algebraic Model for Separated Turbulent Flows." AIAA Paper No. 78-257, AIAA 16th Aerospace Sciences Meeting, Huntsville, Alabama, January 1978.

19. Taylor, D. and Toline, F. R. "Summary of Exhaust Gas Ejector-Diffuser Research." AEDC-TR-68-84 (AD-842812), October 1968.

20. FlÜgel, G. "The Design of Jet Pumps." NACA TM 982 (Berechnung von Strahlapparaten) VDI-Forschungsheft 395, March—April 1939, pp. 1-21.

21. Fortini, A. "Performance Investigation of a Nonpumping Rocket-Ejector System for Altitude Simulation." NASA TN D-257, October 1959.

22. Hill, J. A. F. et al. "Mach Number Measurements in High Speed Wind Tunnels." AGARDOGRAPH 22, October 1952.

23. Dean, Robert C., Jr. *Aerodynamic Measurements.* Gas Turbine Laboratory, Massachusetts Institute of Technology, 1953.

24. Moore, J. A. "Investigation of the Effect of Short Fixed Diffusers on Starting Blowdown Jets in the Mach Number Range from 2.7 to 4.5." NACA TN 3545, January 1956.

25. Neely, James and Matz, R. J. "Aerodynamic Test of the 1/8-Scale J-2 Nozzle Model." AEDC-TR-57-12, October 1957.

26. Shapiro, A. H. *The Dynamics and Thermodynamics of Compressible Fluid Flow.* The Ronald Press Company, New York, New York, 1953, pp. 135.

27. George, D. "Recent Advances in Solid Rocket Motor Performance Prediction Capability." AIAA-81-0033, AIAA 19th Aerospace Sciences Meeting, Los Angeles, California, January 1981.

28. Mason, M. L., Lawrence, E. P., and Re, R. J. "The Effect of Throat Contouring on Two-Dimensional Converging-Diverging Nozzles at Static Conditions." NASA Technical Paper 1704, August 1980.

29. Goldbaum, G. C. "Research Study for Testing of Variable Mach Number Nozzles Aerodynamic Phase—Part II." AEDC-TR-56-10 (AD-98973), October 1956.

30. Smith, H. E. "The Flow Field and Heat Transfer Downstream of a Rearward Facing Step in Supersonic Flow." ARL 67-0056, March 1967.

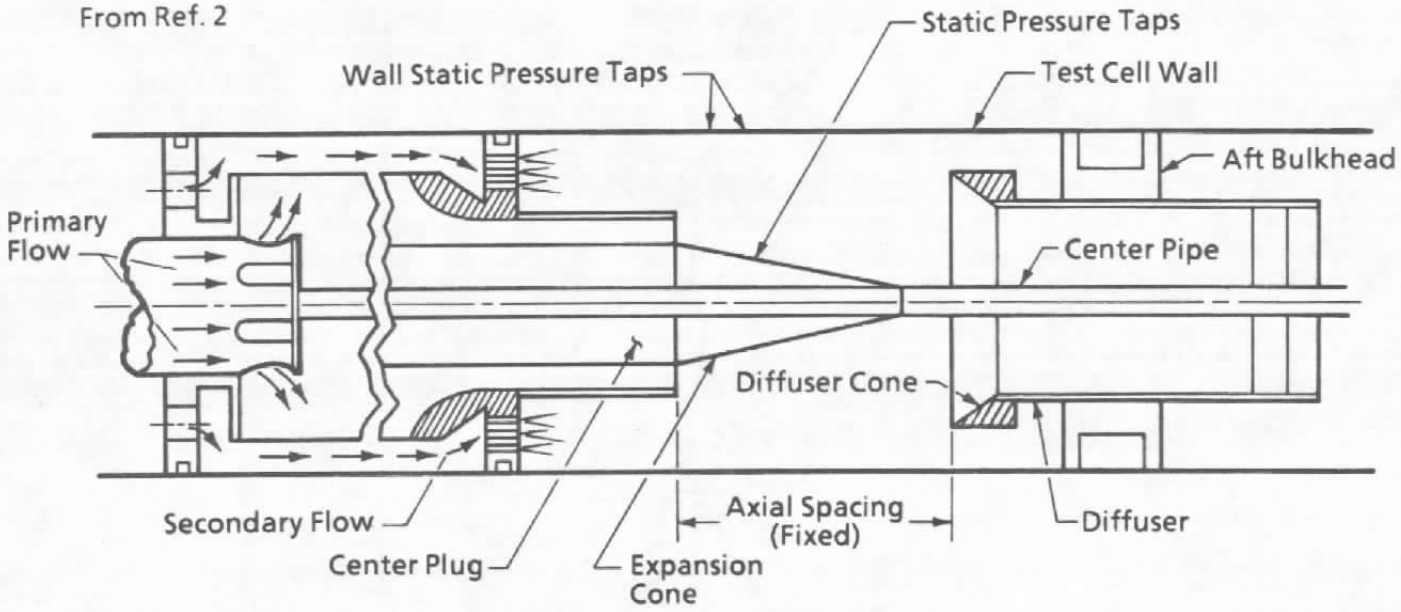

Figure 1. Subscale experimental configuration.

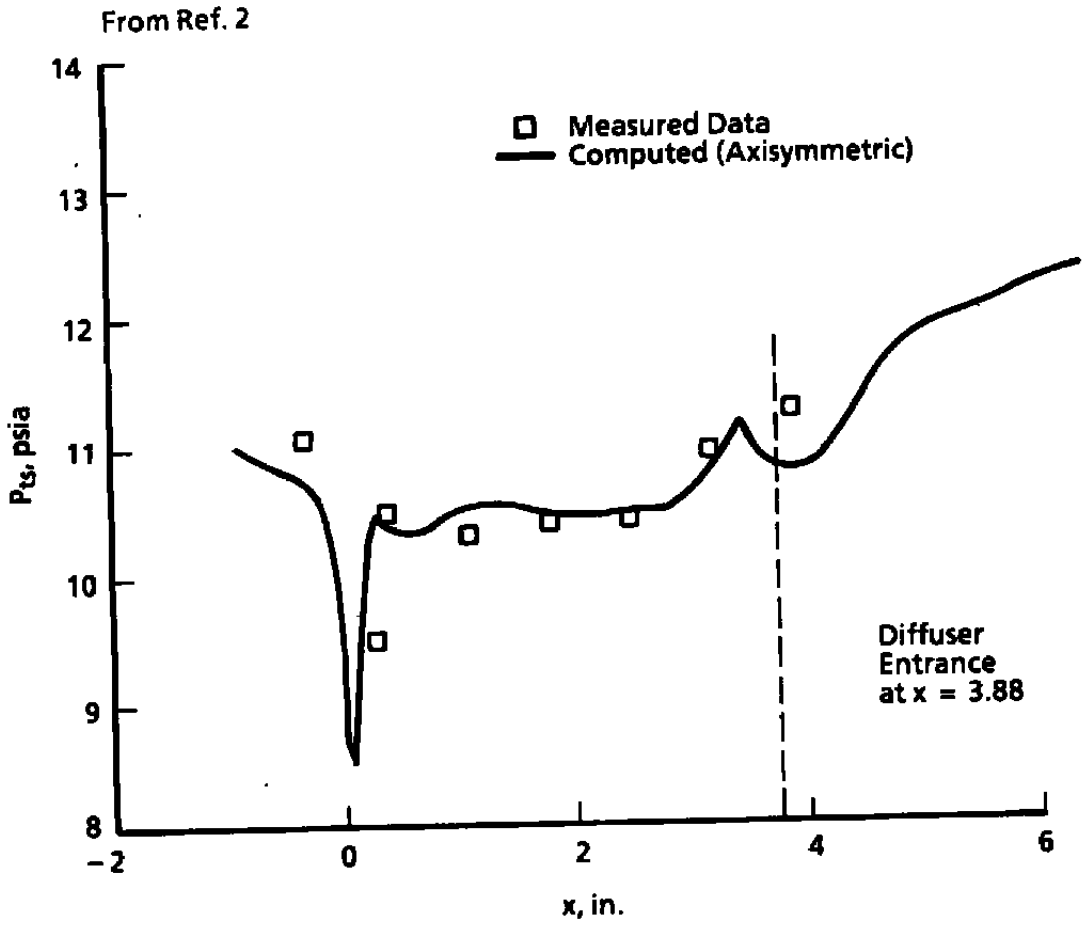

Figure 2. Tube surface static pressure (P_{ts}) versus distance from nozzle exit plane (x) for subscale test.

From Ref. 2

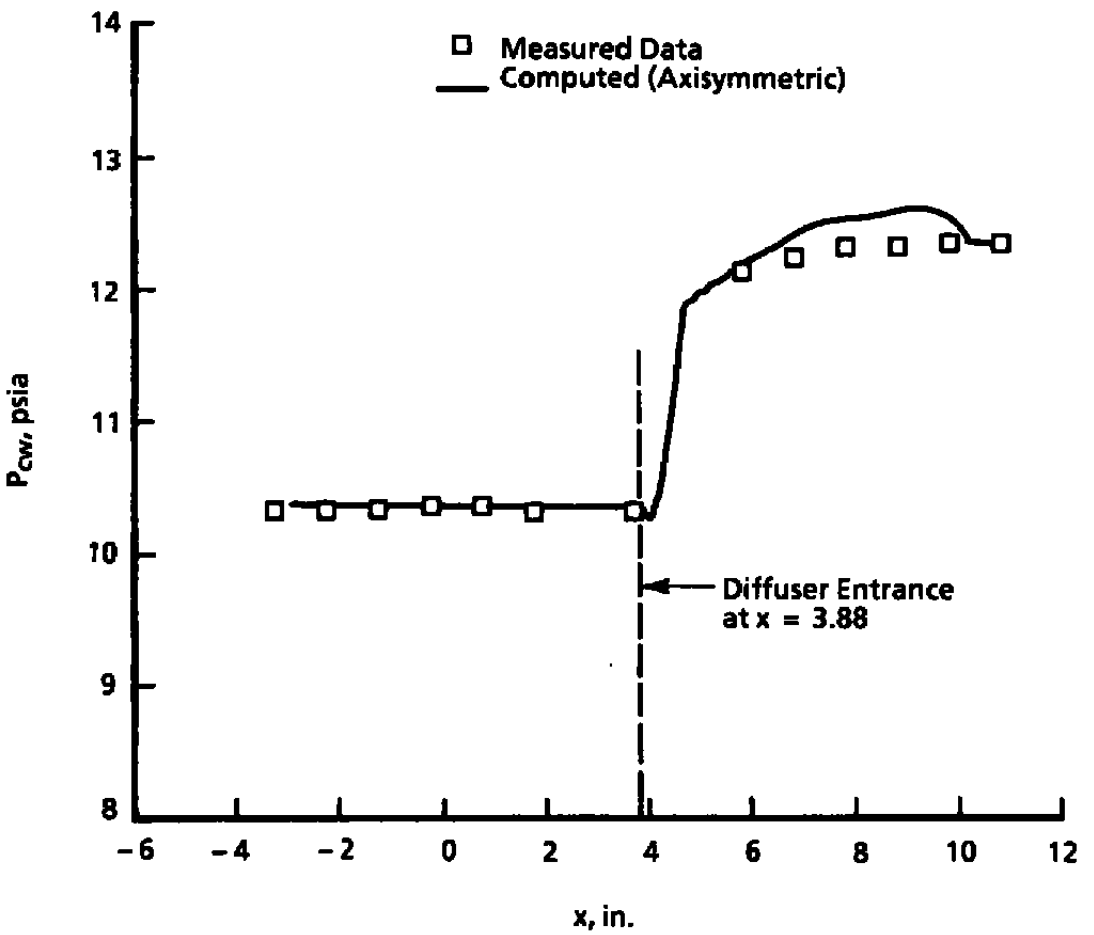

Figure 3. Cell wall static pressure (P_{cw}) versus distance from nozzle exit plane (x) for subscale test.

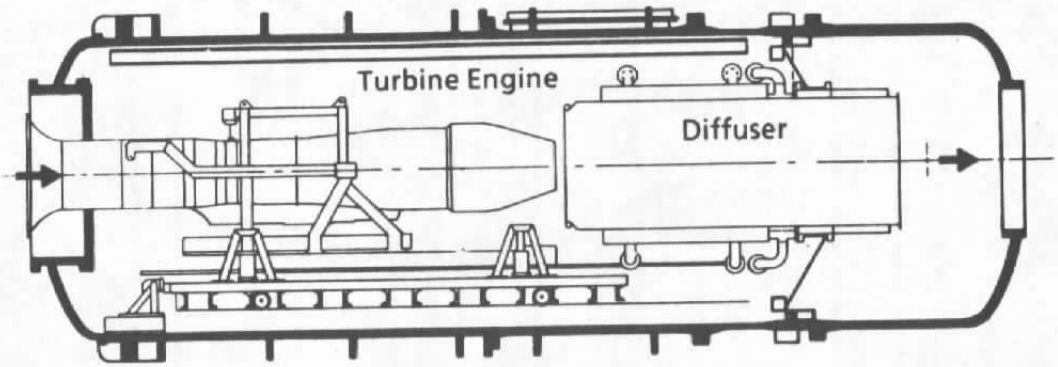

Figure 4. Typical turbine engine test installation.

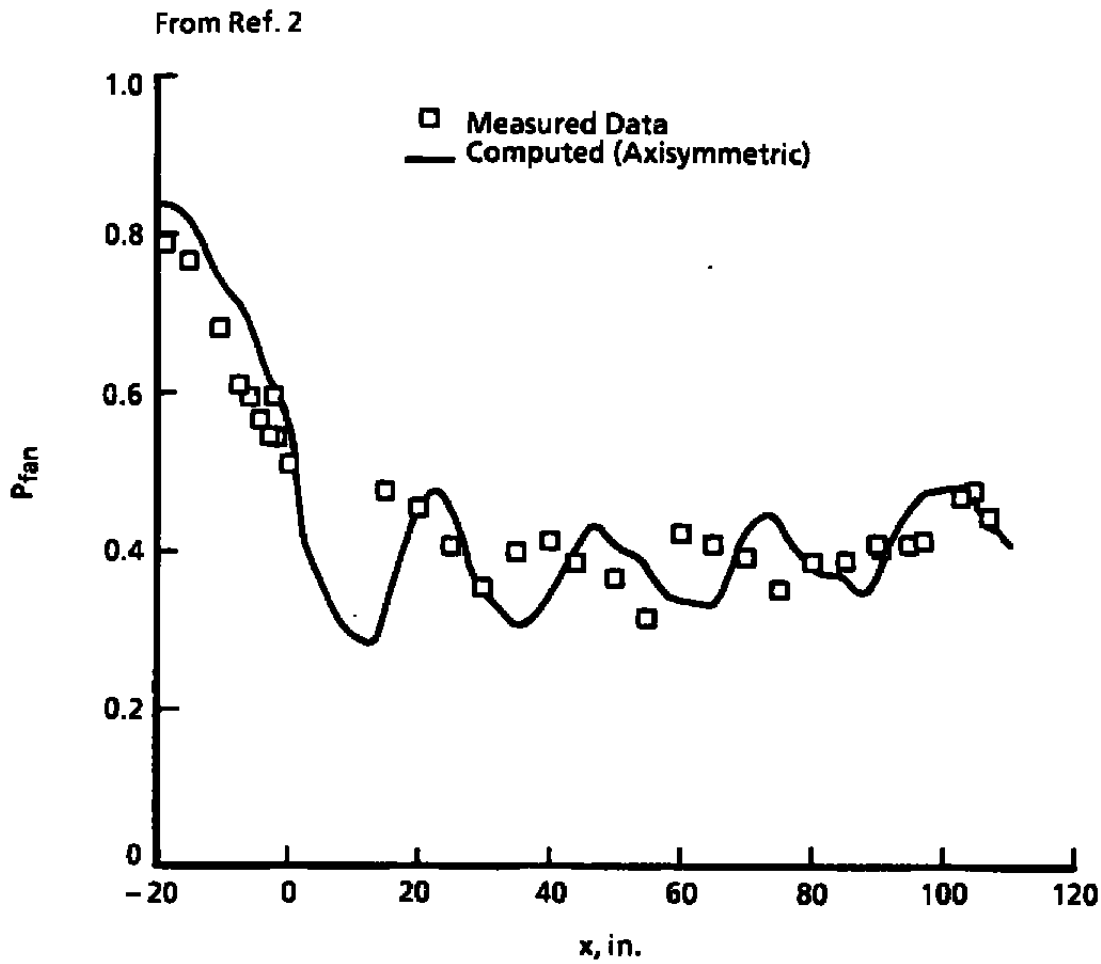

Figure 5. Fan cowl surface pressure (P_{fan}) versus distance from fan stream exit plane (x) for engine/test cell.

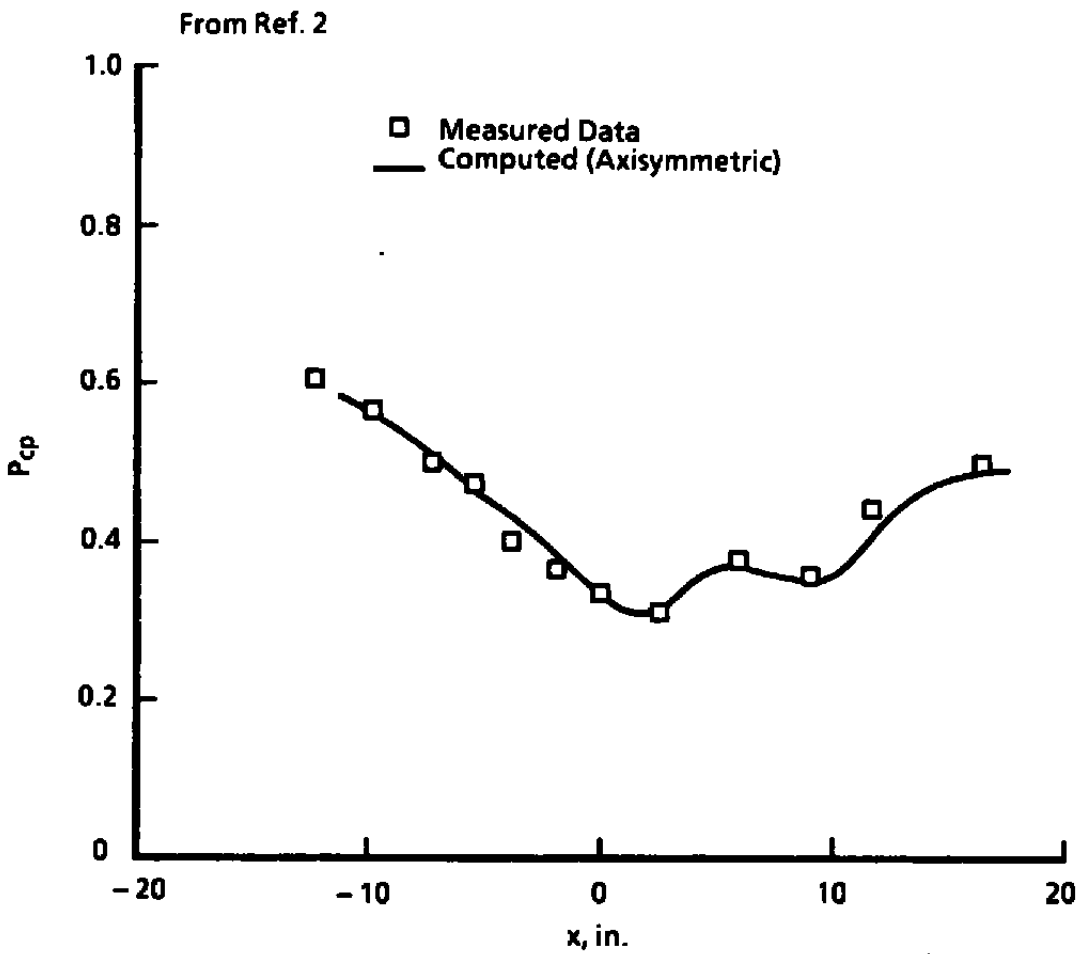

Figure 6. Core plug surface pressure (P_{cp}) versus distance from primary jet exit plane (x) for engine/test cell.

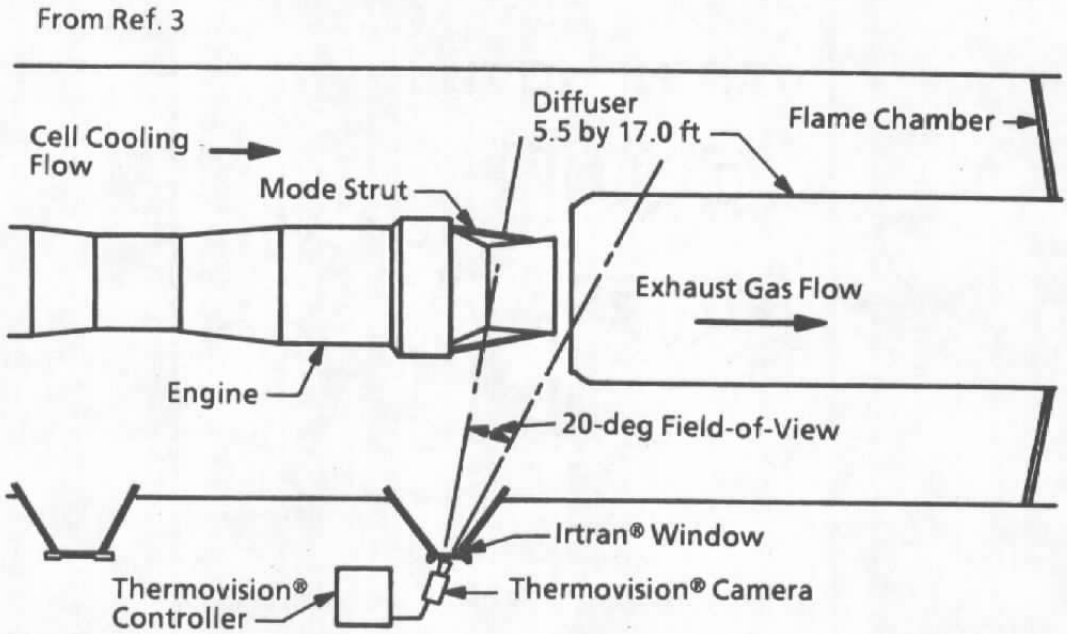

Figure 7. Test configuration for the study of cell heating.

From Ref. 3

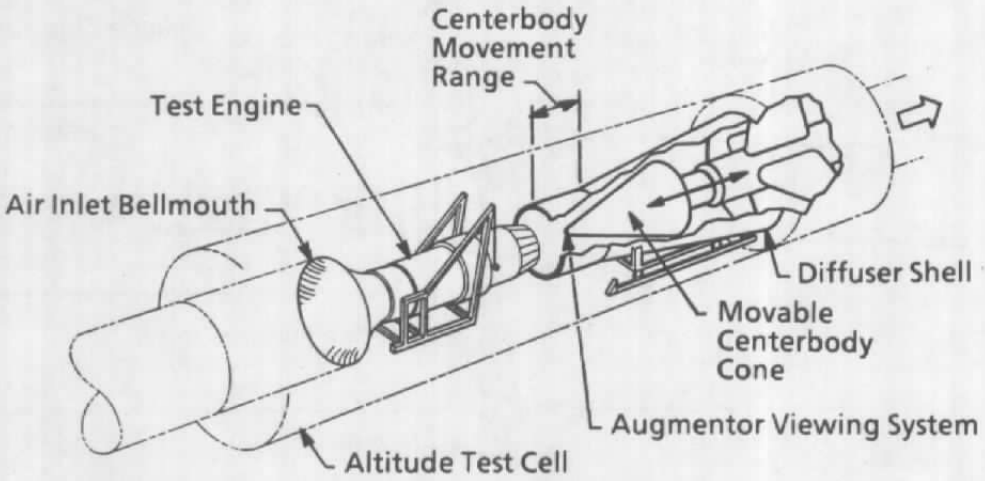

Figure 8. Variable area ejector test configuration.

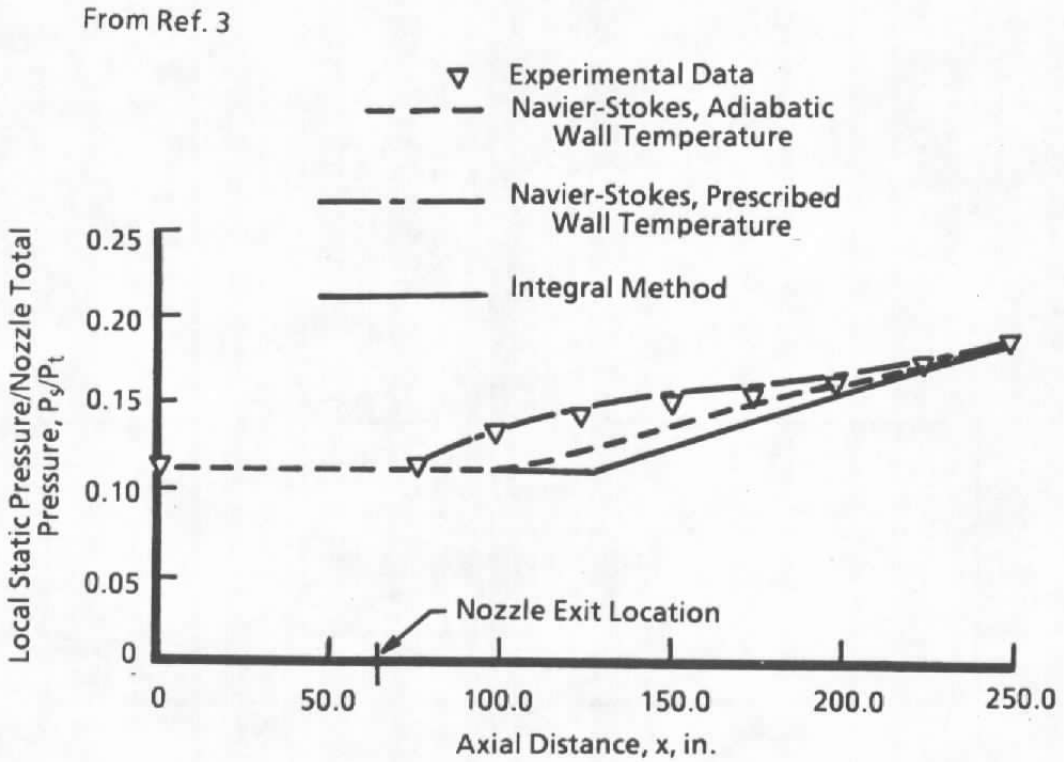

Figure 9. Cell and wall pressures compared to experimental data and integral method results.

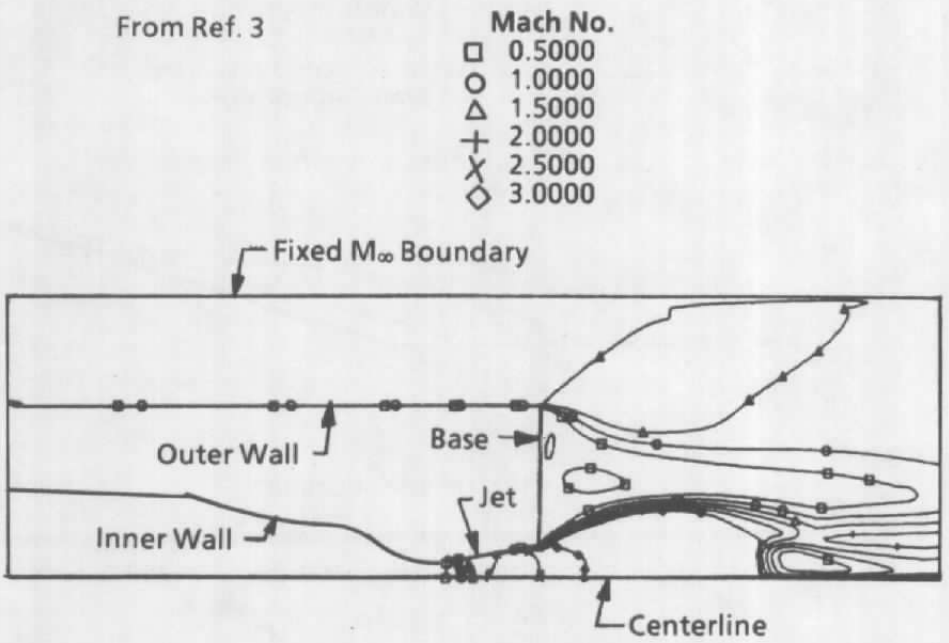

Figure 10. Base flow test case geometry and computed Mach number contours.

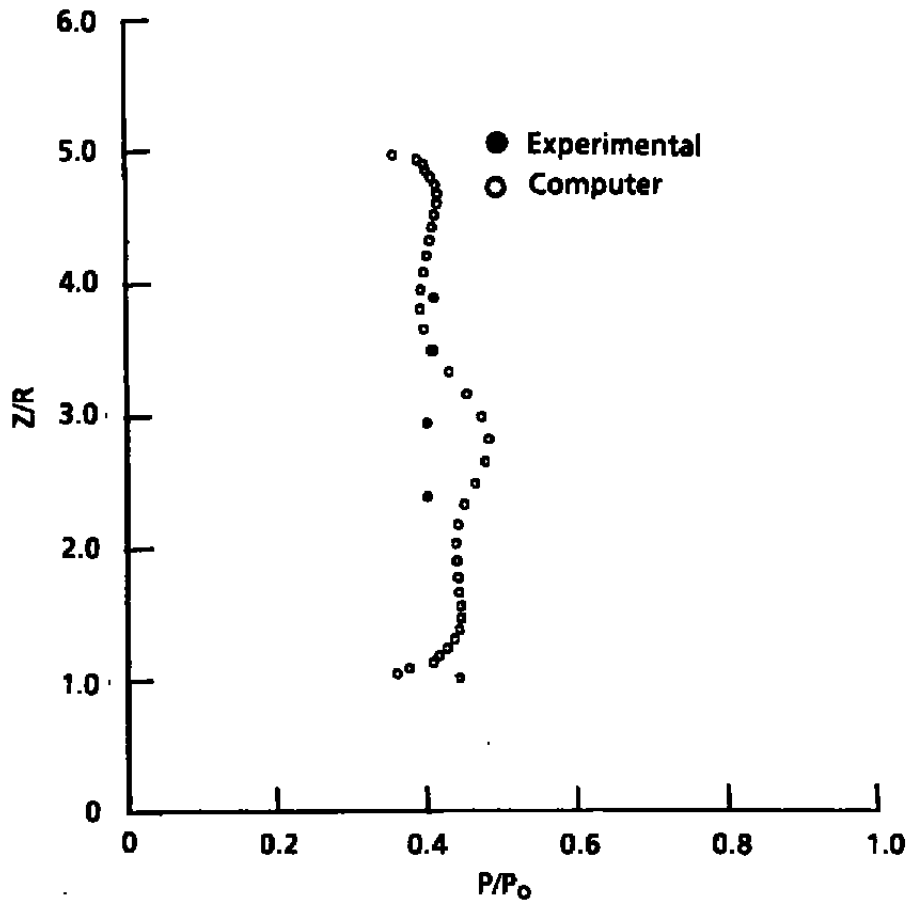

Figure 11. Base flow test case computed versus experimental base-static-to-total-pressure ratio (P/P_o).

From Ref. 5

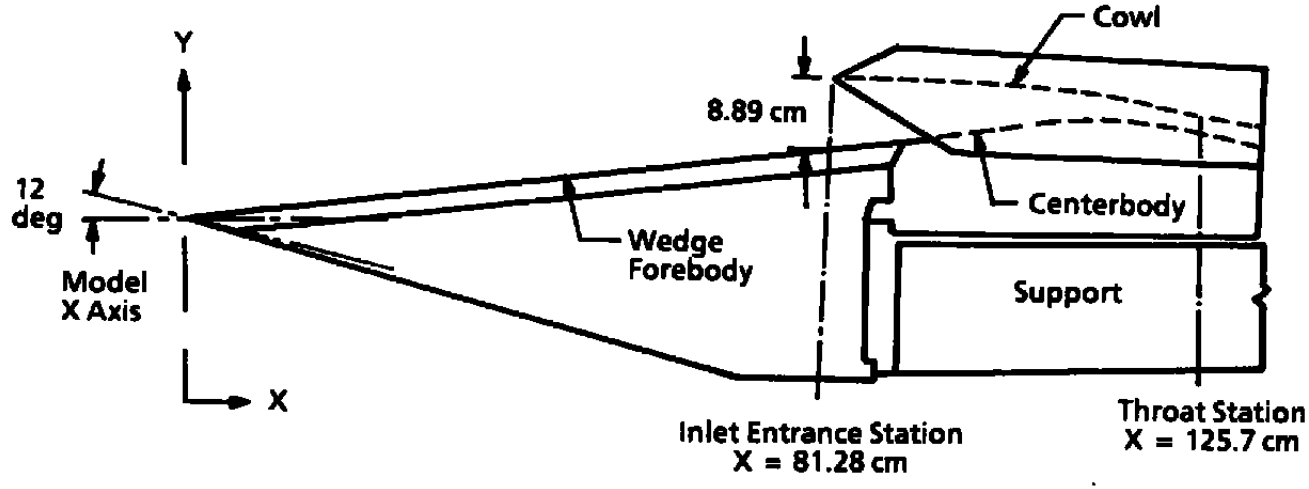

Figure 12. Hypersonic inlet test hardware. (P-2 inlet is shown; P-12 is slightly different.)

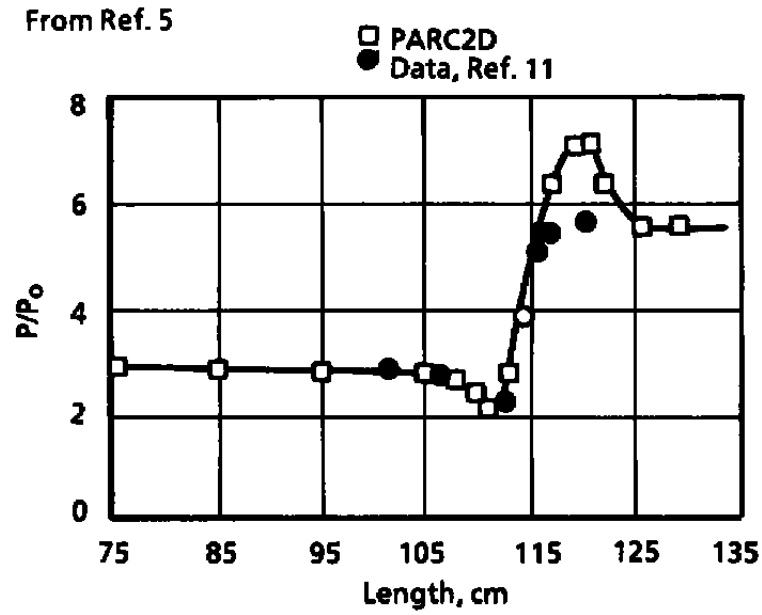

a. Centerbody static pressure for P-2 inlet

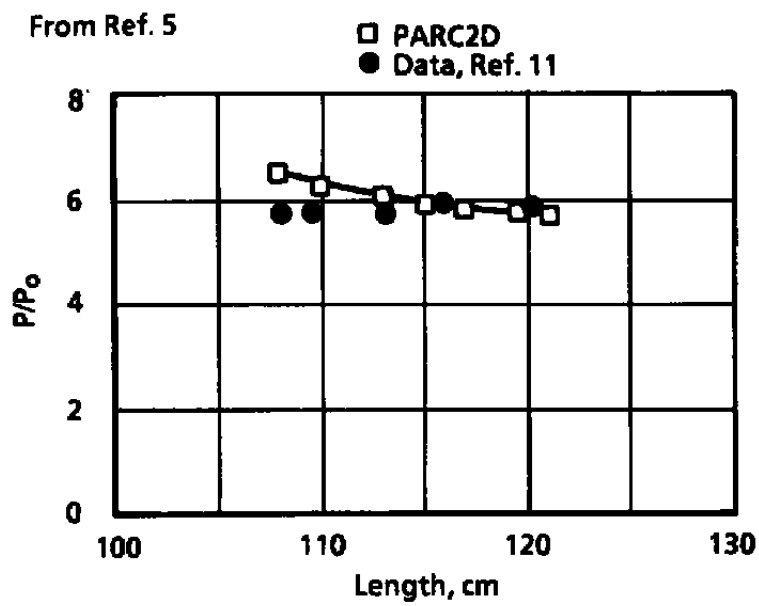

b. Cowl static pressure for P-2 inlet

Figure 13. Comparison of PARC2D results to data at Mach 7.4.

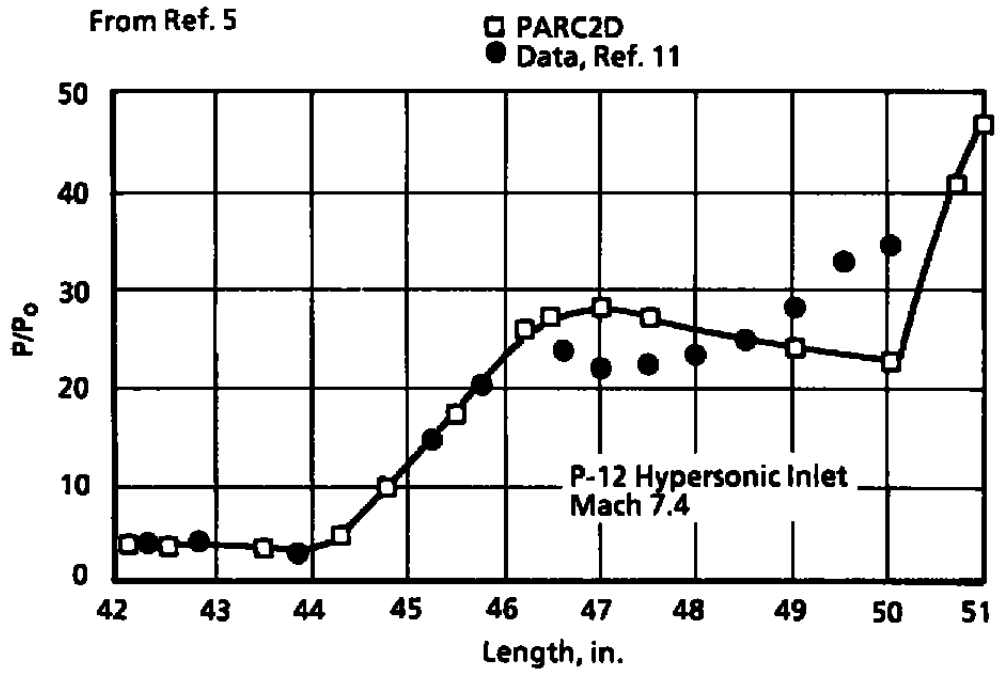

c. Centerbody static pressure for P-12 inlet

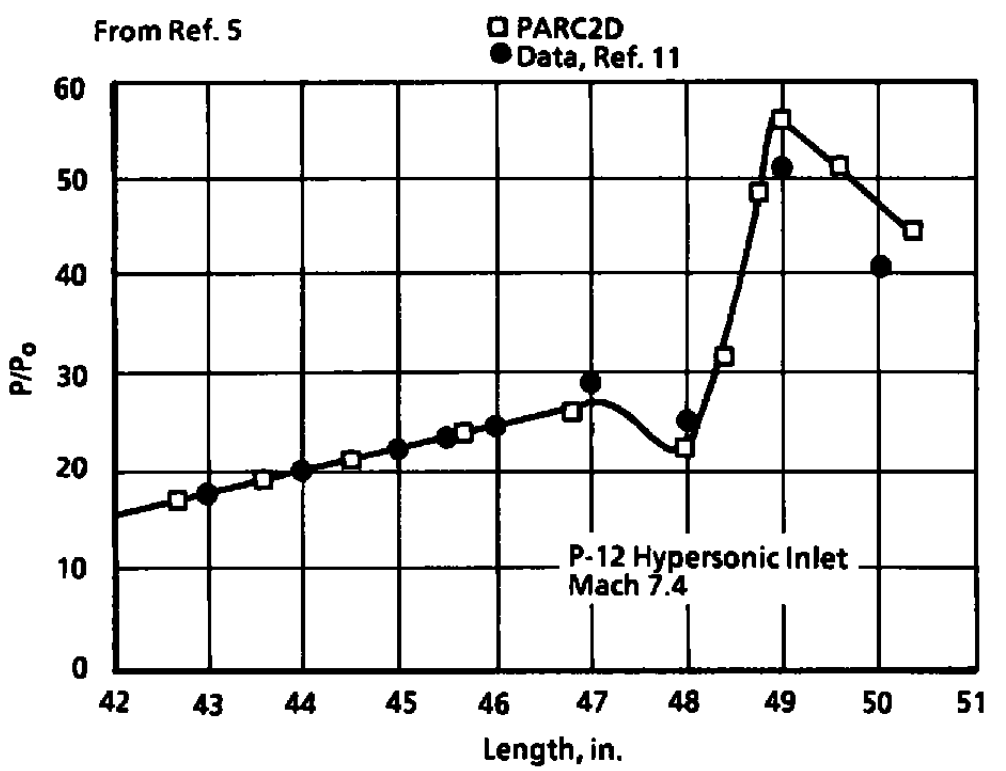

d. Cowl static pressure for P-12 inlet

Figure 13. Concluded.

From Ref. 6

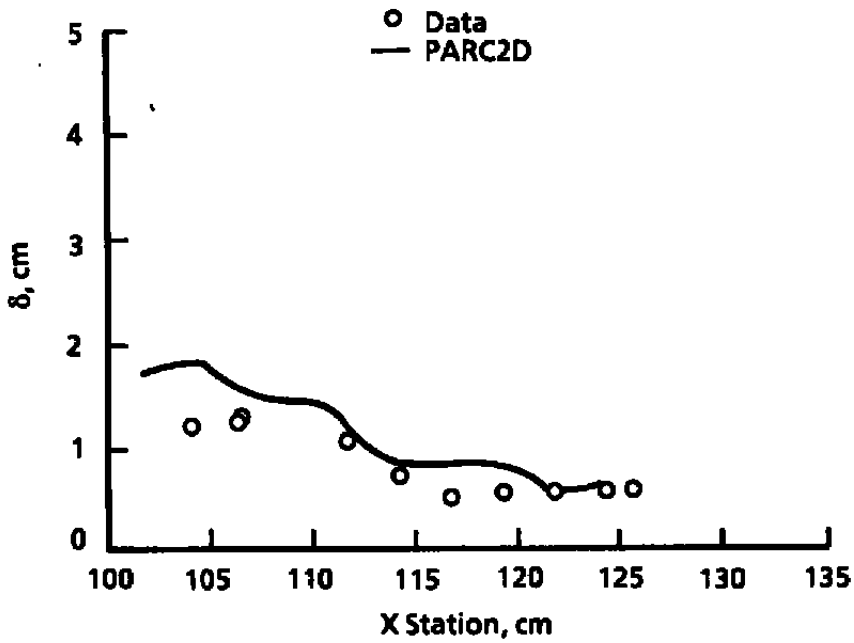

a. Centerbody boundary-layer thickness

From Ref. 6

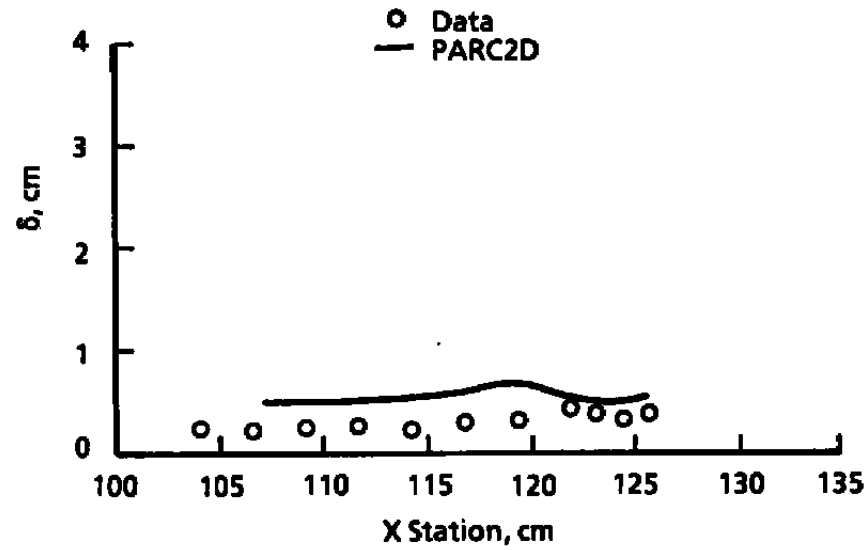

b. Cowl boundary-layer thickness

Figure 14. Boundary-layer growth in a hypersonic inlet.

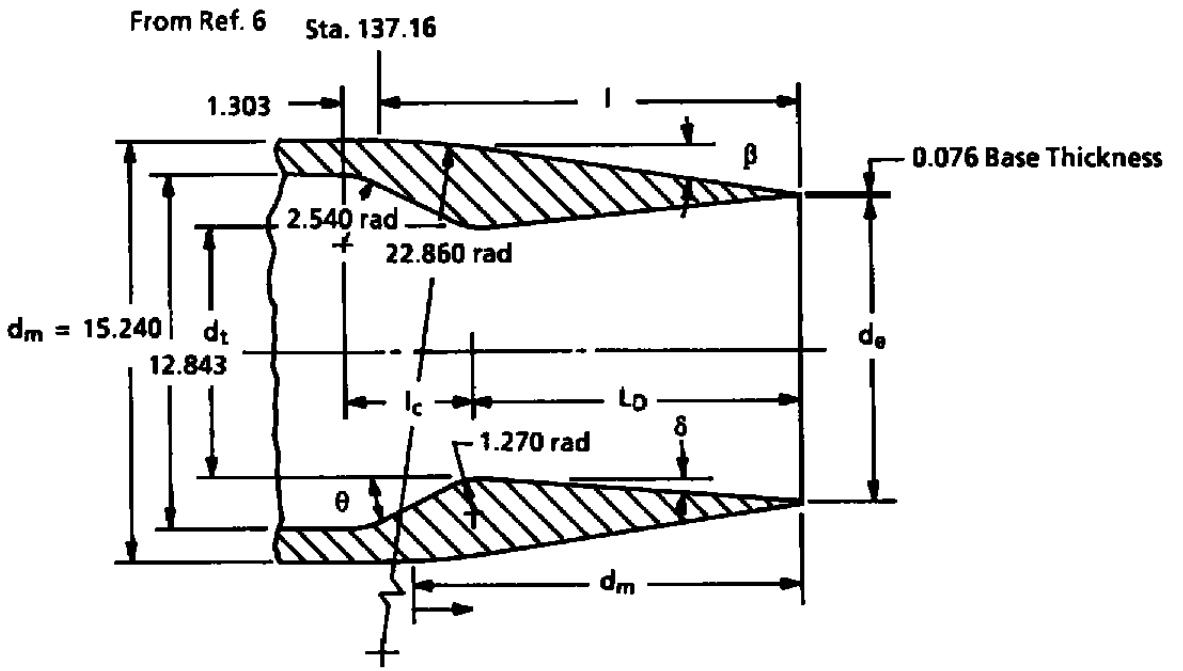

$(P_t/P_o)_{des}$	A_e/A_t	d_t/d_m	l_c/d_m	L_D/d_m	θ, deg	δ, deg	l/d_m	d_e/d_m
4.25	1.25	0.5	0.286	0.8	42.35	2.12	1.0	0.559

Figure 15. Geometry for the convergent/divergent nozzle.

From Ref. 6

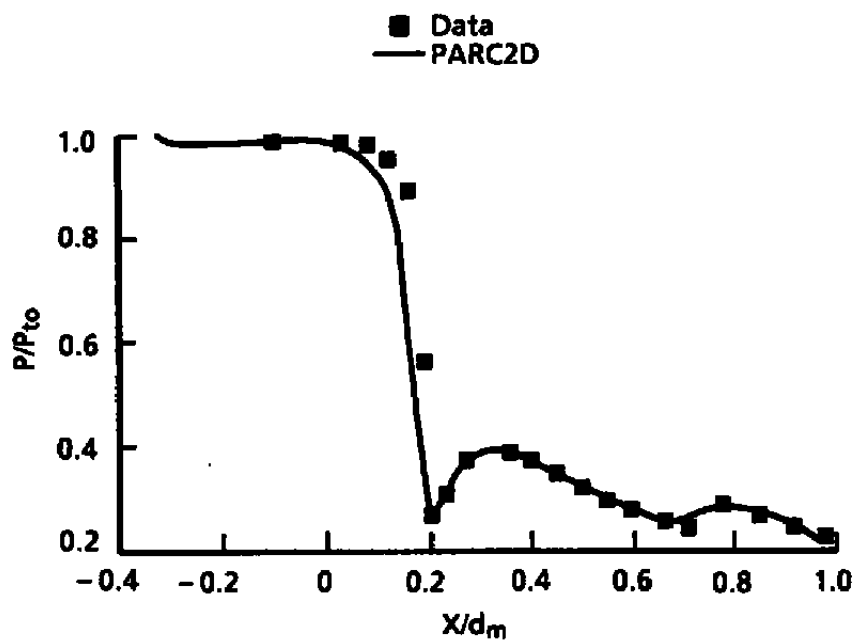

Figure 16. Surface static pressure for the convergent/divergent nozzle.

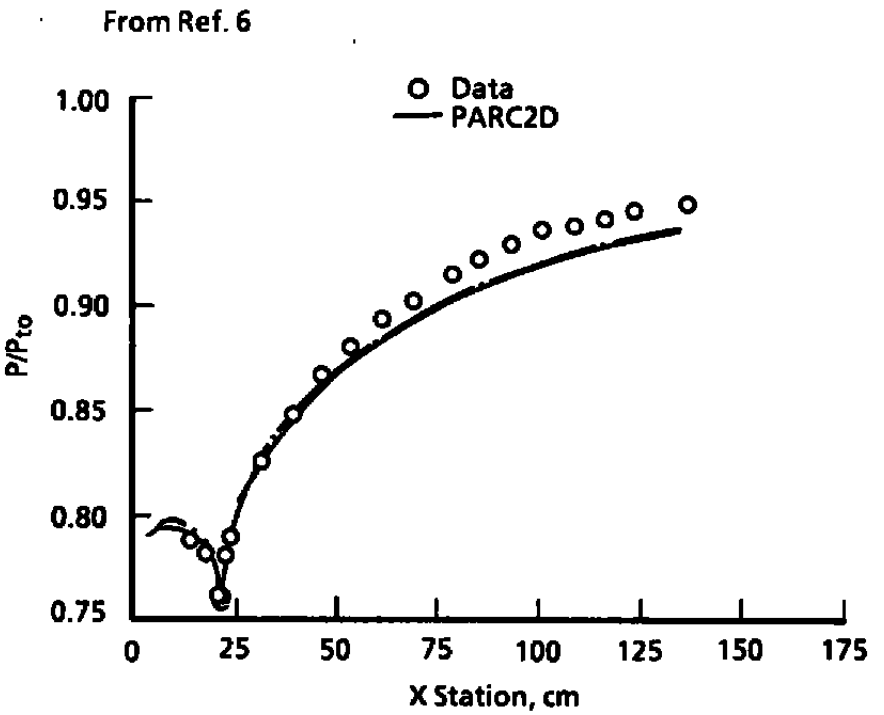

Figure 17. Surface static pressure for the subsonic diffuser.

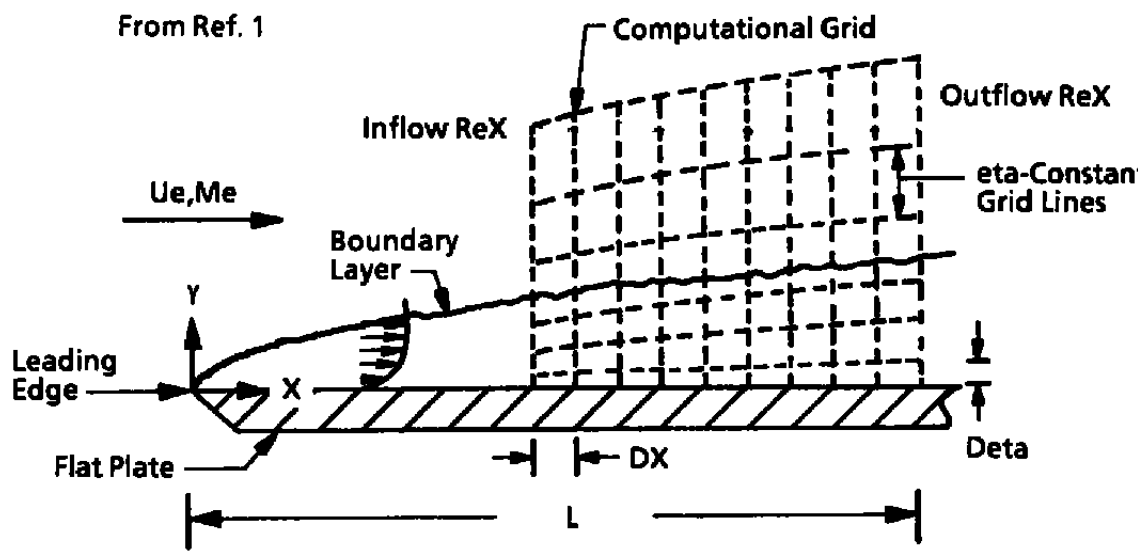

Figure 18. Geometry and basic formulation for flat plate calibration case.

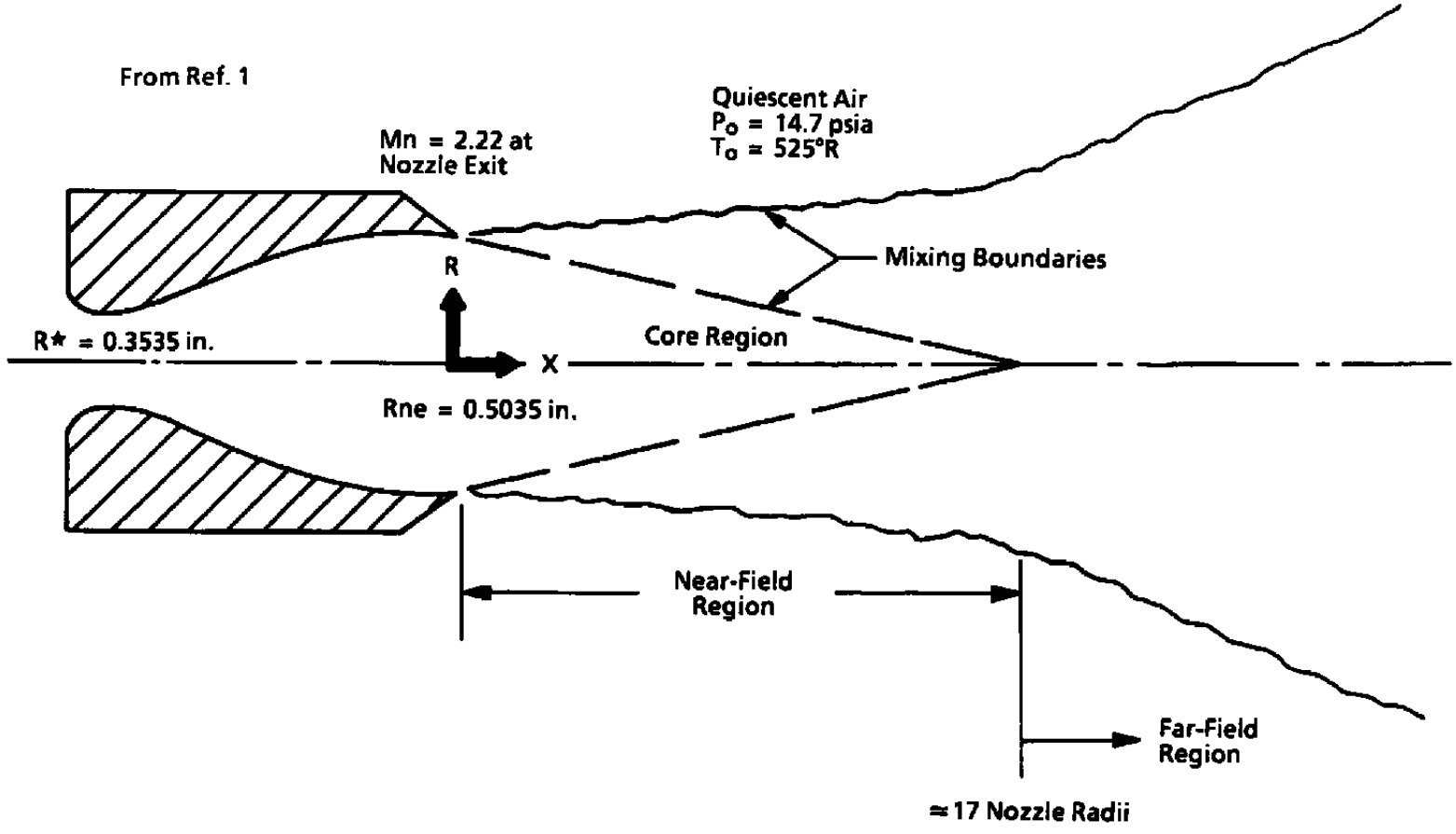

Figure 19. Supersonic nozzle flow basic formulation.

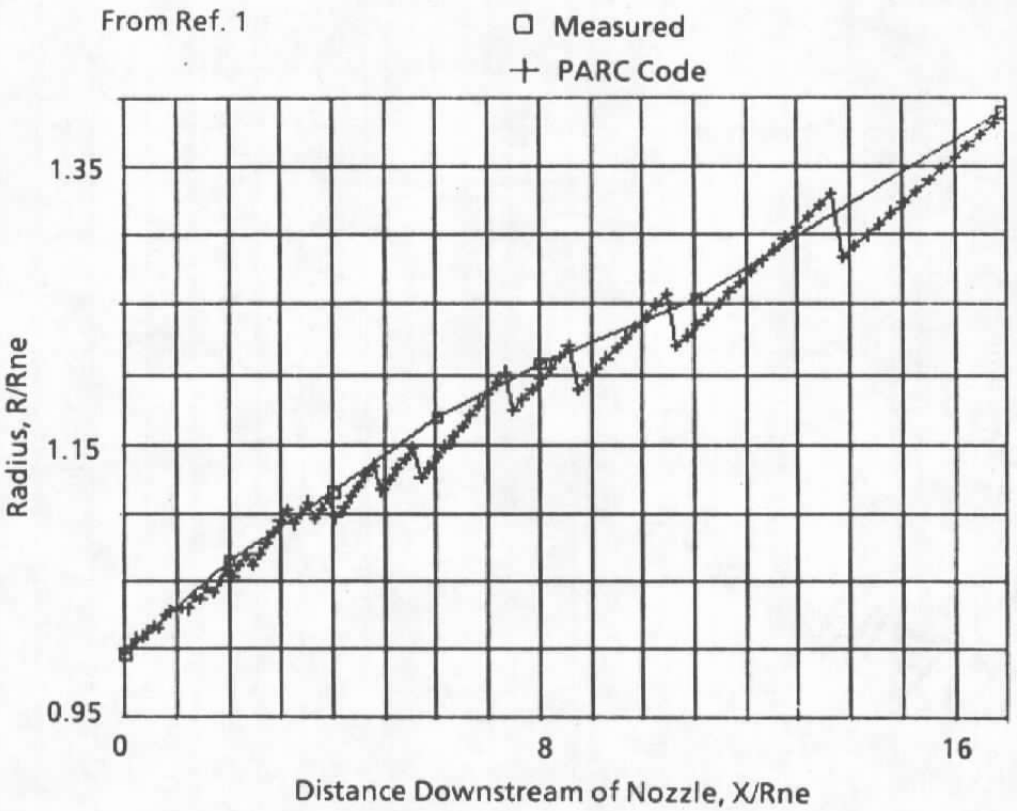

Figure 20. Near-field results for supersonic nozzle.

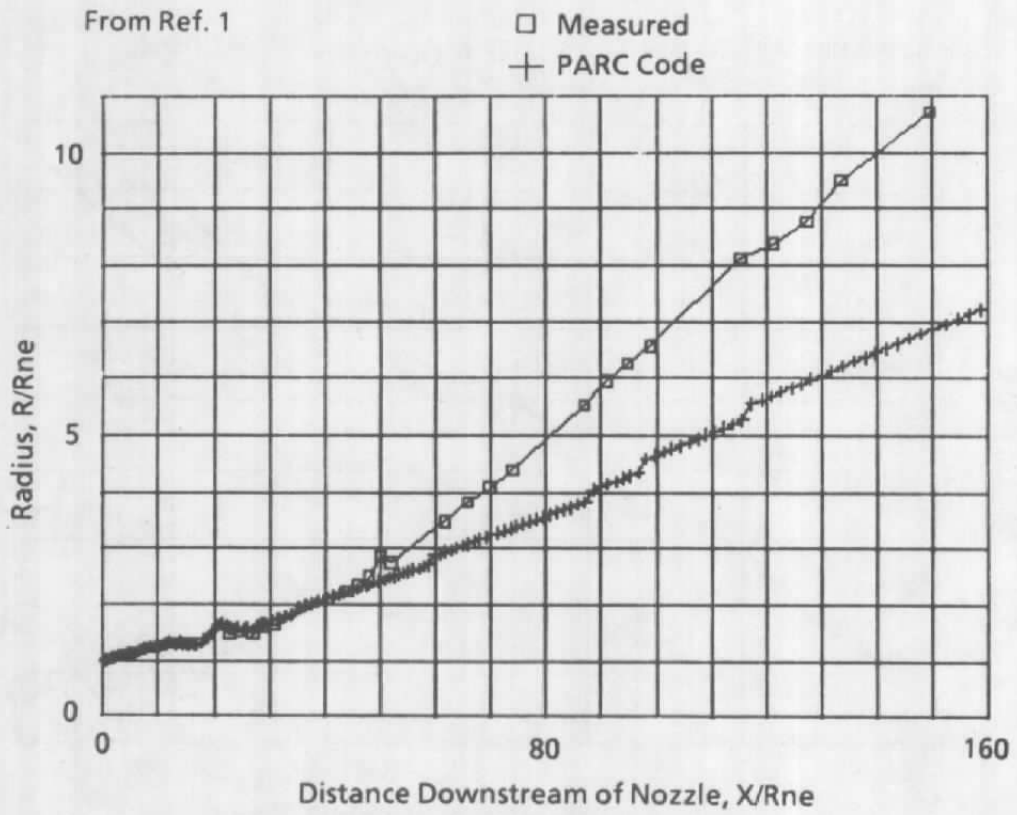

Figure 21. Far-field results for supersonic nozzle.

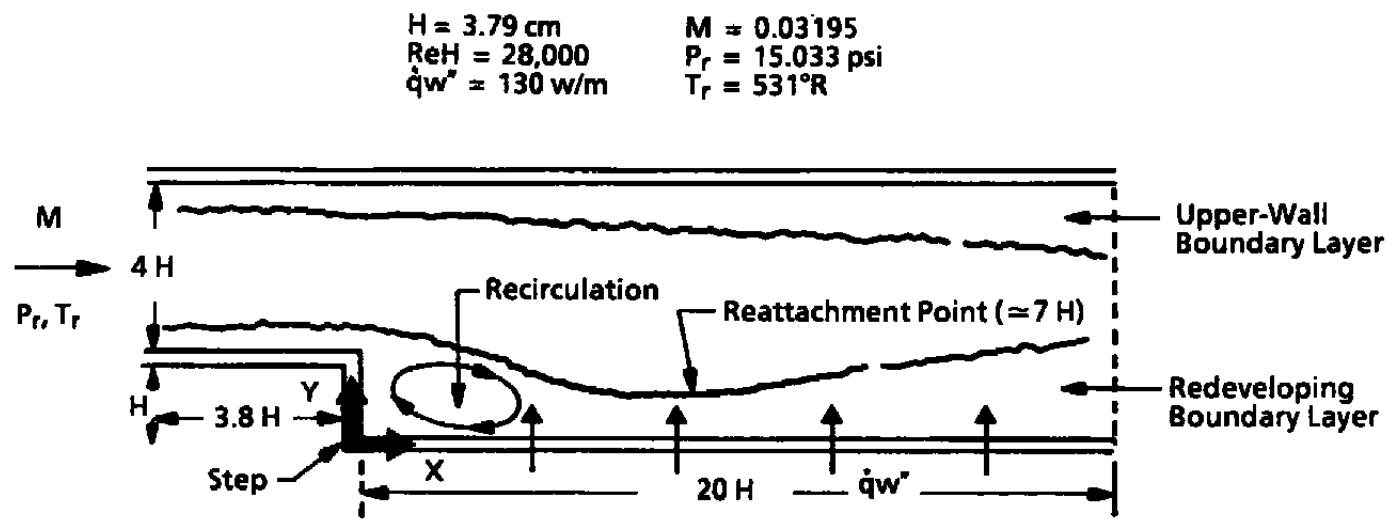

Figure 22. Rearward-facing step basic formulation.

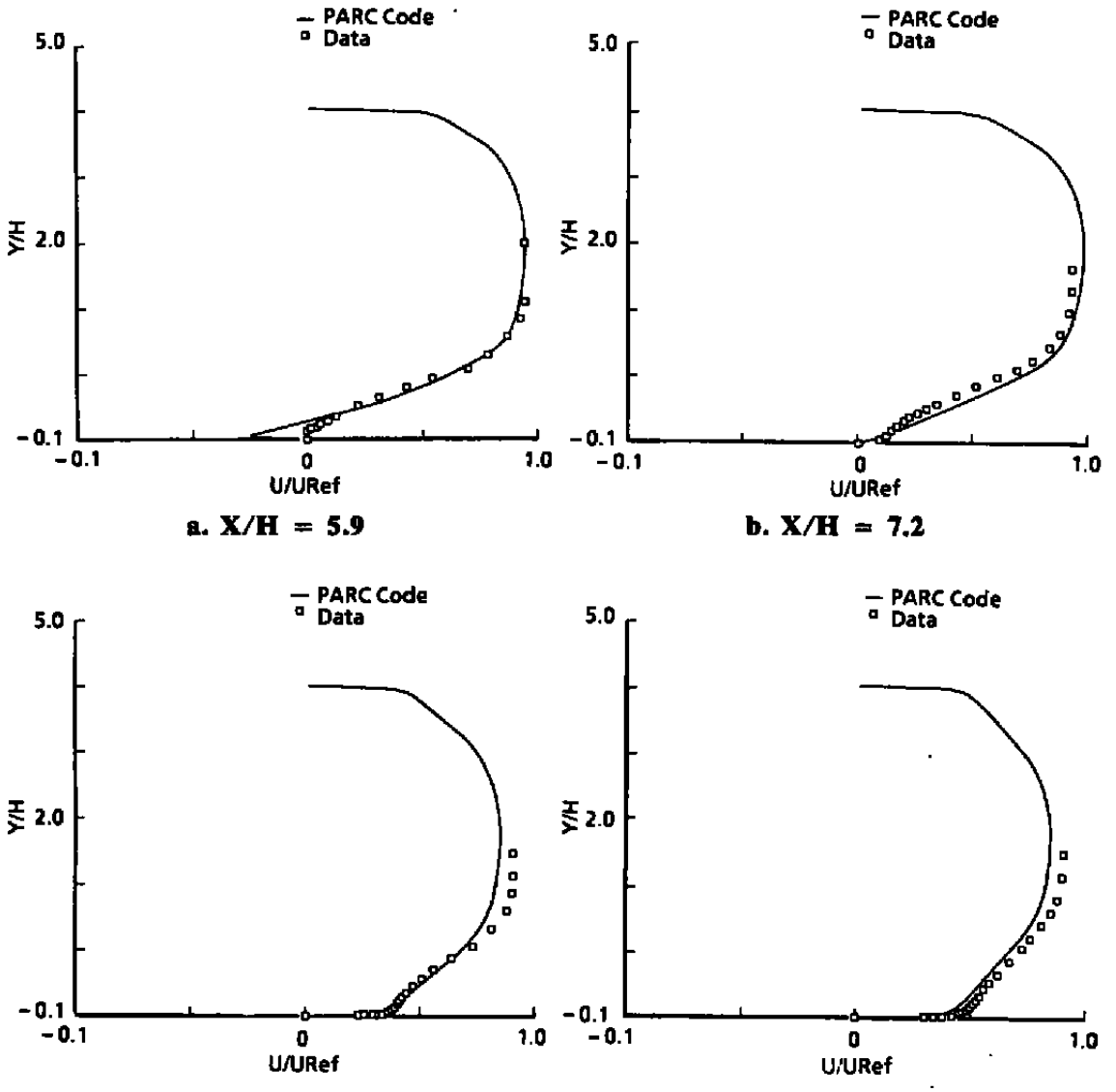

a. X/H = 5.9

b. X/H = 7.2

c. X/H = 12.2

d. X/H = 17.5

Figure 23. Velocity profiles downstream of rearward-facing step.

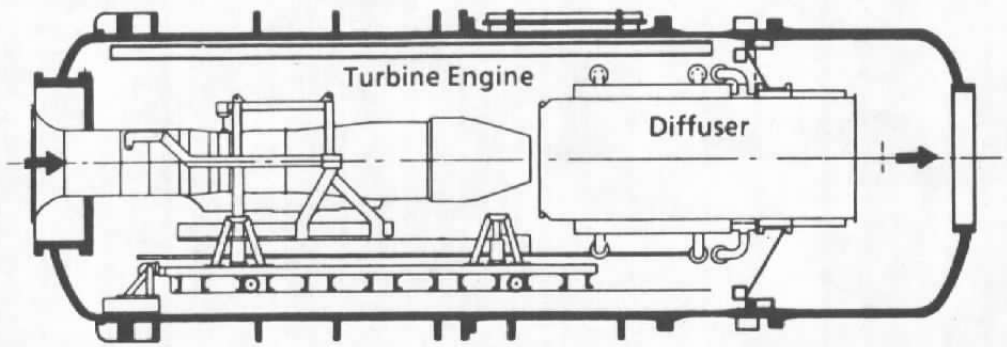

a. Typical turbine engine test installation

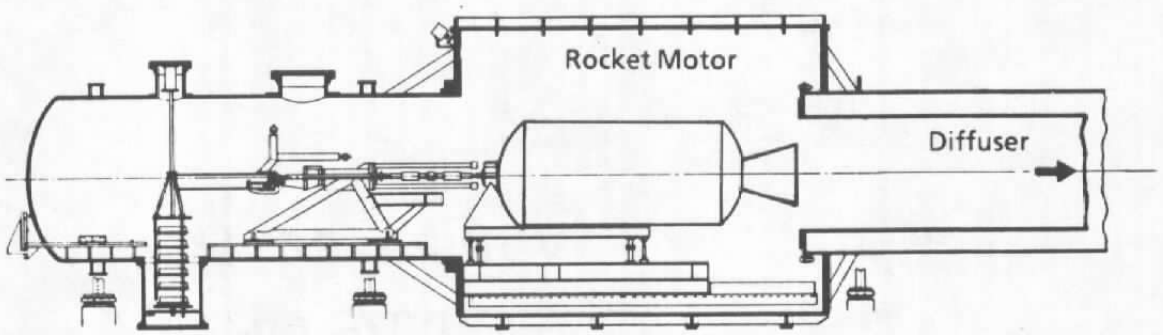

b. Typical rocket motor test installation

Figure 24. Examples of free-jet flows in the ETF.

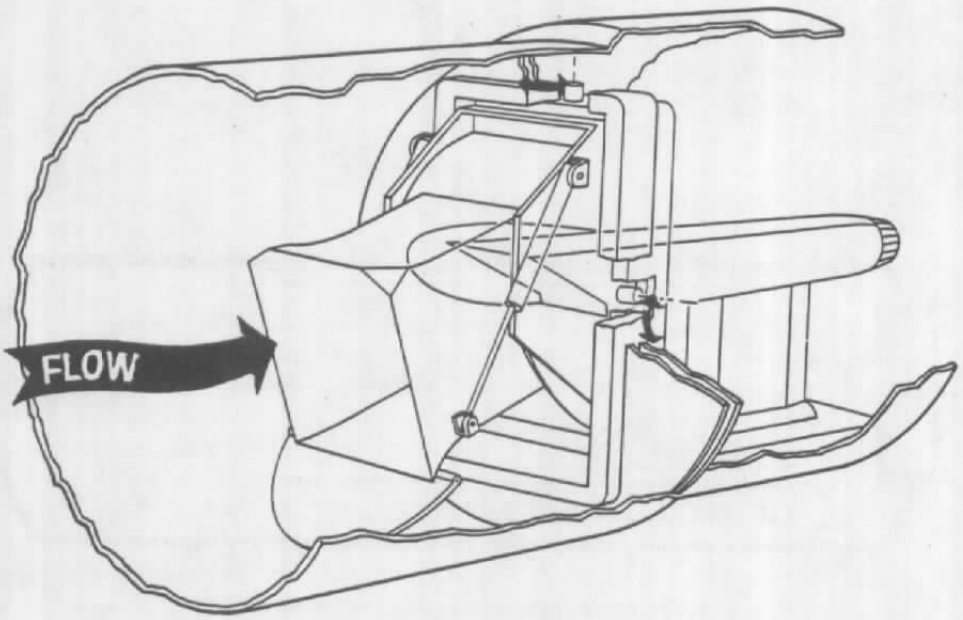

c. Subsonic inlet/engine compatibility testing

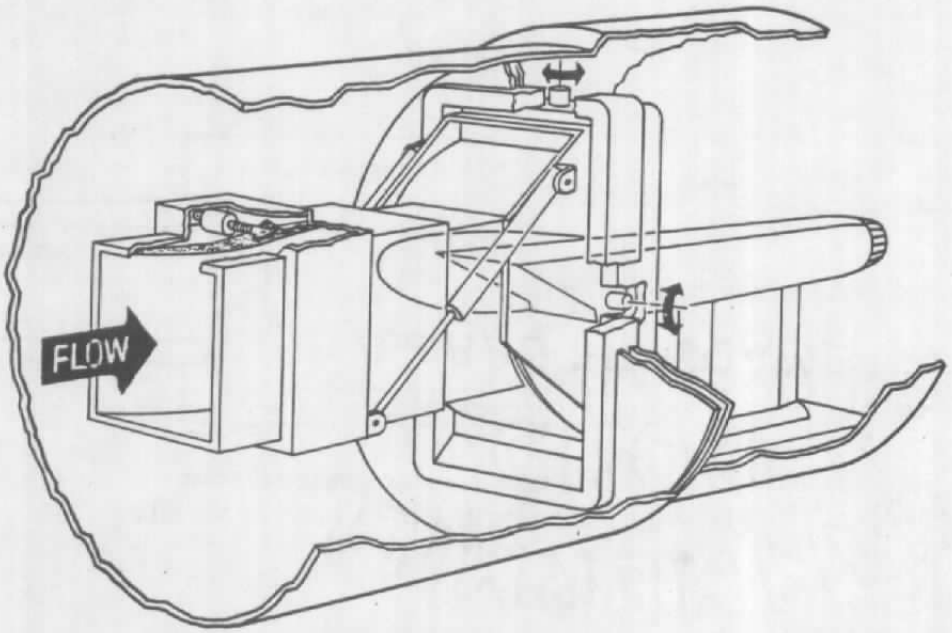

d. Supersonic free-jet inlet/engine compatibility testing

Figure 24. Concluded.

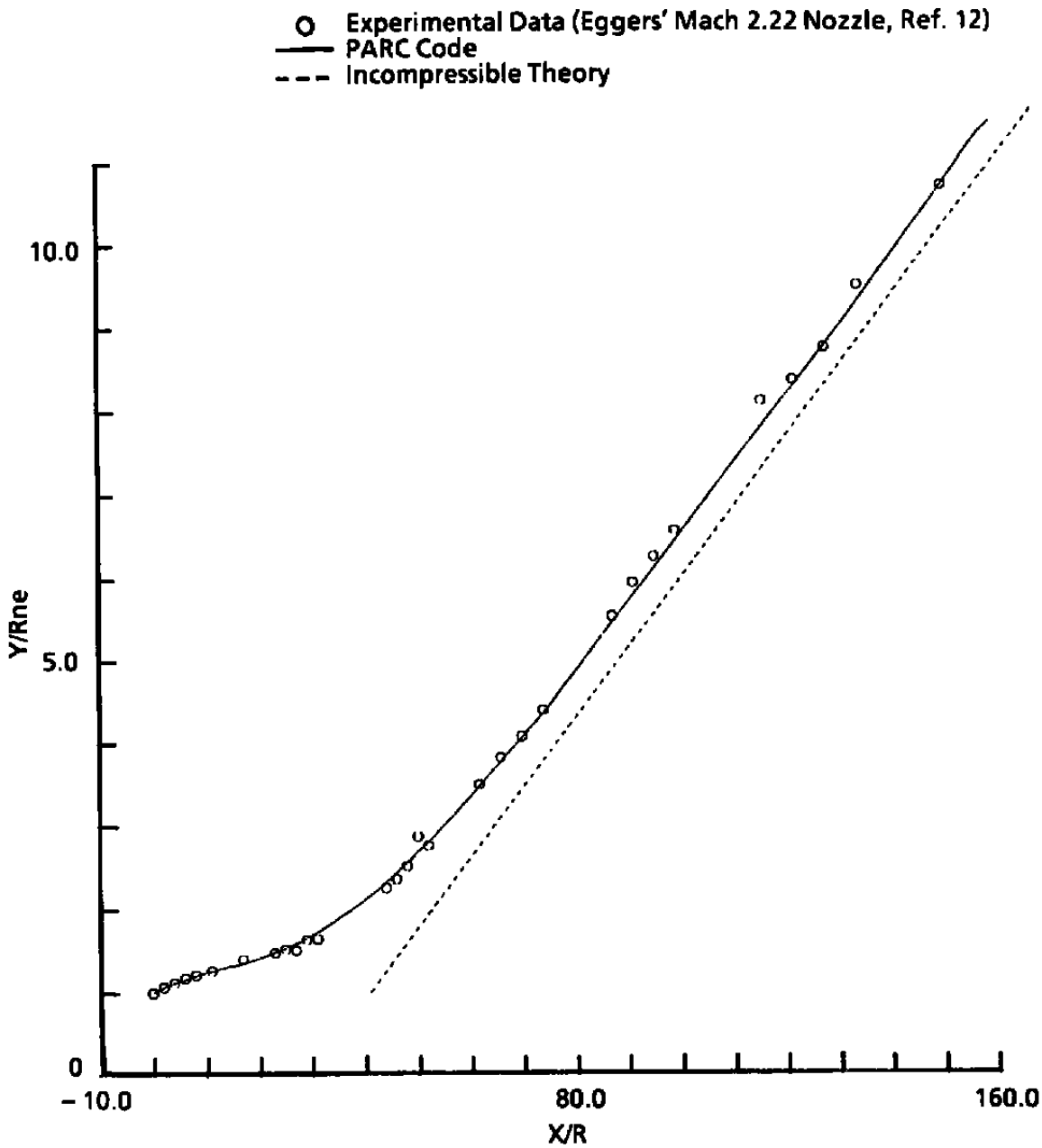

Figure 25. Far-field spread rate using the new turbulence model.

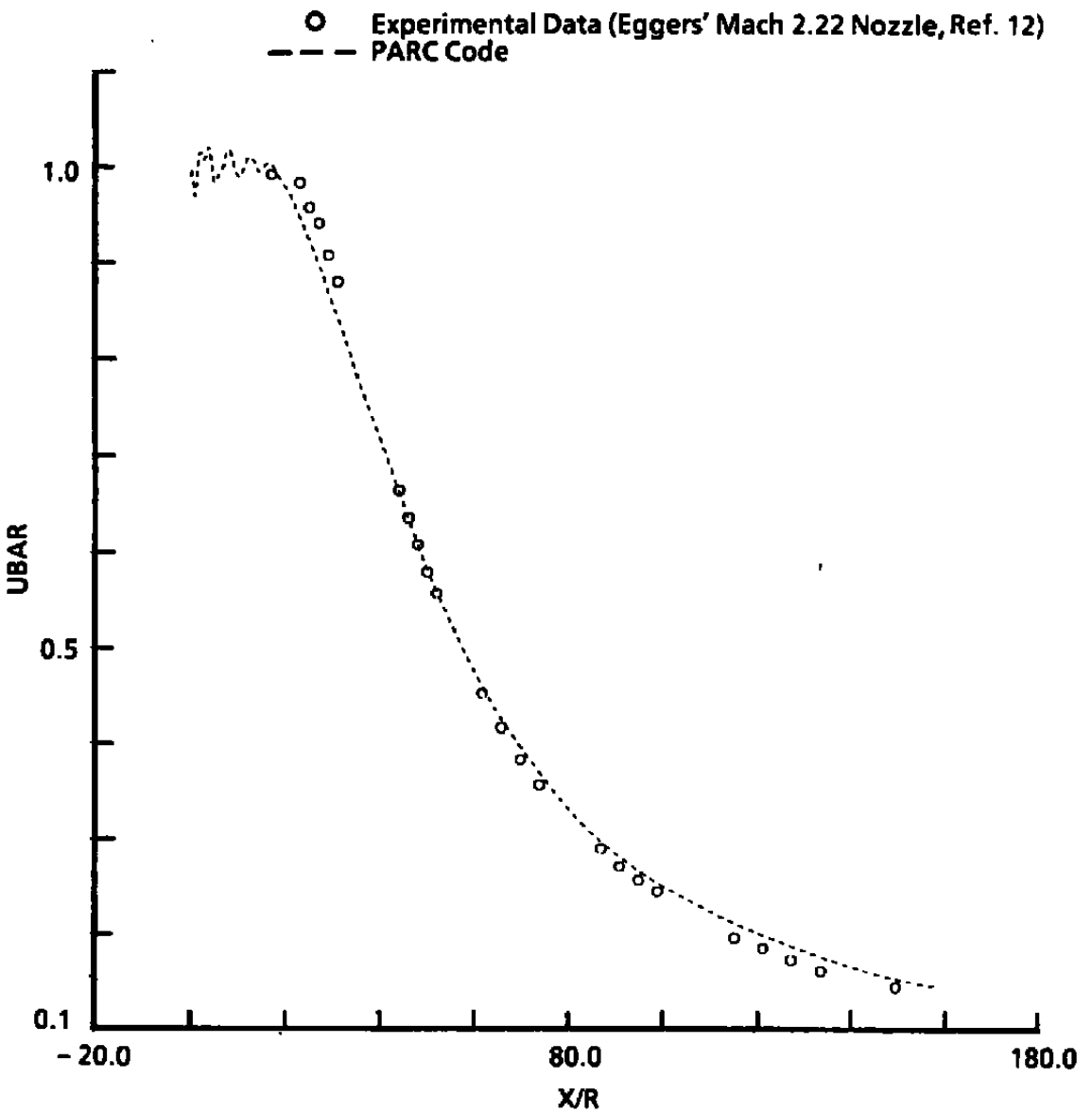

Figure 26. Far-field velocity profiles using the new turbulence model.

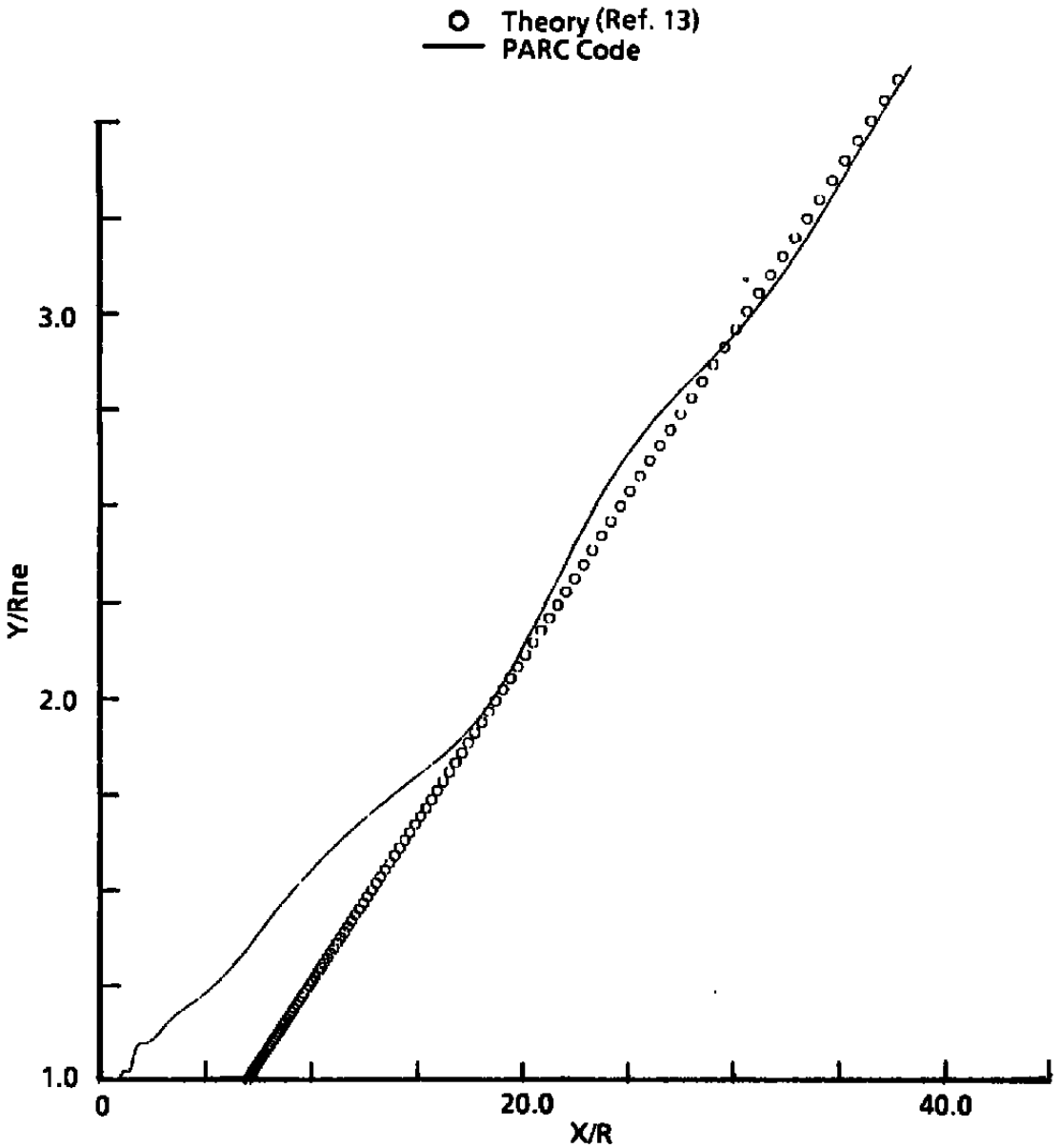

Figure 27. Subsonic jet spread rate compared to $b_{1/2} = 0.0848x$.

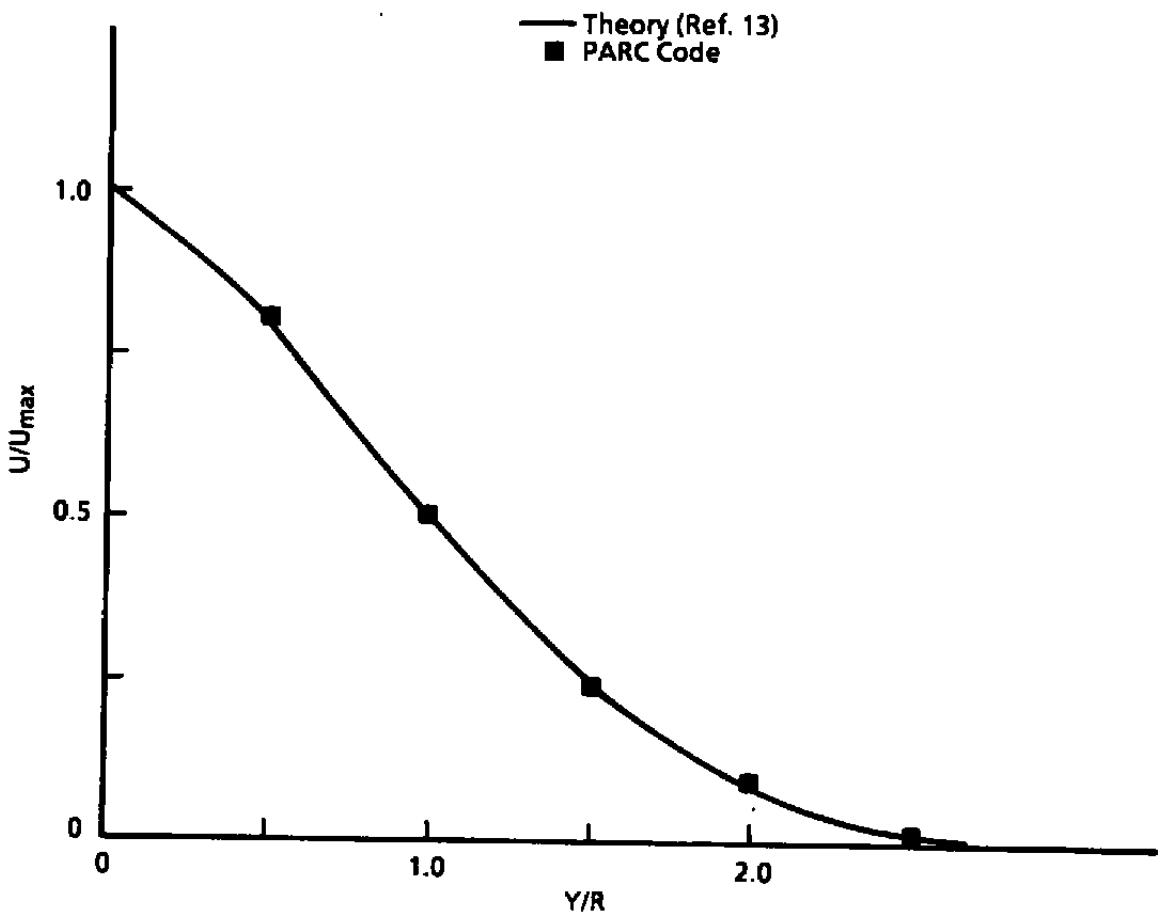

Figure 28. Subsonic jet velocity profiles, nondimensionalized.

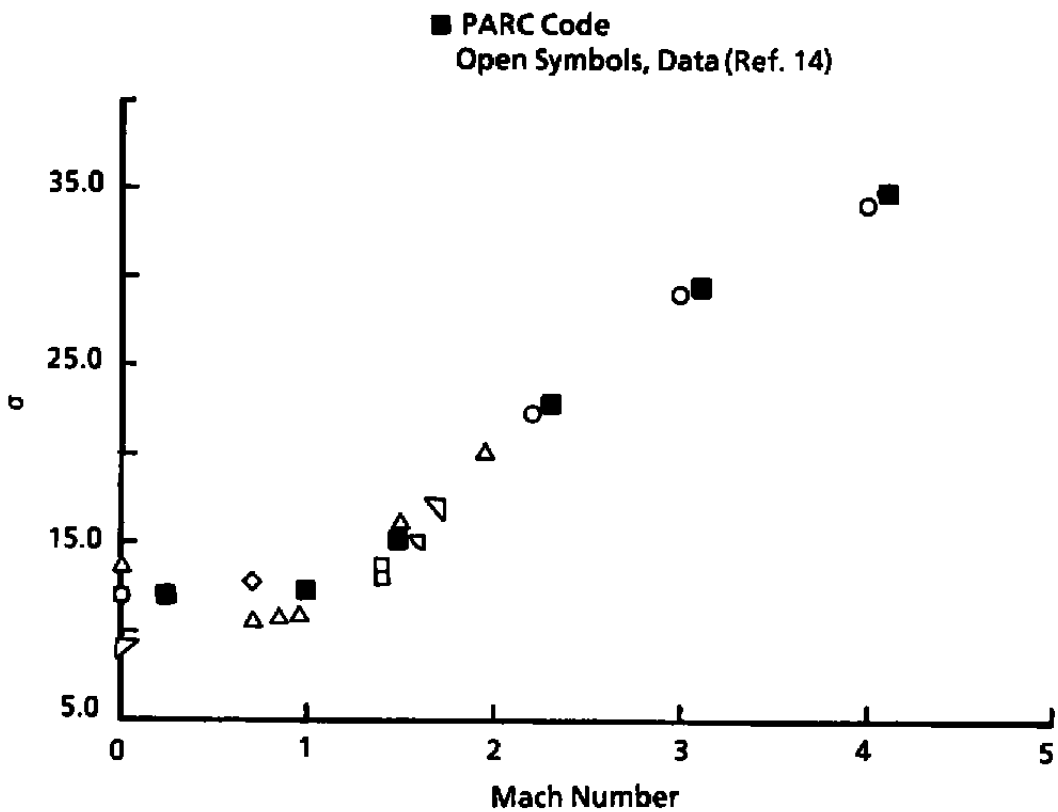

Figure 29. Supersonic jet spread rate comparison.

From Ref. 21

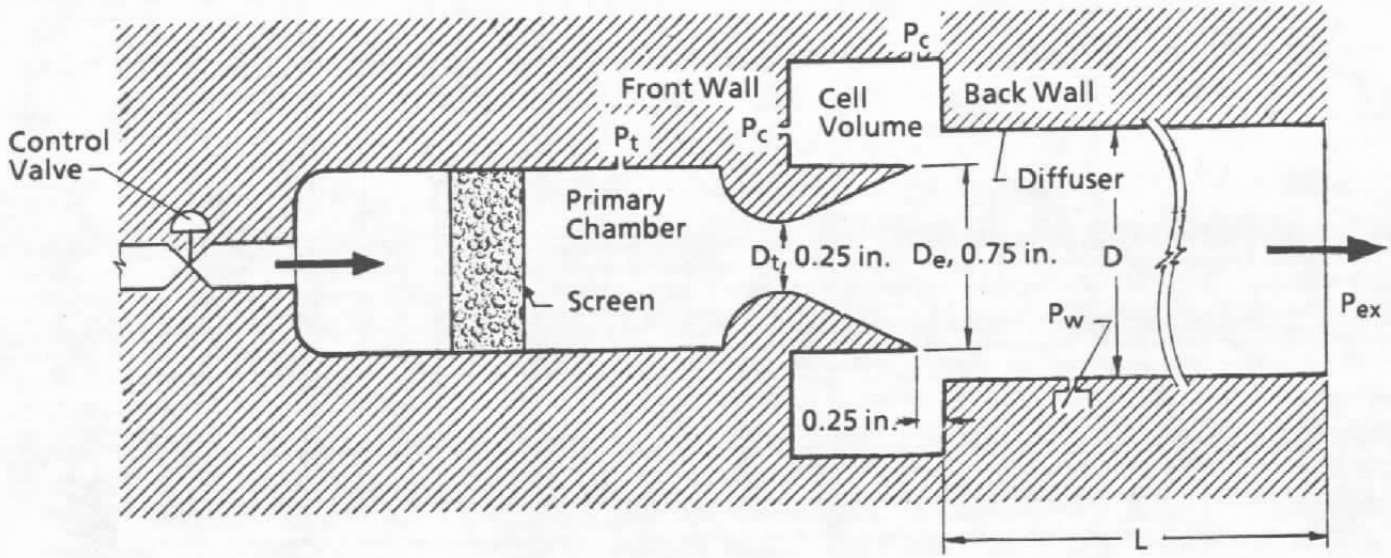

Figure 30. Test apparatus used to obtain calibration data.

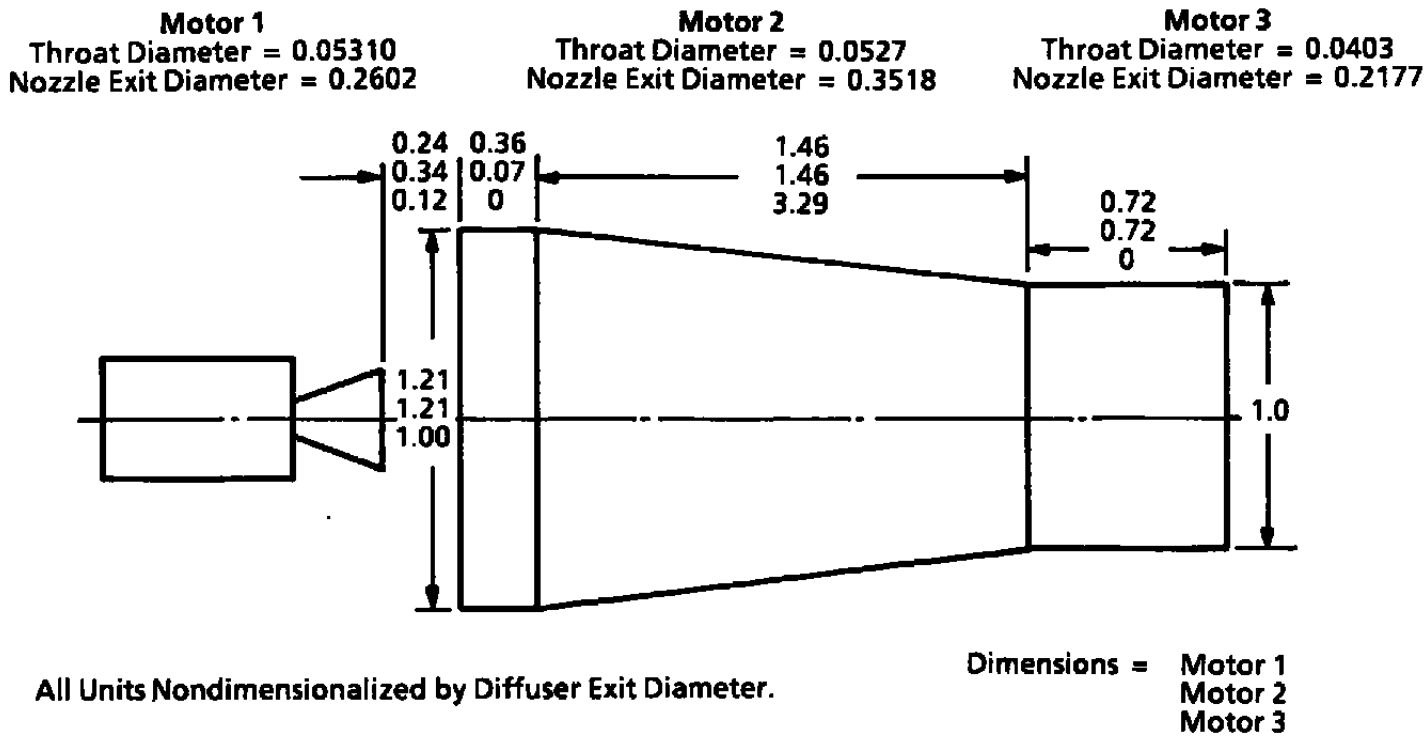

Figure 31. Rocket motor configurations.

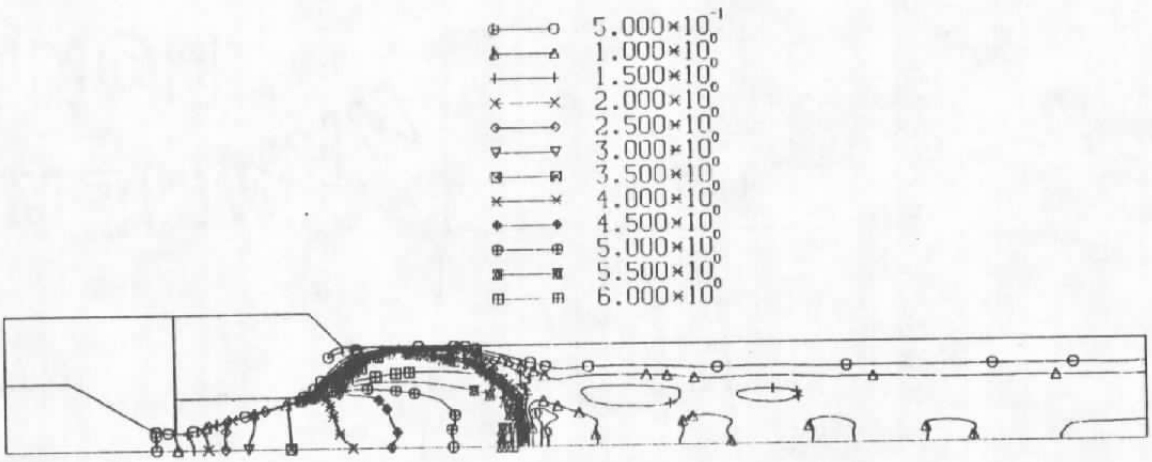

a. Mach number contours

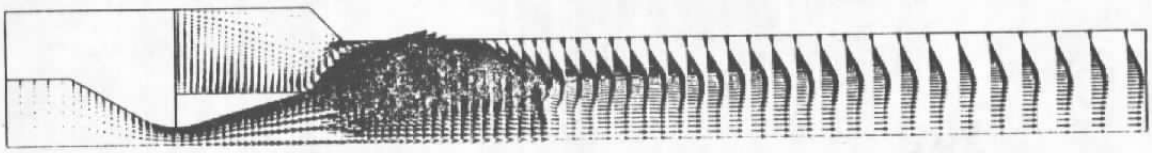

b. Velocity vectors

Figure 32. Flow solution for Case 1.

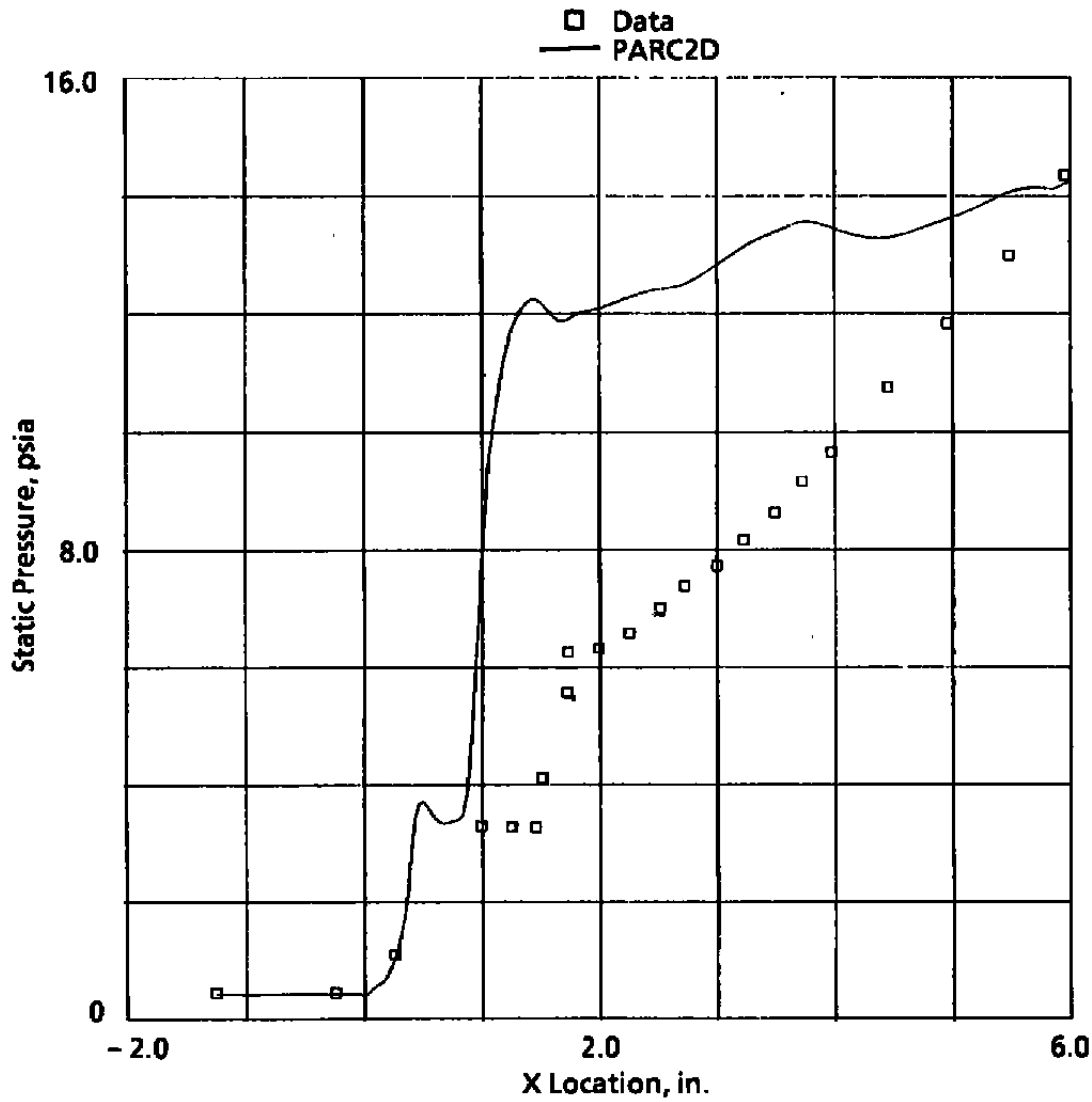

Figure 33. Diffuser wall static pressure comparison for Case 1.

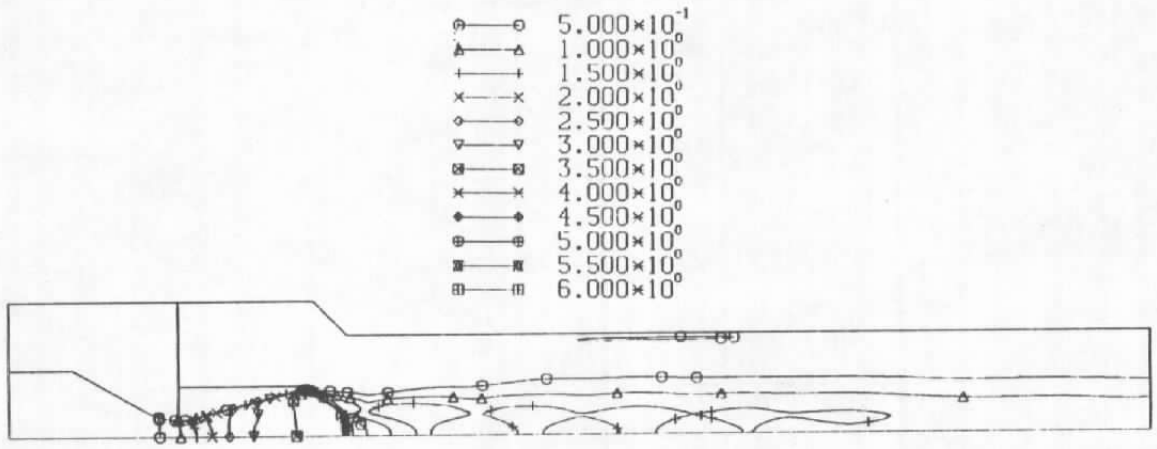

a. Mach number contours

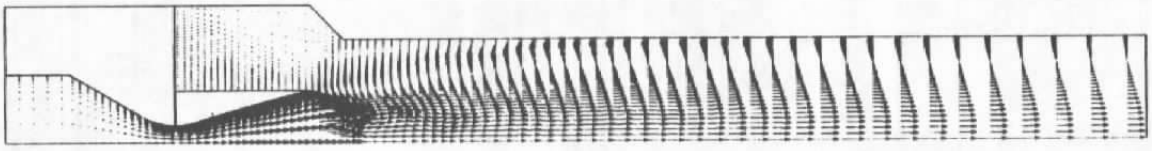

b. Velocity vectors

Figure 34. Flow solution for Case 2.

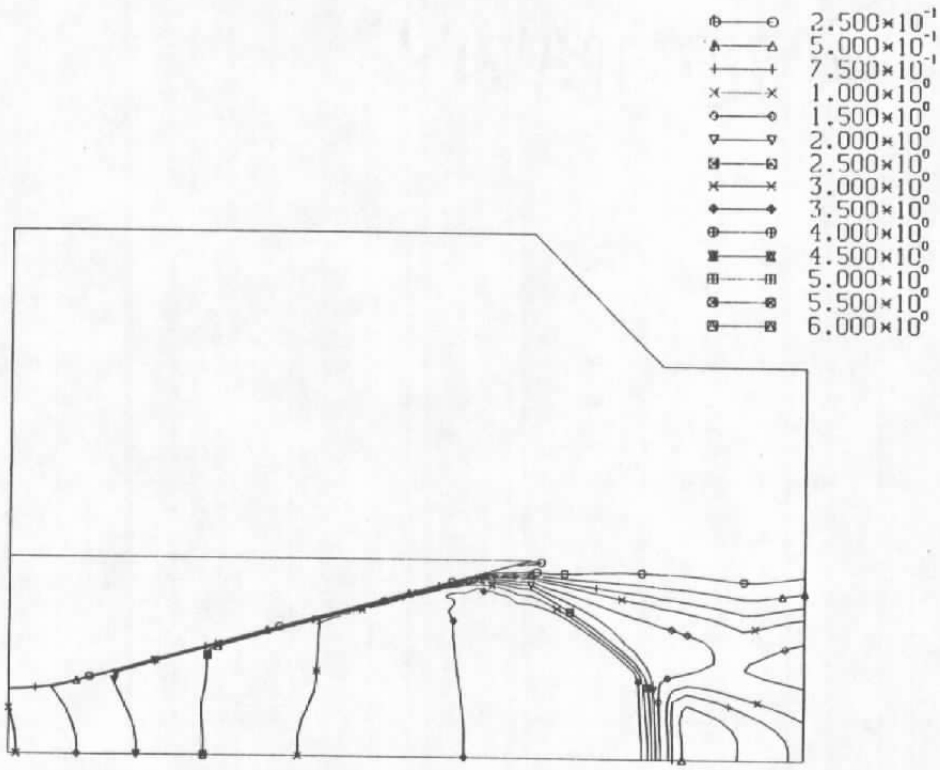

a. Mach number contours

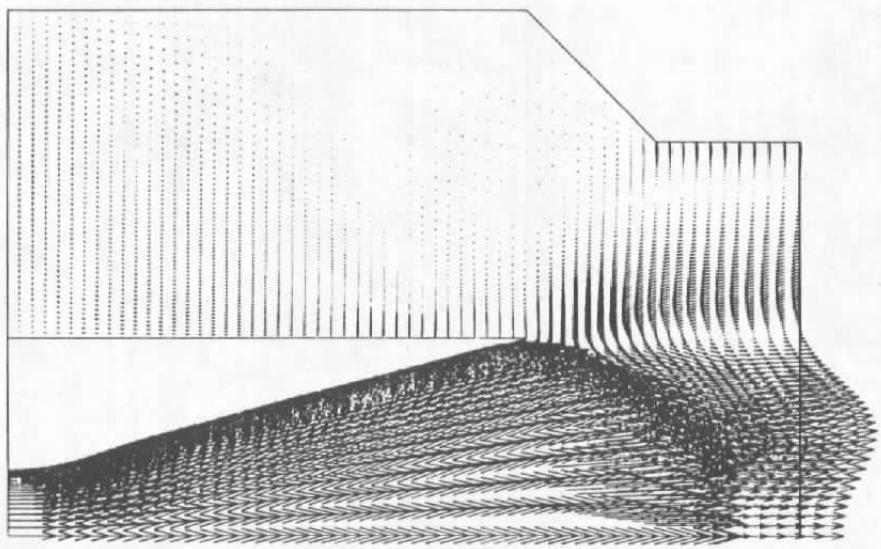

b. Velocity vectors

Figure 35. Nozzle flow solution for Case 2.

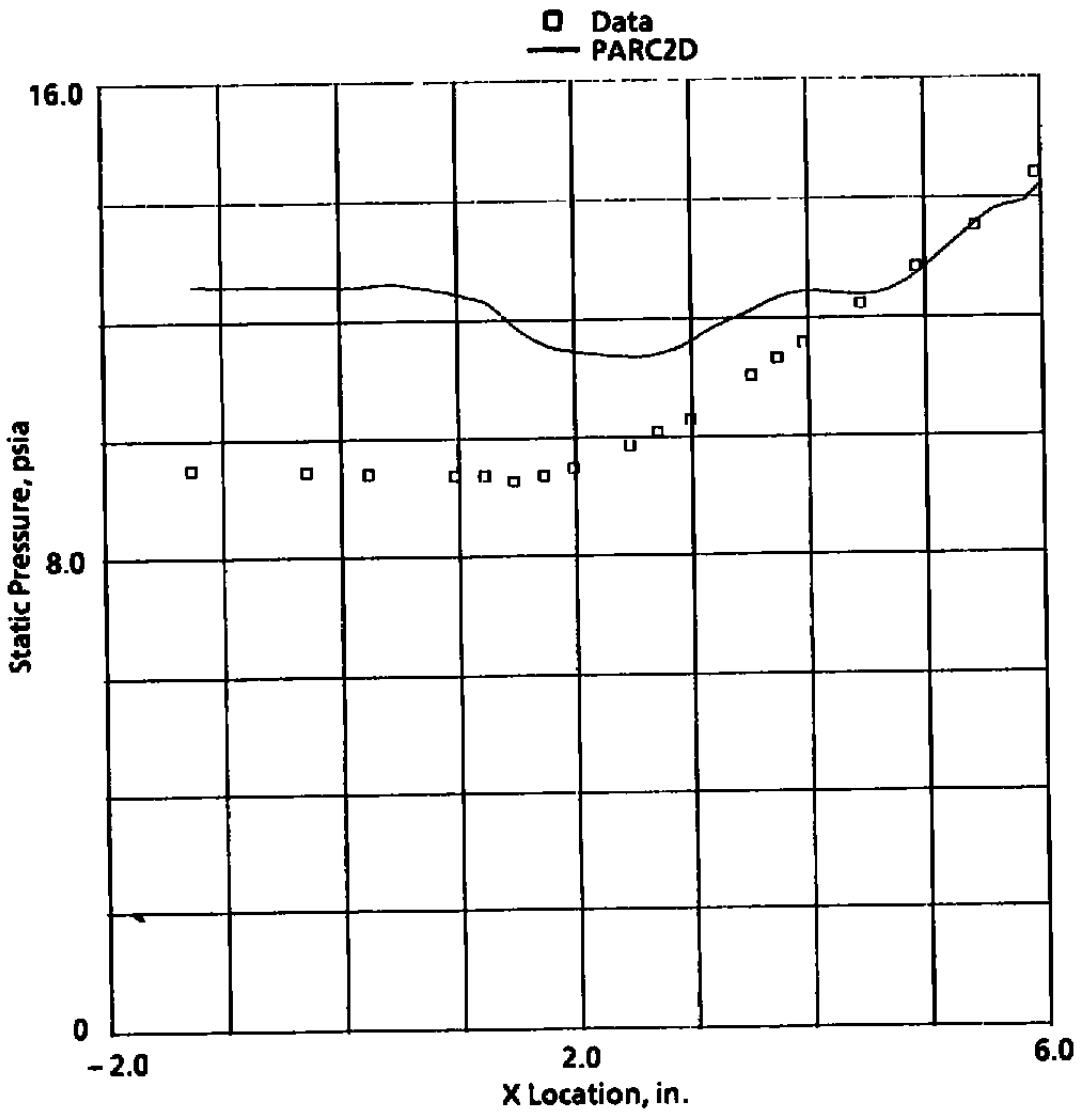

Figure 36. Diffuser wall static pressure comparison for Case 2.

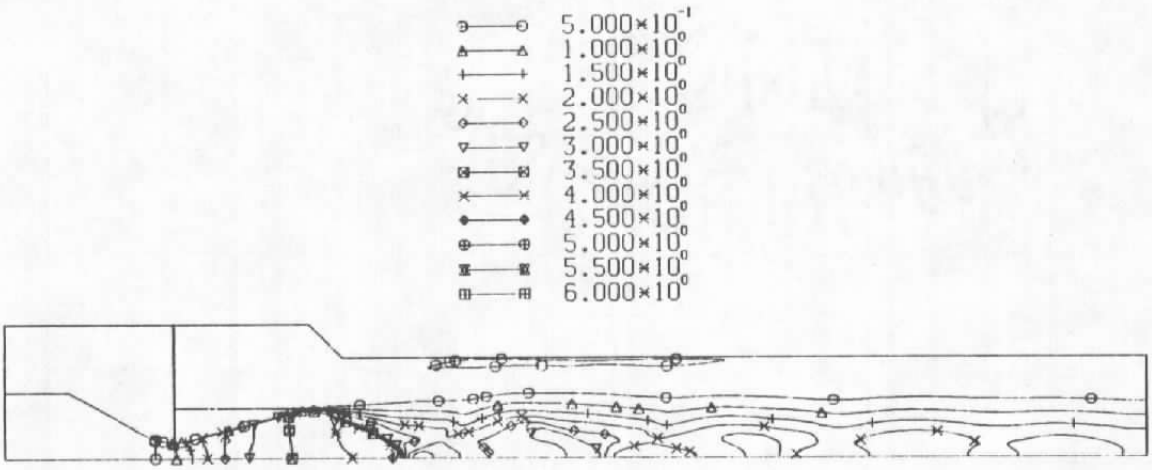

a. Mach number contours

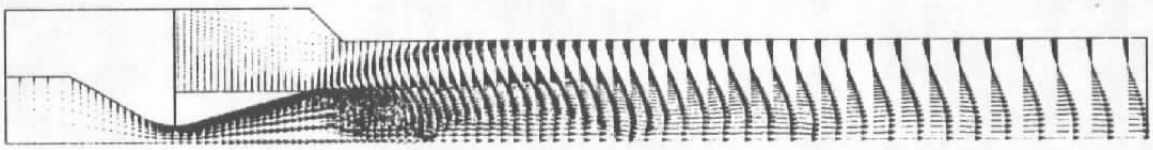

b. Velocity vectors

Figure 37. Flow solution for Case 3.

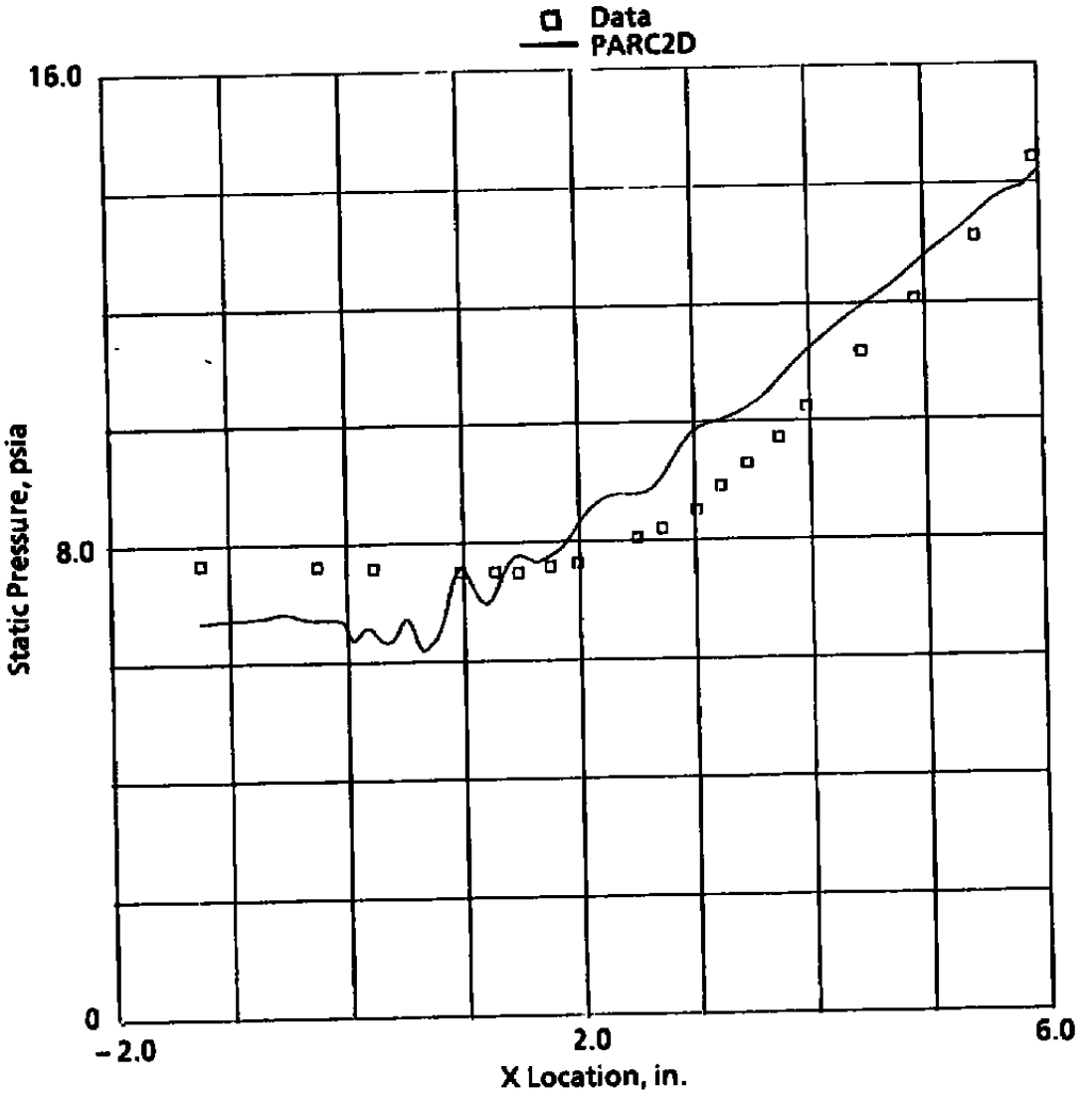

Figure 38. Diffuser wall static pressure comparison for Case 3.

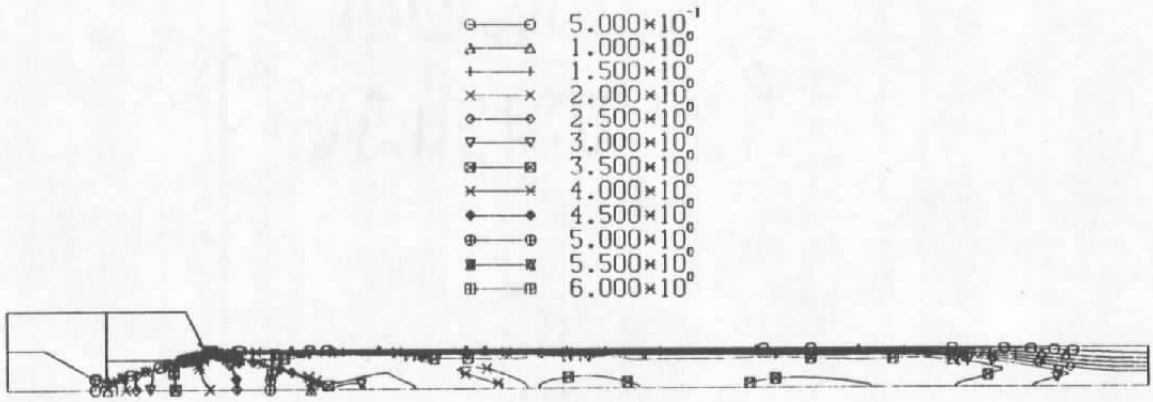

a. Mach number contours

b. Velocity vectors

Figure 39. Flow solution for Case 4.

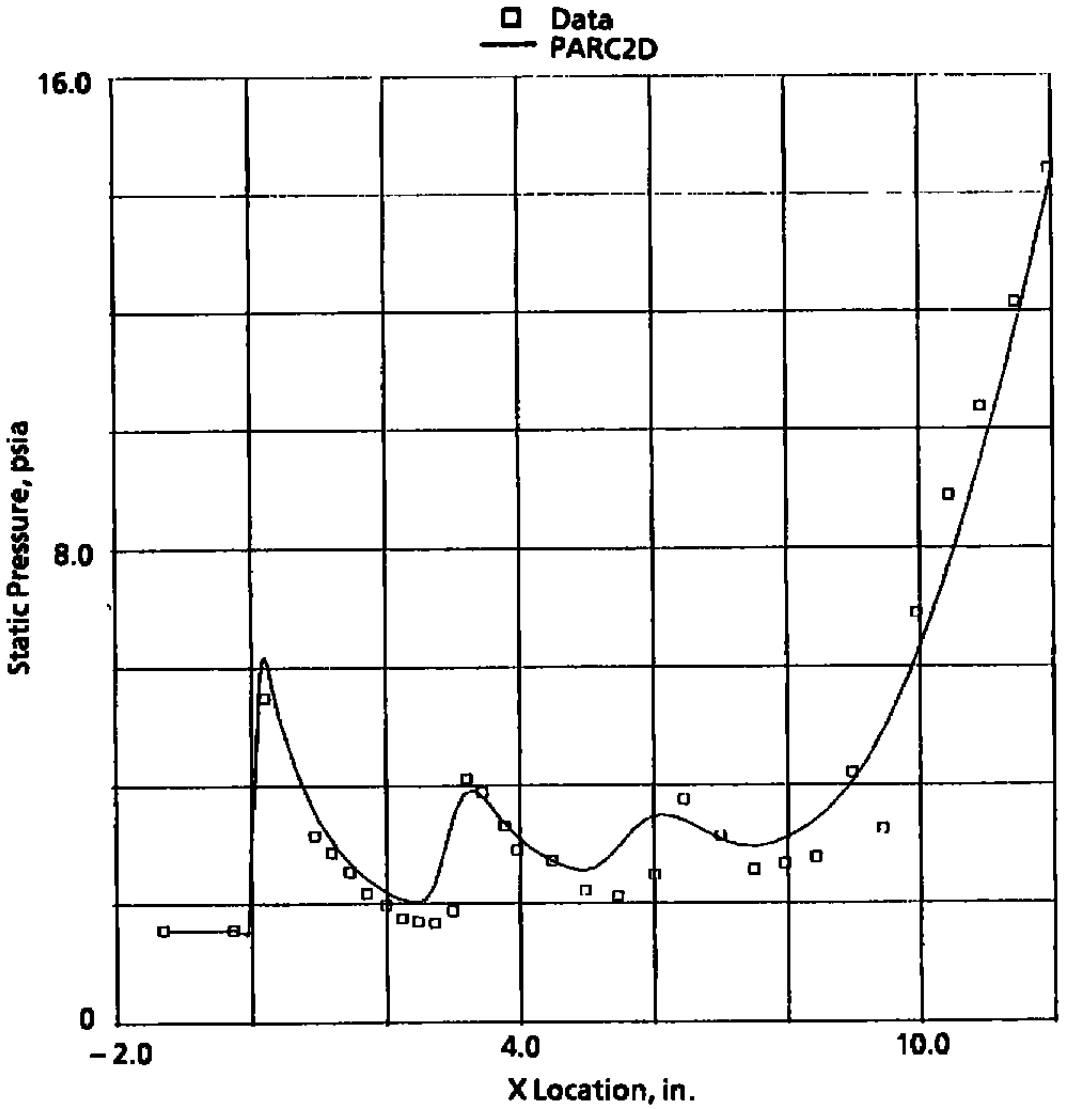

Figure 40. Diffuser wall static pressure comparison for Case 4.

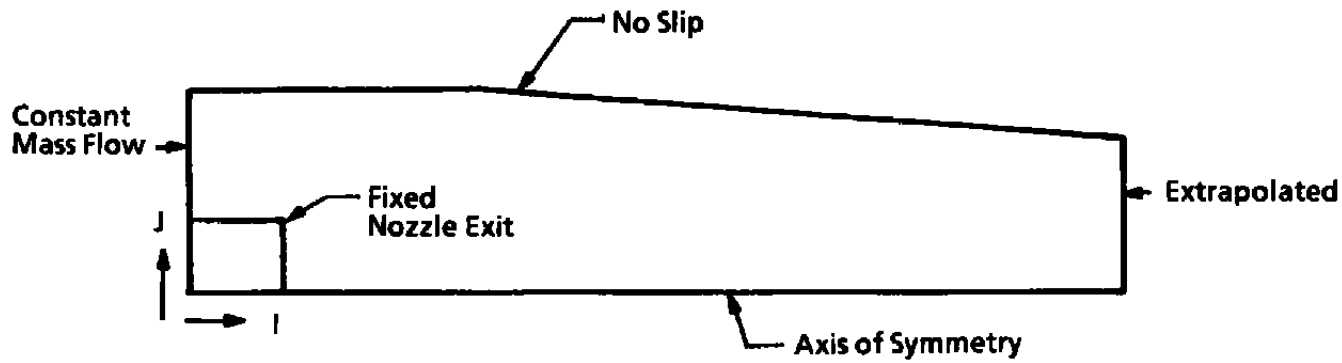

Figure 41. Rocket motor boundary conditions.

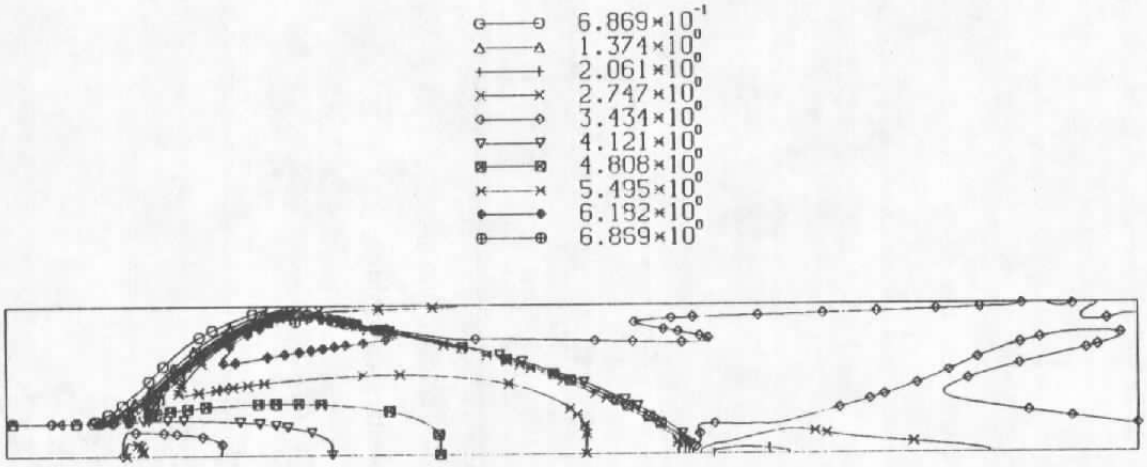

a. Mach number contours

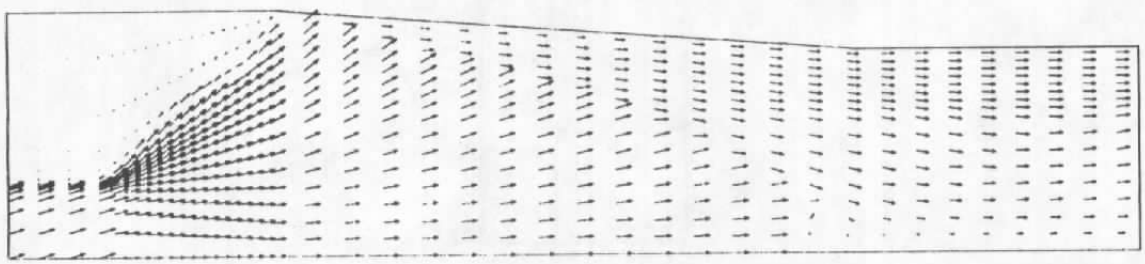

b. Velocity vectors

Figure 42. Motor 1 flow solution with secondary flow.

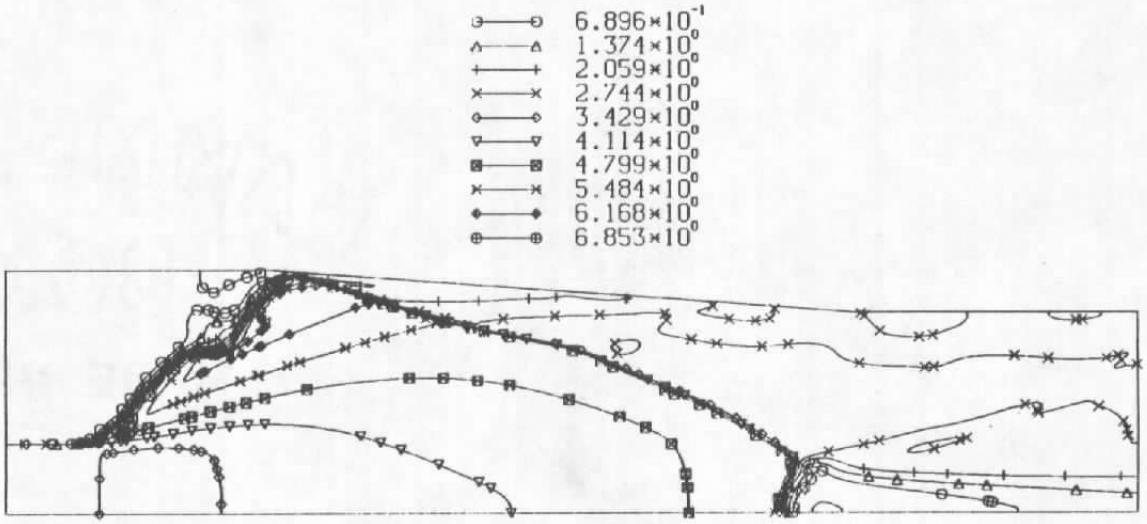

a. Mach number contours

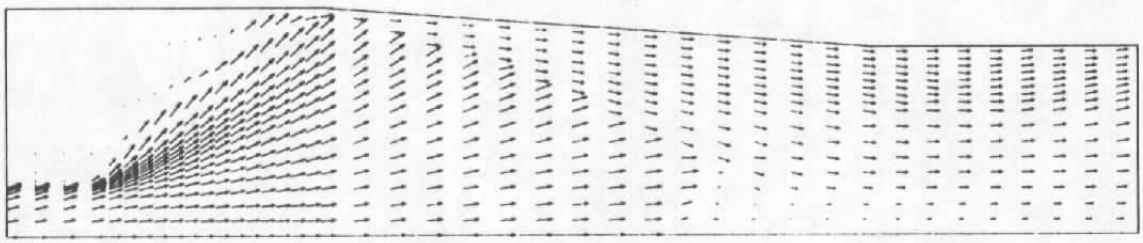

b. Velocity vectors

Figure 43. Motor 2 flow solution with secondary flow.

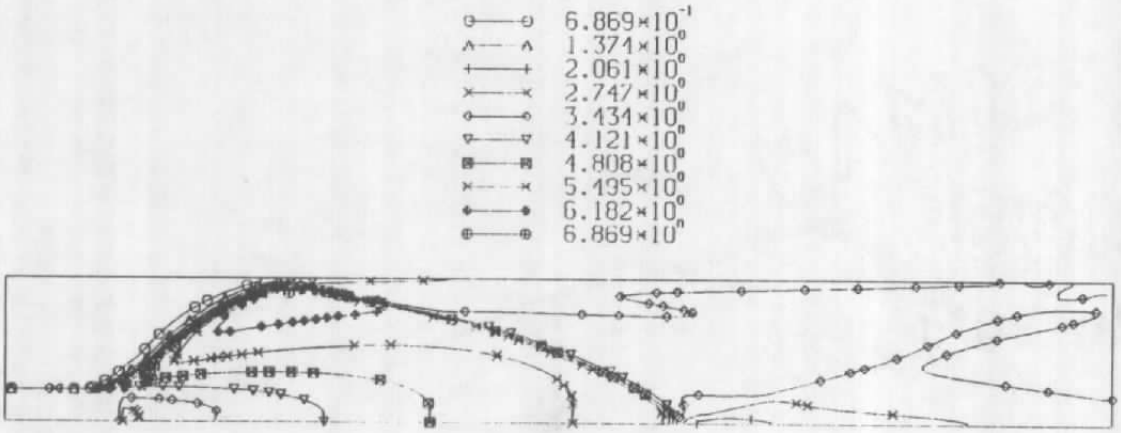

a. Mach number contours

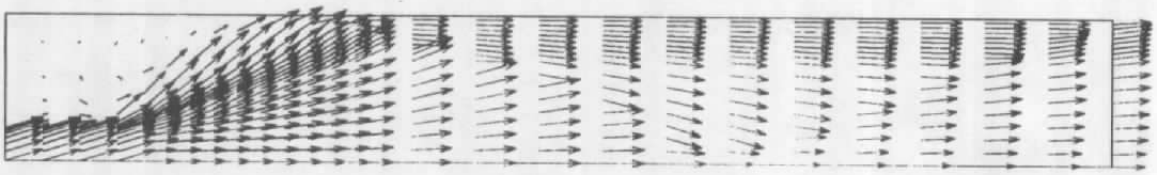

b. Velocity vectors

Figure 44. Motor 3 flow solution with secondary flow.

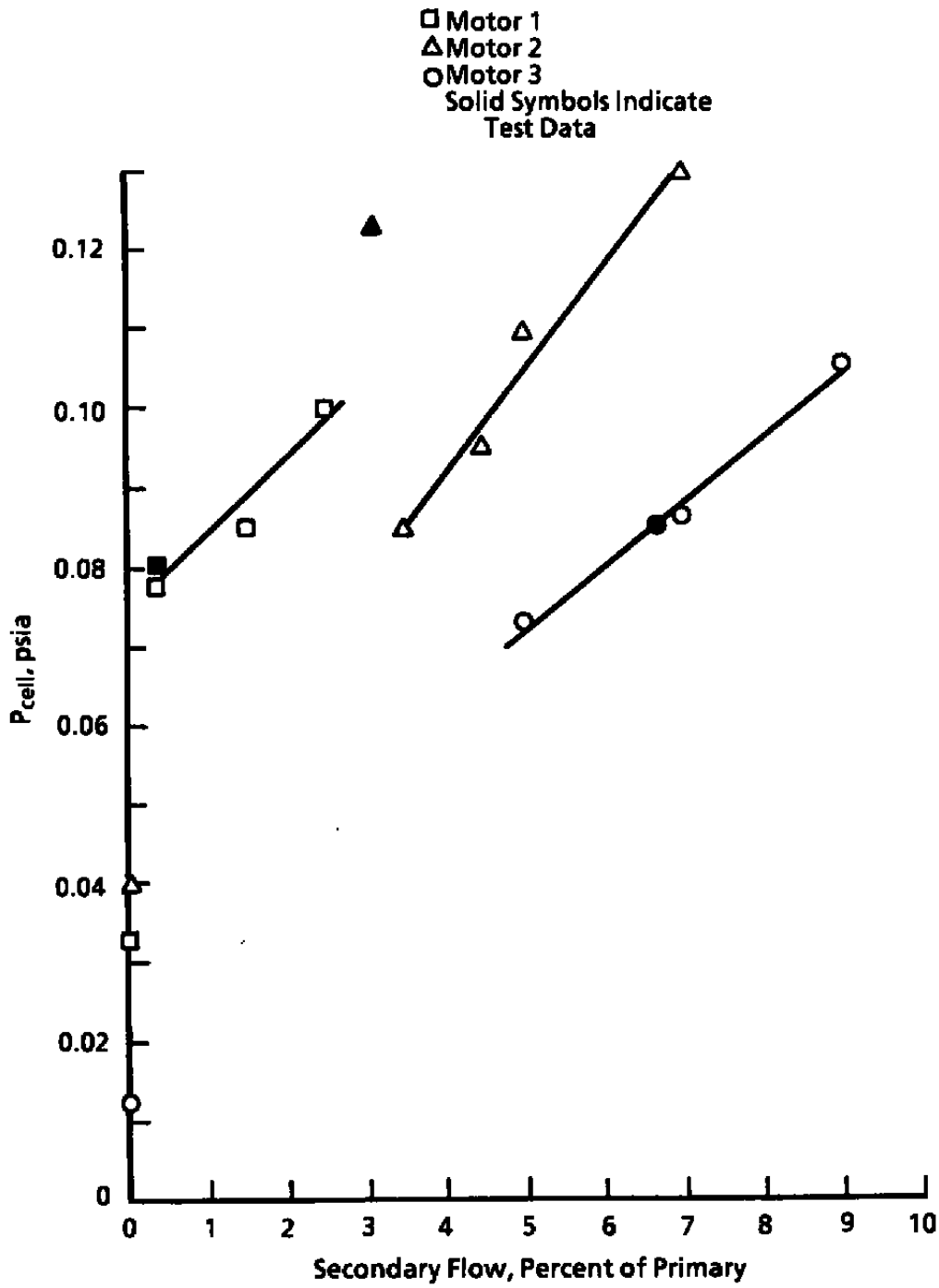

Figure 45. Cell pressure versus secondary flow percent for all three motors.

Sta. 104.47

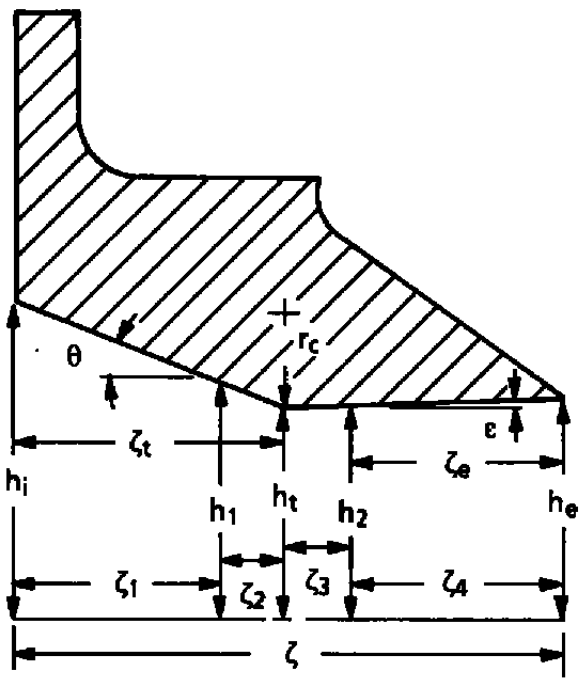

Parameter	Dimensions	Parameter	Dimensions
A_e, cm^2	30.29	ζ_t	5.78
A_ζ, cm^2	27.81	ζ_1	5.54
A_e/A_t	1.09	ζ_2	0.24
h_e	1.49	ζ_3	0.01
h_i	3.52	ζ_4	5.76
h_t	1.37	M_d	1.35
h_1	1.41	NPR_d	2.97
h_2	1.37	r_c	0.68
ζ	11.56	θ, deg	20.84
ζ_e	5.78	ε, deg	1.21

Figure 46. 2-D/C-D nozzle geometry.

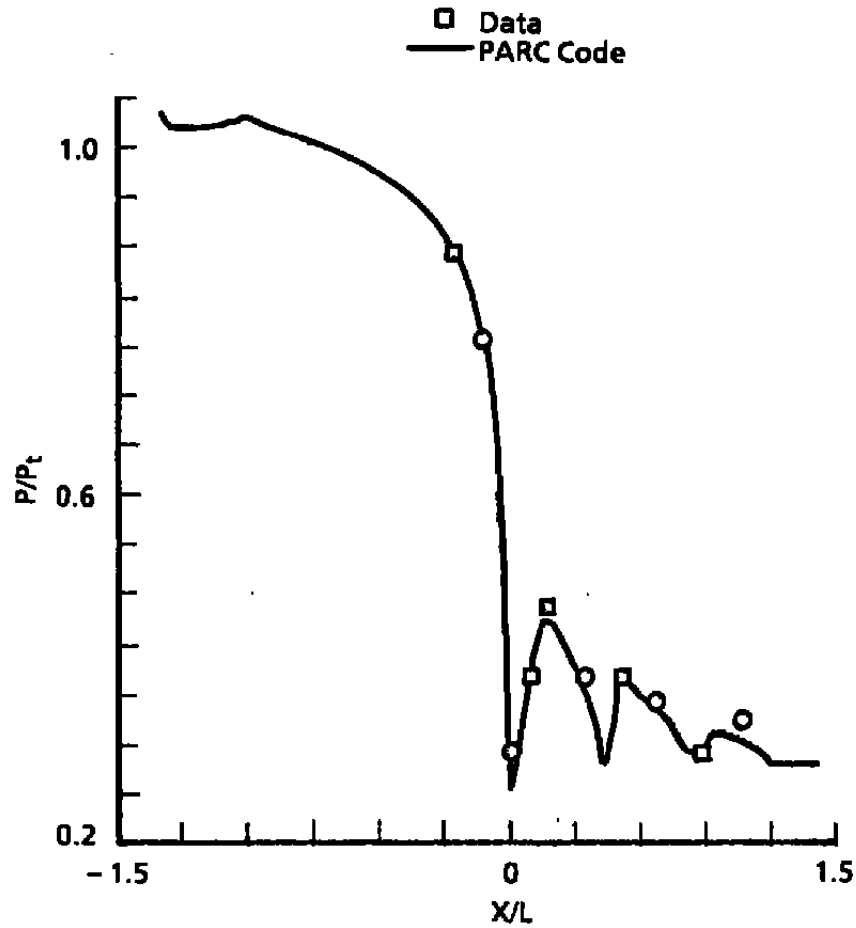

Figure 47. Case 1 wall static pressures for Langley nozzle.

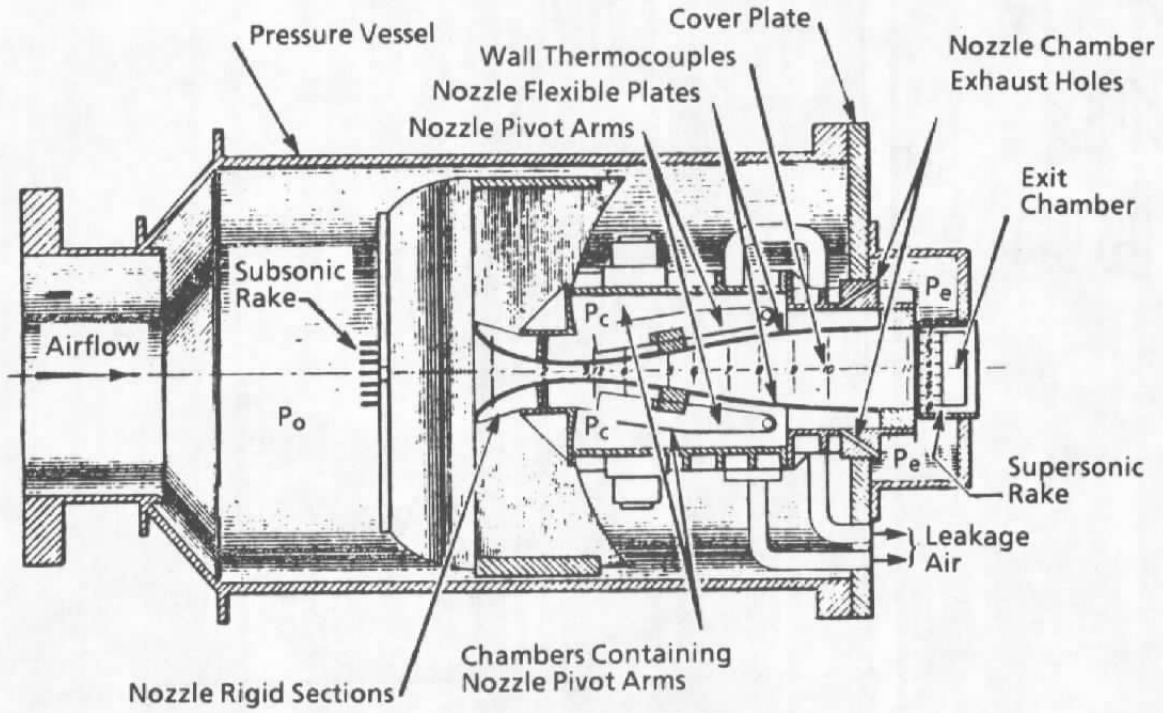

Figure 48. Six-by-six free-jet test installation.

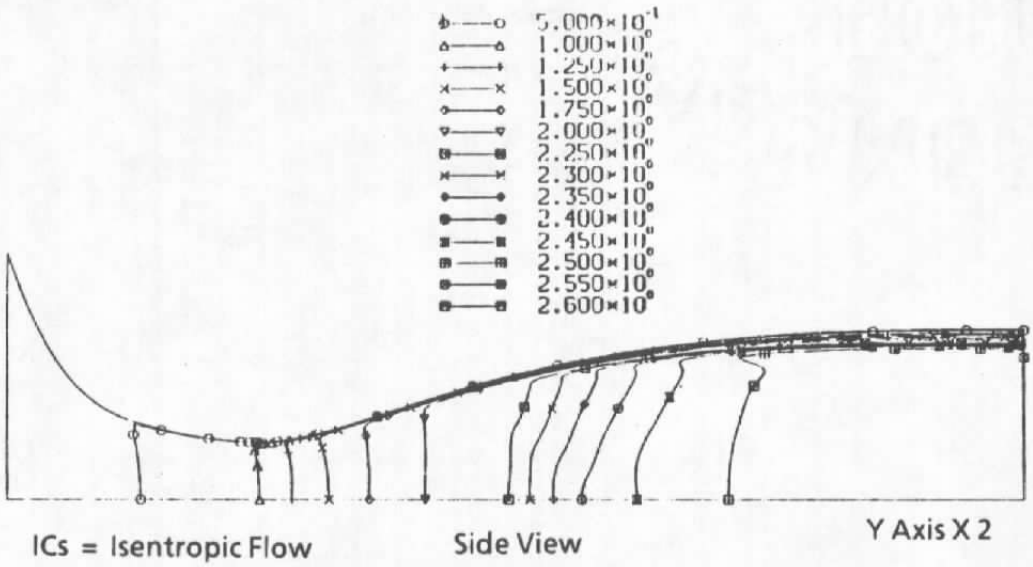

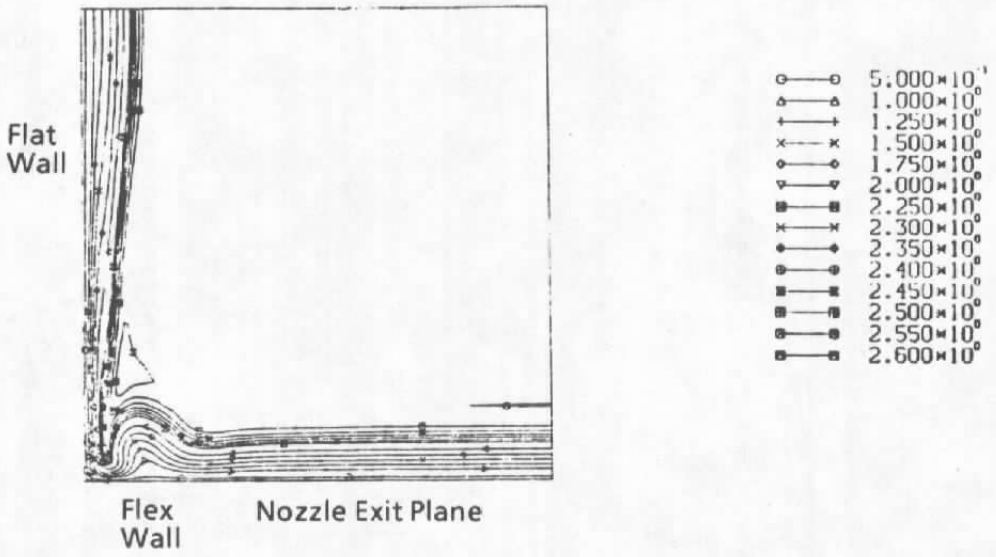

Figure 49. Six-by-six nozzle PARC solution.

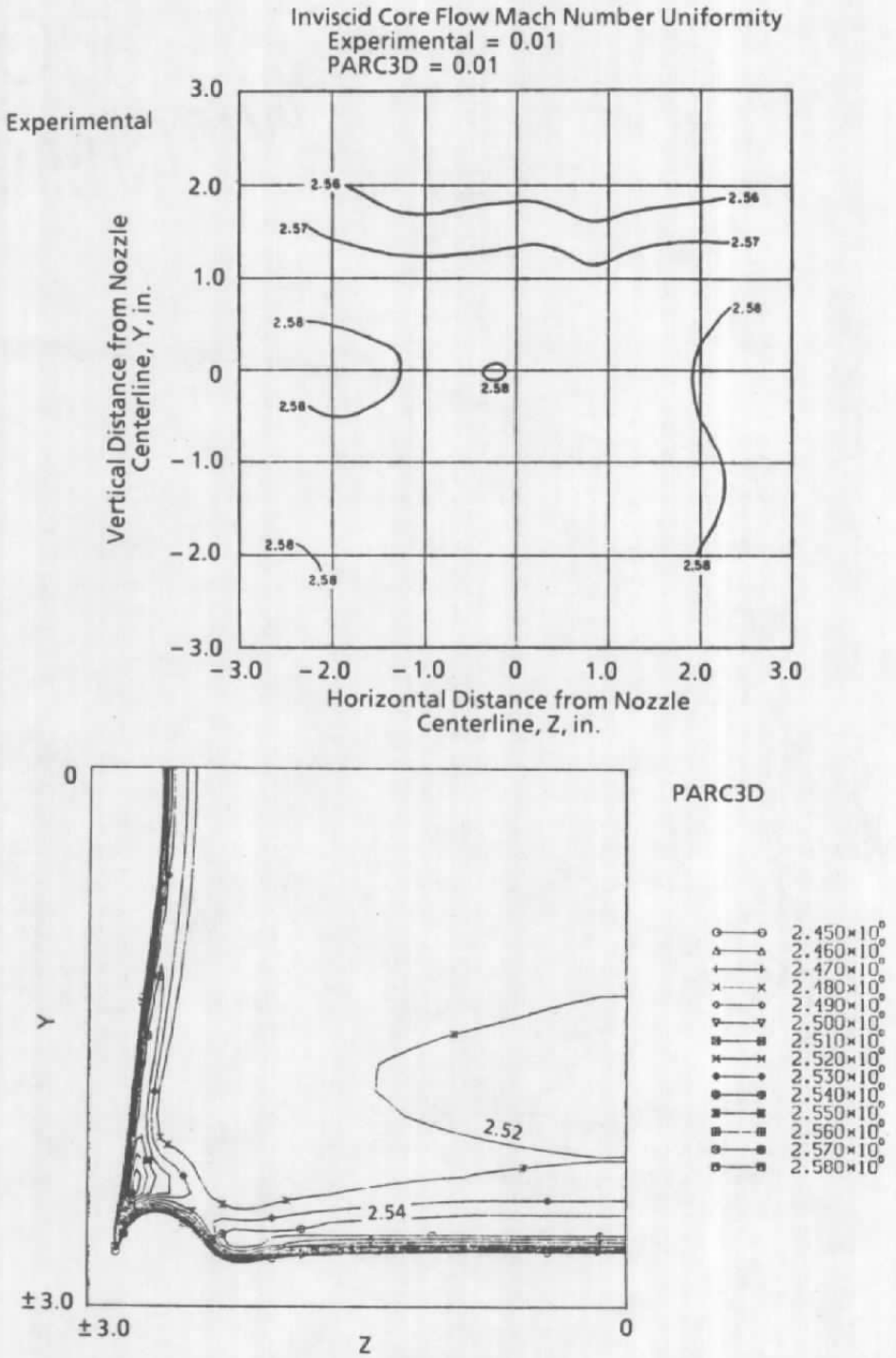

Figure 50. Six-by-six nozzle exit plane Mach number uniformity comparison.

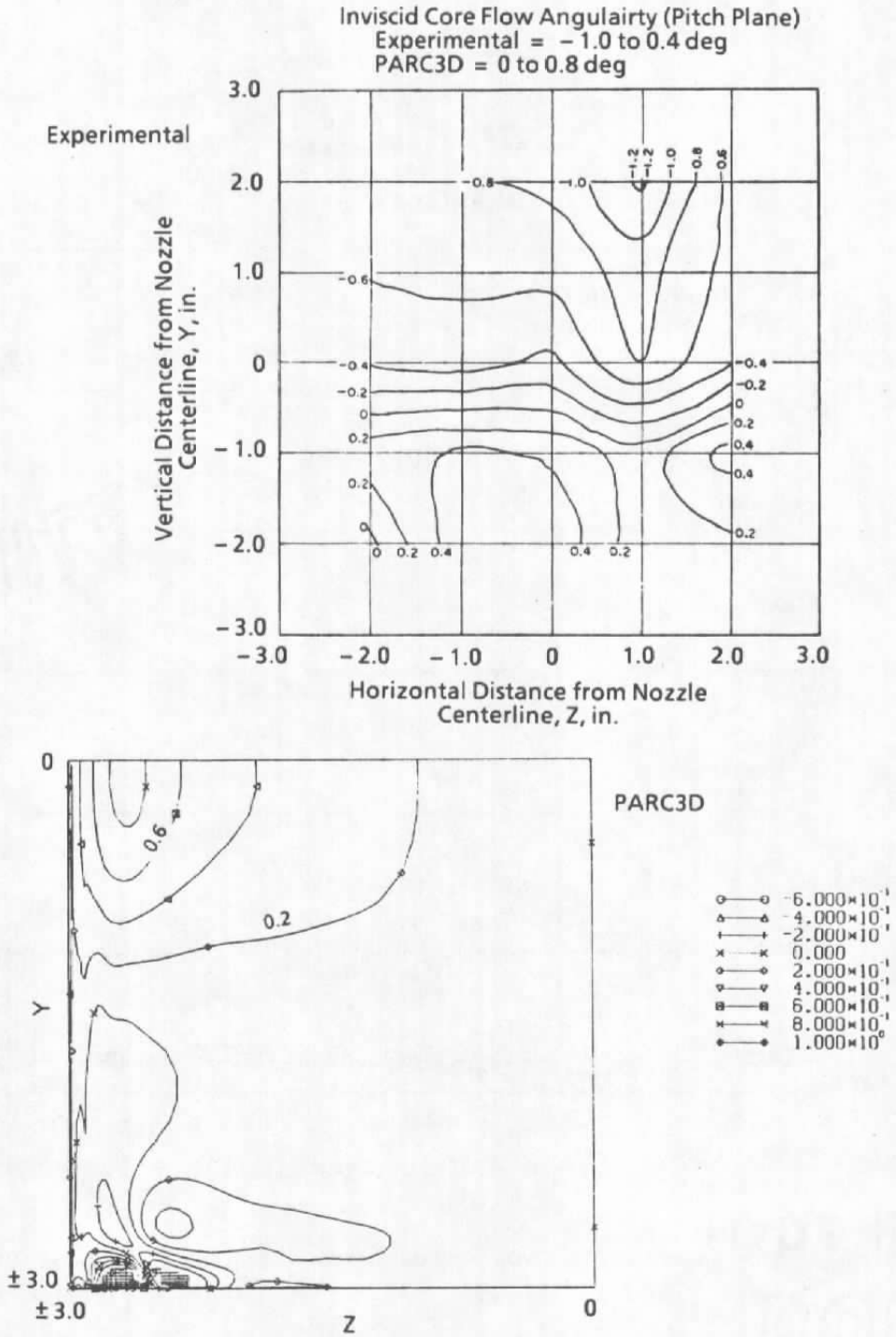

Figure 51. Six-by-six nozzle exit plane flow angularity comparison.

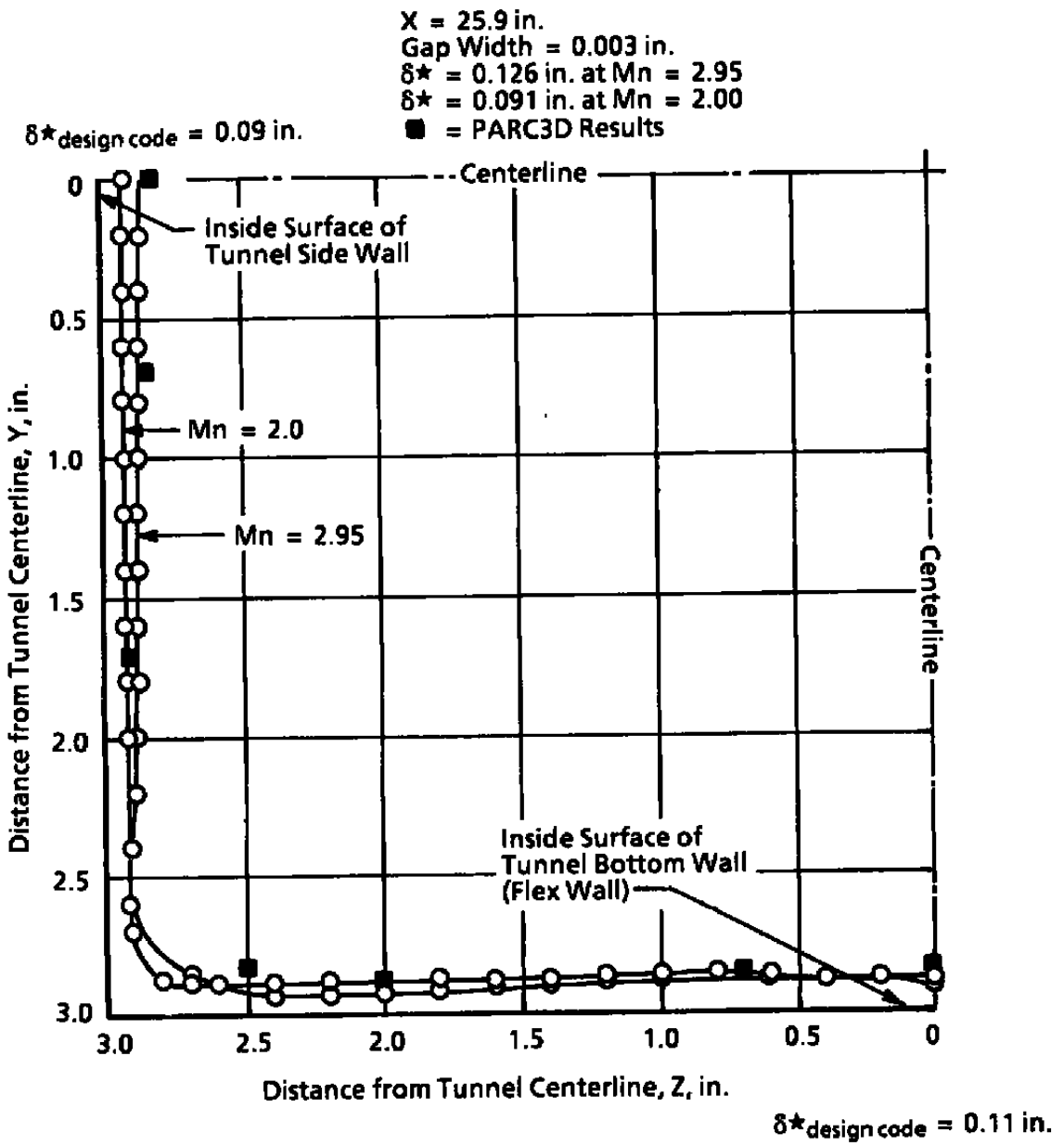

Figure 52. Six-by-six nozzle exit plane boundary-layer displacement thickness comparison.

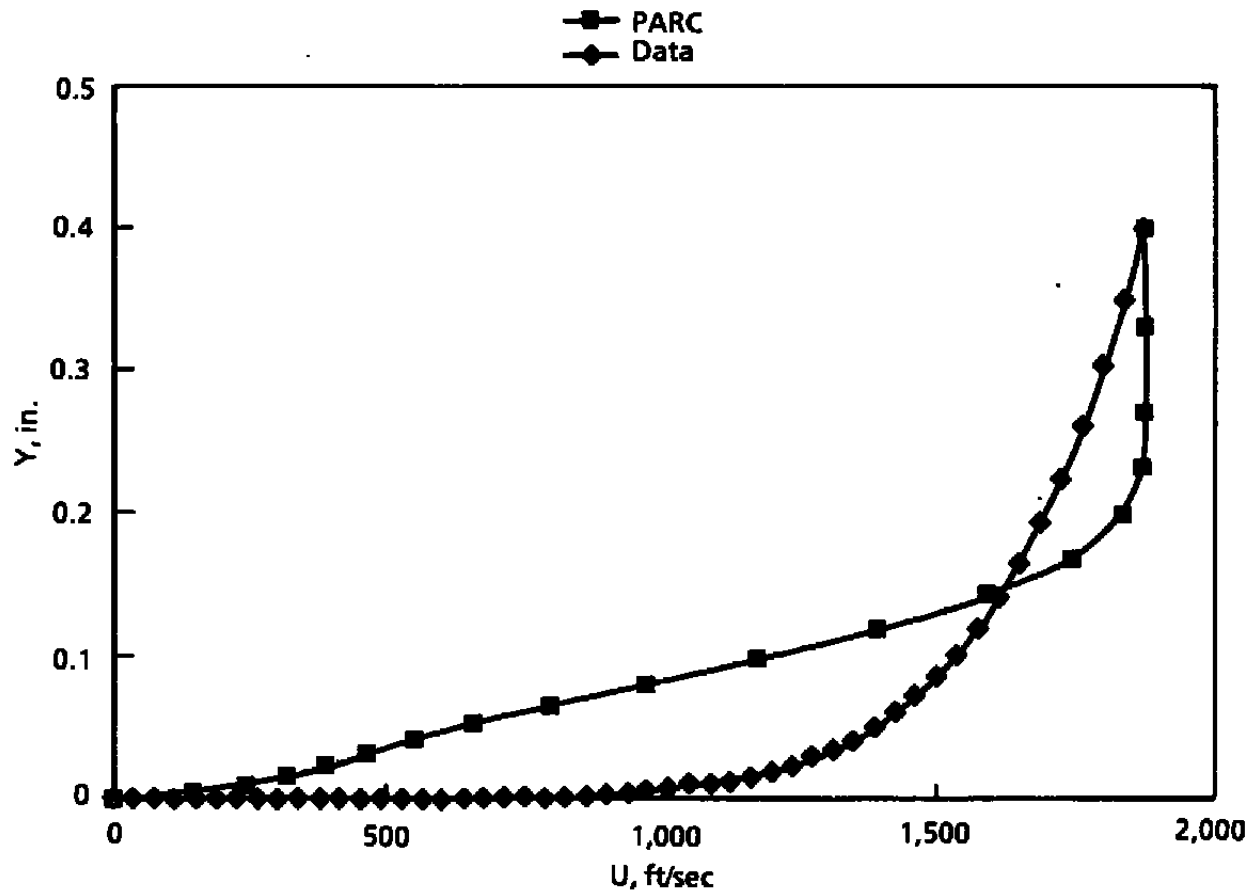

Figure 53. Six-by-six nozzle exit plane boundary-layer profile comparison.

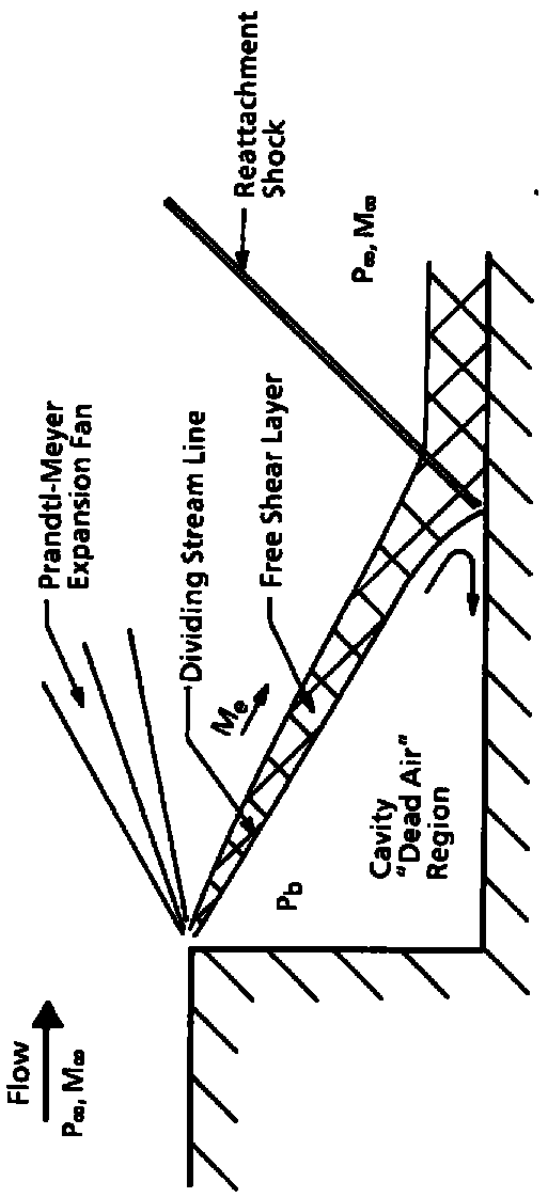

Figure 54. Rearward-facing step problem geometry and flow-field description.

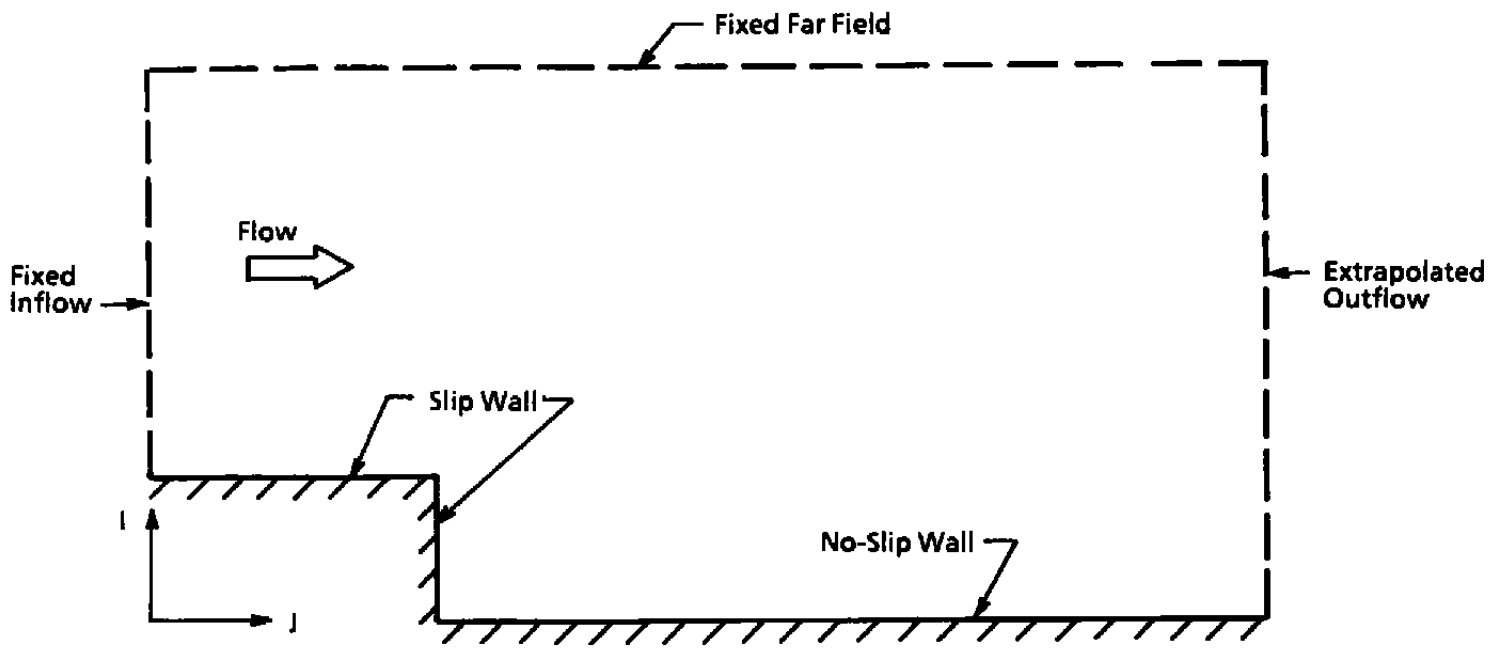

Figure 55. Rearward-facing step boundary conditions.

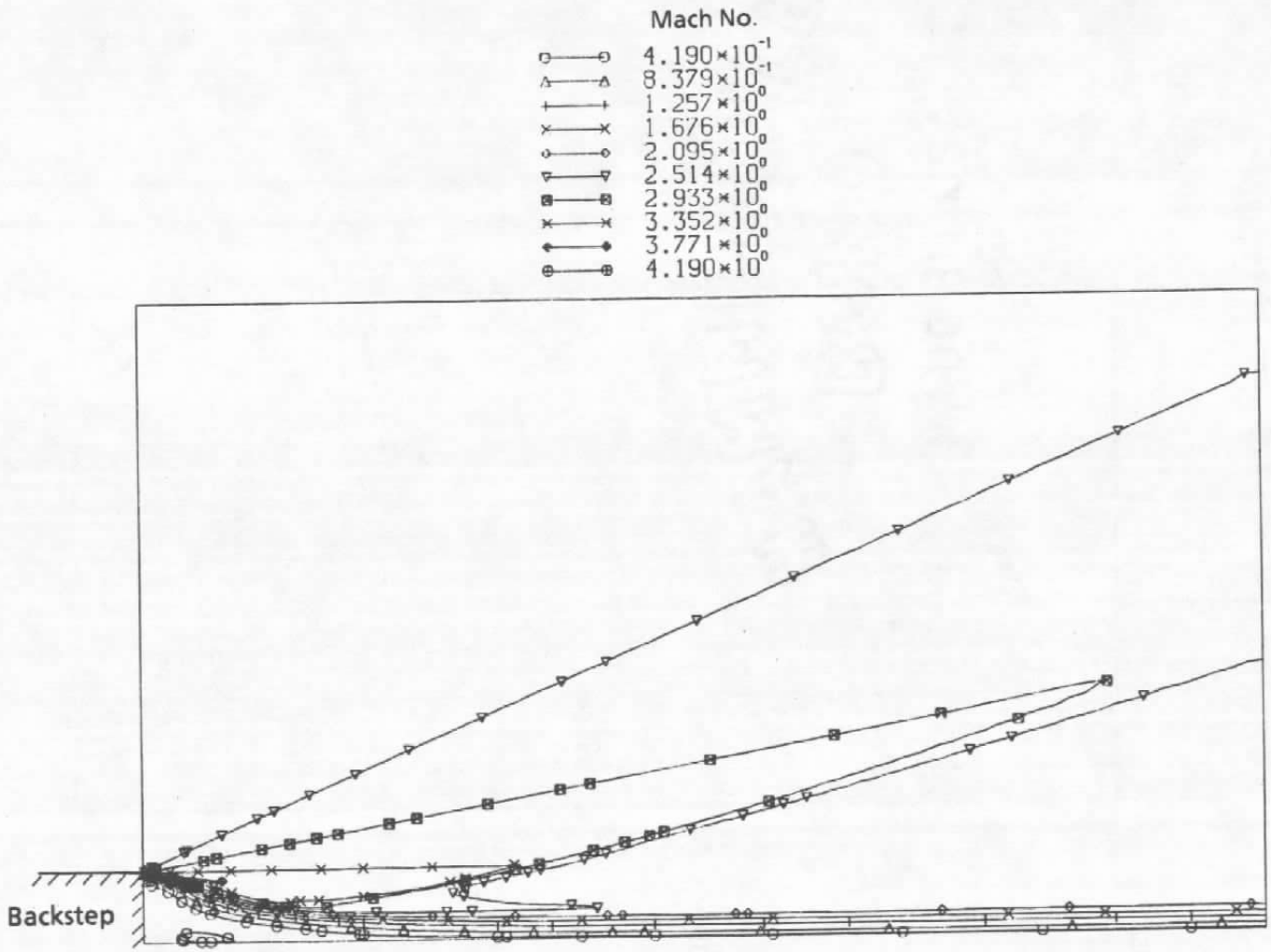

Figure 56. Rearward-facing step Mach 2.5 flow solution.

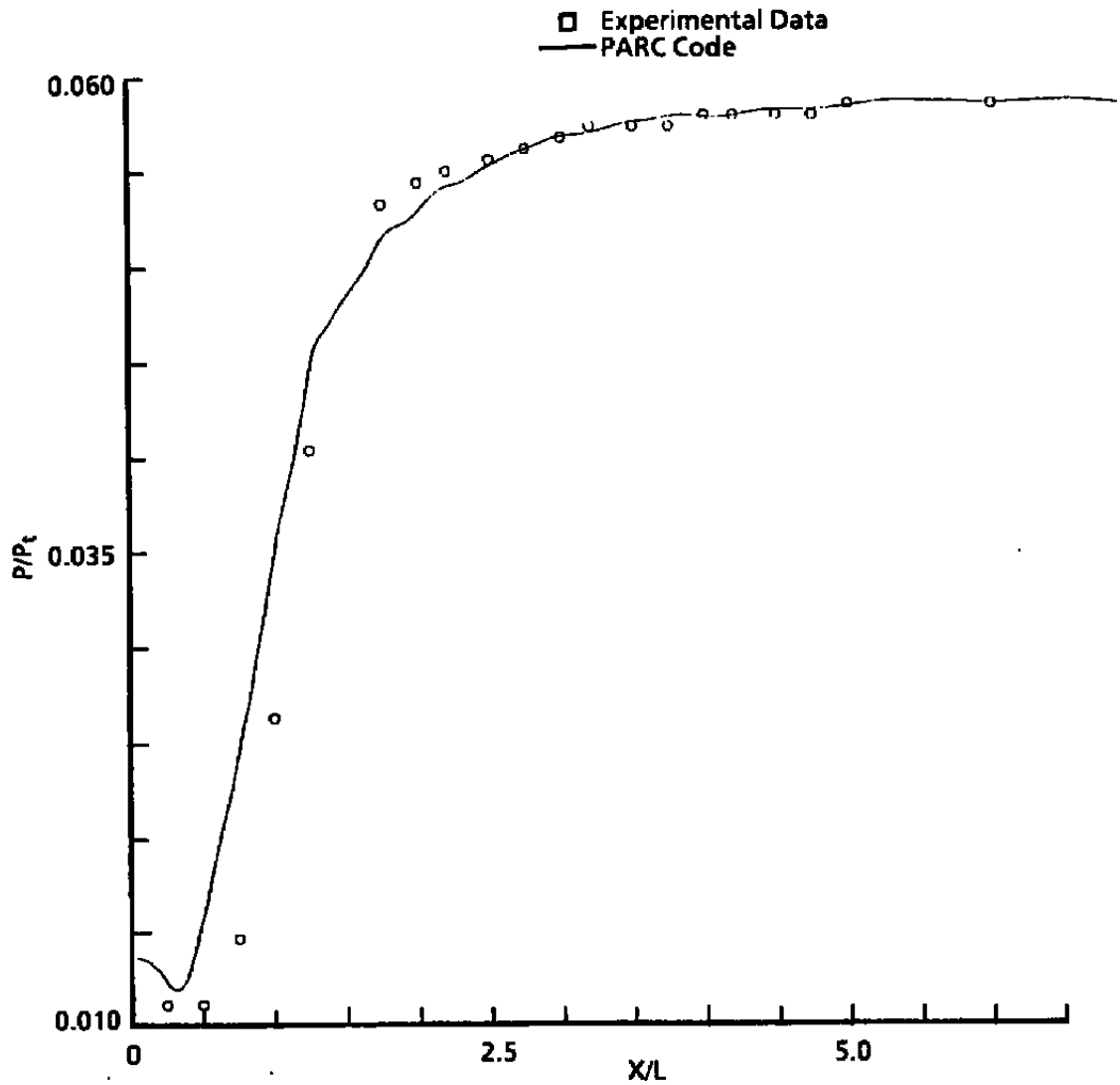

Figure 57. Rearward-facing step Mach 2.5 wall static pressure comparison.

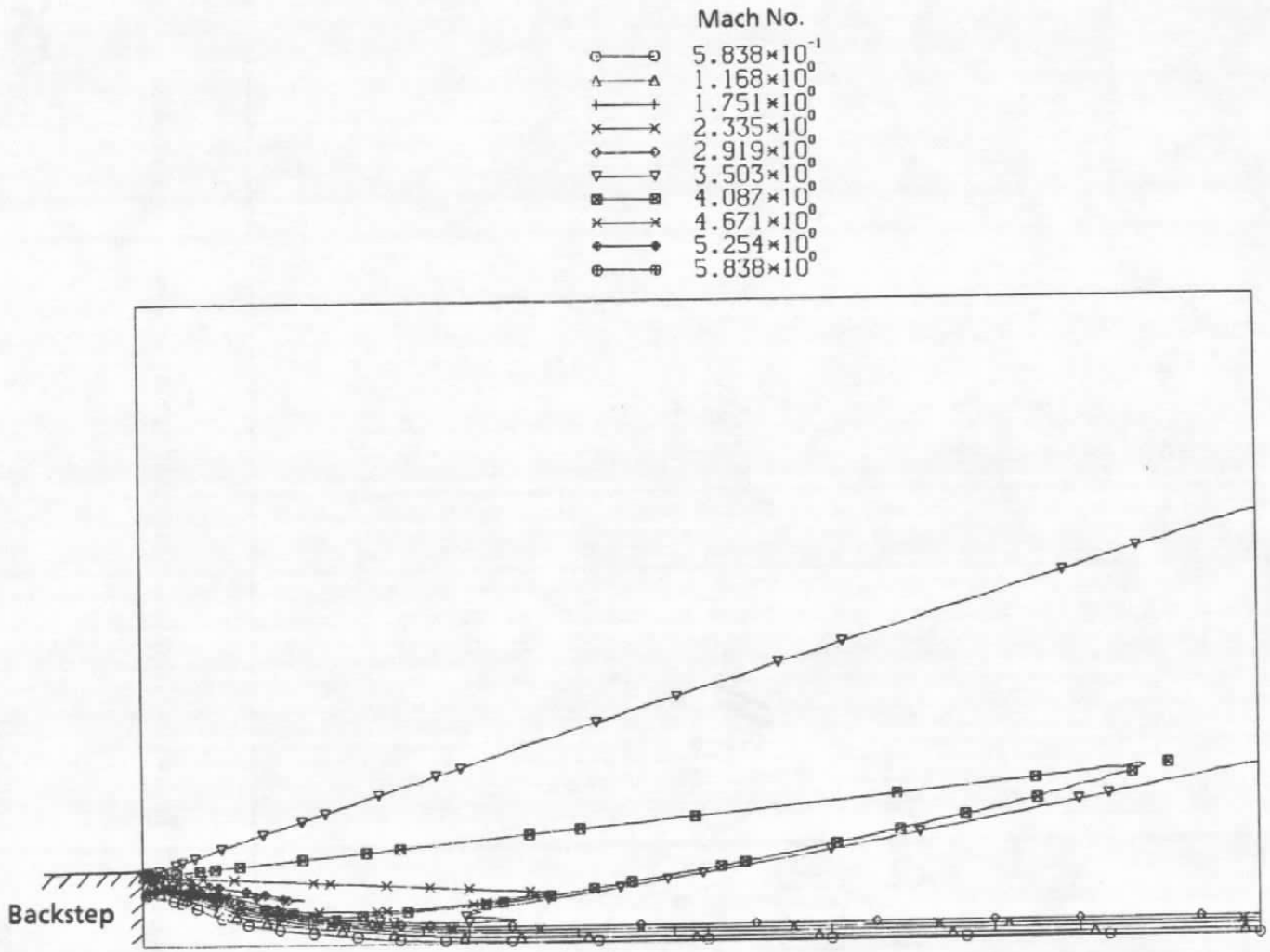

Figure 58. Rearward-facing step Mach 3.5 flow solution.

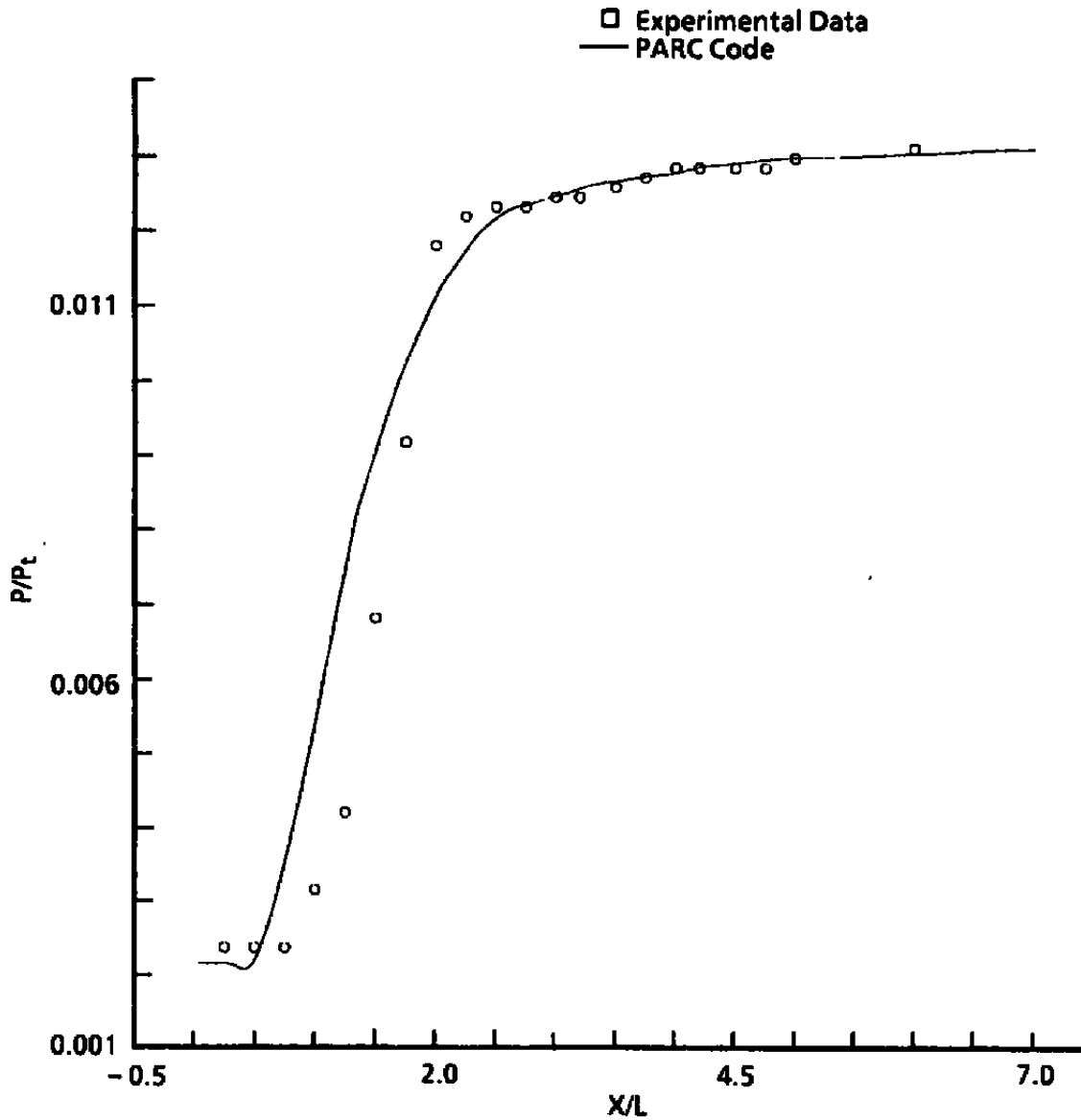

Figure 59. Rearward-facing step Mach 3.5 wall static pressure comparison.

Figure 60. Rearward-facing step Mach 5.0 flow solution.

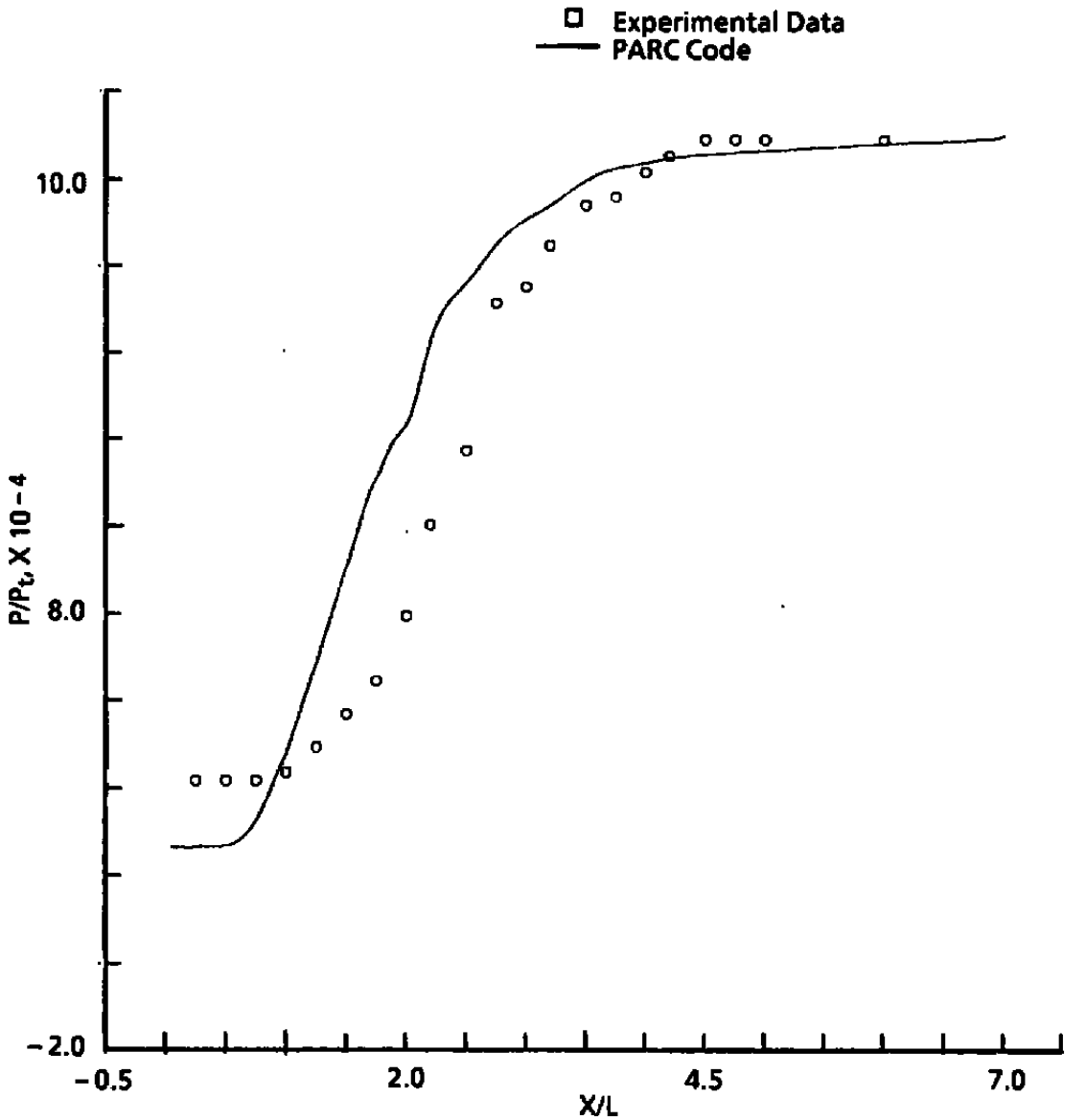

Figure 61. Rearward-facing step Mach 5.0 wall static pressure comparison.

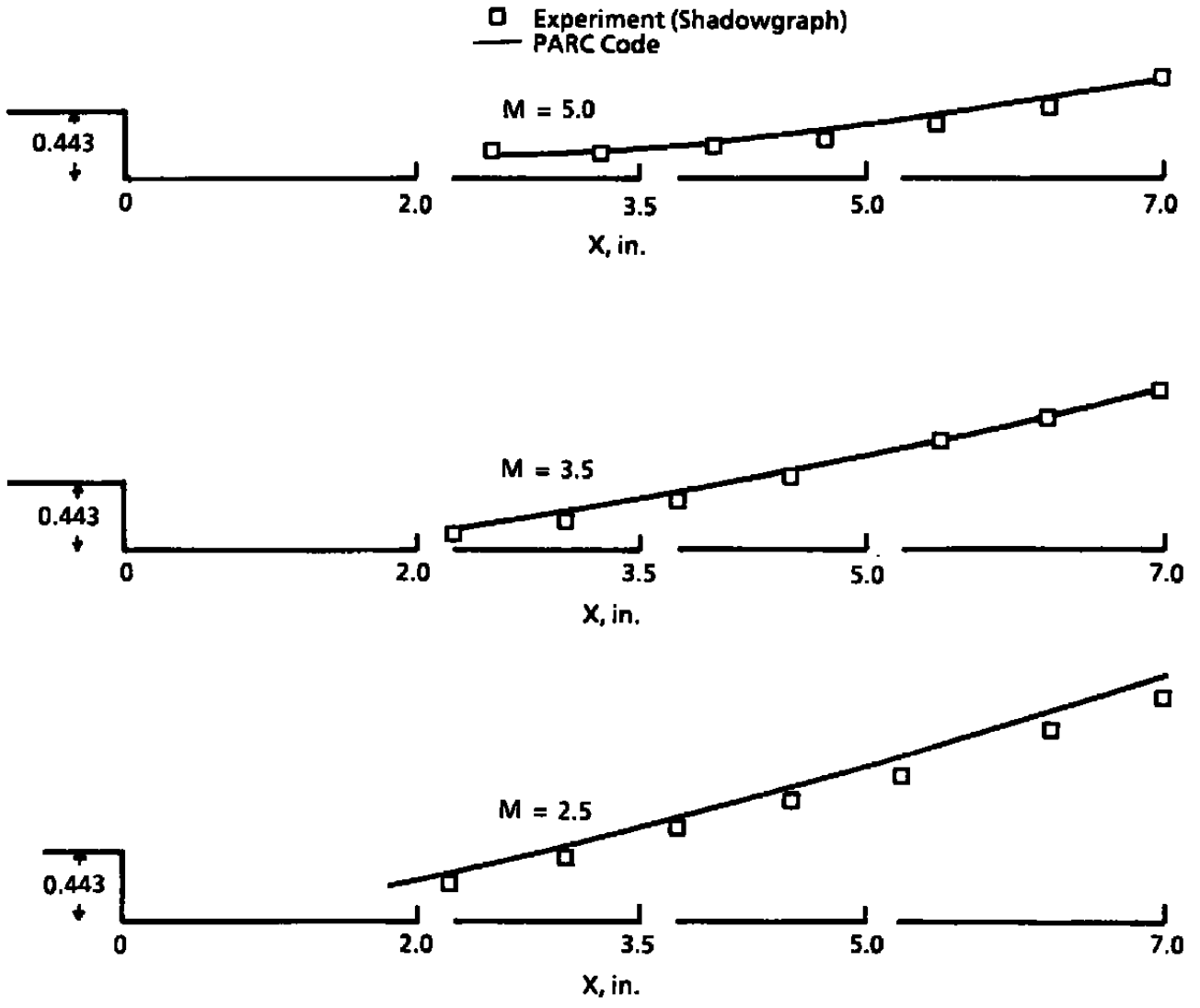

Figure 62. Rearward-facing step reattachment shock location comparison.

Table 1. PARC2D Calibration Activity Prior to 1989

Configuration	Ref.	Calibration Date	Conditions	Comparisons
High-bypass Turbine Engine Exhaust/Diffuser Interaction	2	Surface Pressures (Core Plug and Fan Duct) and Test Cell Pressure	Nozzle Pressure Ratio P_r = 2.5, Simulation at 35,000 ft, Altitude Reynolds Number (Length) Re_L = 7×10^5	Within ±25 percent (Large Deviation Because of Shift in Peak Locations)
Test Cell Heating Turbine Engine/Diffuser Interaction	3	Qualitative Comparison of Computed vs. Experiment (Thermovision® Pictures)	Overexpanded Nozzle Flow, Test Cell Pressure at 13.5 psia, M_E = 1.38 (Mach No. Nozzle Exit)	Agreed Qualitatively
Variable Area Ejector	3	Diffuser Wall Static Pressure	P_s/P_t = 0.11 (Cell Static Pressure to Nozzle Total Pressure), (P_E/p_T = 0.18 Diffuser Exit)	±5 percent
Centered Propulsive Jet	3	Base Pressures	Free-Stream Mach Number of 1.4 and a Jet Exit Mach Number of 2.3	±10 percent
Hypersonic Inlets (P-2, P-12)	5	Centerbody and Cowl Static Pessures	Inlet Mach Number M_α = 7.4, $Re_\alpha = 8.86 \times 10^6$/m (Free-Stream Reynolds No.)	P_2 = ±15 percent Cowl P_{12}, 10 percent Centerbody P_{12}, ±30 percent
2-D Hypersonic Inlet	6	Centerbody Boundary-Layer Growth	Inlet Mach Number M_α = 7.4, $Re_\alpha = 8.86 \times 10^6$/m	±50 percent (Transition to Turbulent Flow Incorrectly Modeled)
Axisymmetric Nozzle	6	Surface Static Pressure	P_T/P_a = 4.25 (Nozzle Total to Ambient), M_{exit} = 1.6 (Nozzle Exit Mach No.)	±5 percent
Subsonic Diffuser (Axisymmetric)	16	Surface Static Pressures	Inlet Pressure Ratio P_s/P_t = 0.8	±5 percent
Flat Plate	1	Profile Temperatures, Velocities, Skin Friction Shape Factor, Stanton Number	Laminar and Turbulent Flow, Various Reynolds Numbers ($Re_L = 2 \times 10^5$ to 5×10^6) and Mach Numbers (0.1 to 2.5)	±5 percent to ±10 percent
Supersonic Jet Axisymmetric	1	Profile of Wake Velocities and Spread Rates	Jet Mach No. = 2.22 P_a = 14.7 P_{sia}, T_a = 525°R (Ambient Conditions)	Near Field ±5 percent for Field ±40 percent (Far-Field Turbulence Incorrectly Modeled)
Rearward-Facing Step Subsonic	1	Profile Velocities, Wall Temperatures, Skin Friction	Re_h = 28,000 h = 3.79 cm M_α = 0.03195	±10 percent

Table 2. Rocket Motor Test Cases

Characteristic	Motor 1	Motor 2	Motor 3
Diffuser Area to Throat Area Ratio, Ad/A*	503.49	523.80	589.29
Diffuser Area to Nozzle Exit Area Ratio, Ad/Ane	11.31	21.77	20.32
Rocket Motor Chamber Pressure, psia	822.50	800.00	565.00
Test Data Percent Secondary Flow, lbm/sec	0.36	3.10	6.70
Test Data Cell Pressure, psia	0.08	0.12	0.08

Table 3. Wall Coordinates for the Six-by-Six Nozzle (X = 0 at Nozzle Throat)

X, in.	Y, in.	X, in.	Y, in.
−8.54	4.34	4.27	1.45
−8.34	4.05	4.50	1.49
−8.12	3.75	4.74	1.53
−7.90	3.47	4.97	1.57
−7.67	3.22	5.20	1.60
−7.45	2.99	5.43	1.64
−7.23	2.78	5.66	1.68
−7.00	2.59	5.90	1.71
−6.55	2.26	6.36	1.79
−6.33	2.12	6.59	1.83
−6.10	2.00	6.83	1.86
−5.87	1.89	7.06	1.89
−5.65	1.79	7.29	1.93
−5.42	1.71	7.52	1.97
−5.19	1.63	7.75	2.00
−4.96	1.57	8.70	2.13
−4.50	1.46	9.63	2.25
−4.27	1.42	10.09	2.30
−4.04	1.38	10.56	2.35
−3.81	1.35	11.02	2.40
−3.58	1.32	11.48	2.45
−3.35	1.29	11.95	2.49
−3.12	1.26	12.41	2.53
−2.90	1.23	12.87	2.57
−2.67	1.20	13.34	2.61
−2.43	1.18	13.80	2.64
−2.20	1.16	14.27	2.68
−1.97	1.14	14.73	2.71
−1.74	1.12	15.20	2.73
−1.51	1.10	15.66	2.76
−1.28	1.09	16.13	2.79
−1.05	1.07	16.59	2.81
−0.82	1.06	17.06	2.83
−0.59	1.05	17.52	2.85
−0.36	1.04	17.99	2.87
−0.13	1.03	18.45	2.89
0.10	1.03	18.92	2.90
0.33	1.02	19.38	2.92
0.56	1.03	19.85	2.93
0.79	1.03	20.31	2.94
1.02	1.05	20.78	2.95
1.49	1.08	21.71	2.97
1.72	1.10	22.18	2.97
1.95	1.12	22.64	2.98
2.18	1.15	23.11	2.98
2.41	1.18	23.57	2.99
2.65	1.21	24.04	2.99
3.11	1.27	24.97	3.00
3.34	1.31	25.44	3.00
3.57	1.34	25.90	3.00
3.81	1.38	26.37	3.00
4.04	1.42	26.83	3.00

Table 4. PARC2D Calibration from 1989 to 1990

Configuration	Ref.	Calibration Data	Conditions	Comparisons
Mach 2.22 nozzle	12	Wake Velocity Profiles and Spread Rates	Jet Mach No. = 2.22 P_a = 14.7 psia, T_a = 525°R (Ambient Conditions)	Near Field ±5 percent Far Field ±10 percent
Subonic Free Jet	13	Theoretical Spread Rate, Velocity Profile	Jet Mach No. = 0.20	< ±10 percent
Supersonic Free Jet	15	Compiled Mixing Spread Rate Data	Jet Mach Nos. = 1.0, 1.6, 3.0, and 4.0	±5 percent
Air Ejector/Diffuser	21	Test Cell Pressure, Diffuser Wall Static Pressures	1. P_t = 630 psia (Total Pressure) Ad/A^* = 36 (Area Diffuser to Area Ejector Throat), L/D = 4 2. P_t = 208 psia Ad/A^* = 36, L/D = 4 3. P_t = 360 psia Ad/A^* = 36, L/D = 4 4. P_t = 460 psia Ad/A^* = 16, L/D = 12	1. Matched Cell Pressure Exactly; Wall Statics Not Matched 2. 30 percent (Cell Pressure) 3. Correct Cell Pressure Value (Oscillate) 4. Matched Cell Pressure, Wall Static with Slight Shift in Peak Locations
Rocket Diffuser Systems	N/A	Test Cell Pressure	Nozzle Flow Field Calculated by SPP Code (Ref. 27); See Table 2 Ad/A^* Approx. 500 to 600 P_t (Chamber) Approx. 600 to 800 psia	Motors 1 and 3 Predicted Within Data Uncertainty; Motor 2 Was Outside Uncertainty Range
2-D/C-D Nozzle	28	Wall Static Pressures	Nozzle Exit Mach No., M_E = 1.35 A_e/A_t = 1.09 (Exit to Throat)	Upstream of Throat: Exact Match, Downstream: ±5 percent to ±30 percent (Peaks and Valleys Shifted)
Supersonic Free-Jet Nozzle	29	Mach No. and Flow Angularity Uniformity, Boundary-Layer Profile	M_E = 2.59 (Exit Mach No.) $Re_L = 1.2 \times 10^7$ (Length)	Mach No. Level: ±2 percent Uniformity: ±0.01 percent Flow Angularity: ±1 deg
Reward-Facing Step (Supersonic)	30	Wall Static Pressures, Shock Location	Inlet Mach Nos. M_α = 2.5, 3.5, and 5.0 Step height, h = 0.443 in.	After Reattachment: ±1 percent to 5 percent, Base Region: M_α = 2.5, 3.5: ±5 percent M_α = 5.0 ±50 percent

APPENDIX A

MODIFICATION TO ALGEBRAIC TURBULENCE MODEL MIXING COEFFICIENT

One of the most troublesome aspects of the work reported herein was the large amount of computer time required to get a converged solution. This was driven by the small time-step required to maintain stability. The number of iterations required to get to a converged solution is directly proportional to the size of the time step taken.

One of the major factors controlling the time-step size in the previous examples was the turbulence level in the flow. The PARC2D program limits the rate of change of certain derivatives during the flow solution, and an artificially high turbulence level could cause the limits to be exceeded. The turbulence model generates a value for the turbulent viscosity that is corrected by the constant turbulence mixing coefficient (COFMIX). This correction factor has been required simply because the values calculated without it were much too high. The problems that occurred above, however, indicated that the use of a constant correction might be too simplistic for the actual flow problem. The investigation was also driven by the results reported in Ref. 1, in particular by the complete failure of the turbulence model to adjust for the far-field flow in the Mach 2.22 jet.

To investigate this problem, a modification to the turbulence model was made that provided a correction factor based on the local Mach number of the flow. Mach number was chosen as the independent variable since it provides a reasonable indication of the energy of the flow at a given location. For a given value of Mach number at any particular grid point in the computational domain, the correction factor applied to the turbulent viscosity calculation was changed to

$$\text{COFMIX} = \frac{1}{(1 + 0.3\ \text{Mn}^2)}$$

The variable was limited to a maximum value of 0.47.

NOMENCLATURE

$b_{½}$	Free-jet boundary where the velocity equals ½ centerline velocity
COFMIX	Algebraic turbulence model turbulent mixing coefficient
D	Diffuser diameter
h	Rearward-facing step height
L	Diffuser length
M	Mach number
M_a, M_∞	Free-stream Mach number
M_E	Nozzle exit Mach number
P	Static pressure
P_a	Ambient pressure
P_{cell}	Test cell pressure
P_E	Diffuser exit pressure
P_r	Nozzle pressure ratio
P_t	Total pressure
R	Nozzle exit radius
Re_h	Reynolds number based on step height
Re_l	Reynolds number based on length
Re_∂	Reynolds number based on free-stream conditions
T_a	Ambient temperature

U	Velocity in the axial direction
UBAR	U divided by nozzle exit U
U_{max}	Maximum axial velocity
X	Axial distance downstream of nozzle exit plane
$Y_{½max}$	Radial location where the velocity equals ½ centerline velocity
σ	Spreading parameter
δ^*	Boundary-layer displacement thickness